The Computer aided design of ~~Shape design and interface load analysis for~~ below-knee prosthetic sockets.

by

David Reynolds B.Sc.

A Thesis Submitted for the Degree of
Doctor of Philosophy
in the
Faculty of Engineering

UNIVERSITY OF LONDON

October 1988

Bioengineering Centre
Department of Mechanical Engineering
University College London
Roehampton Lane
LONDON SW15 5PR

Dedicated to my parents

Abstract

The thesis begins with an introduction to the conventional socket design and fabrication procedure. A computer based system is documented which was developed at UCL to design below-knee prosthetic sockets. The first objective in the system's development was to provide an automated facility capable of taking surface measurements of a residual limb and manipulating these data to produce a socket shape using conventional design philosophy.

To refine the system, design must ultimately aim to provide an appropriate socket shape which produces a predetermined load distribution at the limb/socket interface. This requires an improved fundamental understanding of socket loading. An engineering study is presented in which the finite element (FE) method is used to predict interface loads in standing. The main objectives of this work are to produce a 'first generation' FE model which realistically represents the tissues of a loaded residual limb and then to use this model to discover the key parameters which determine interface loads.

Initially, idealised geometry and assumed mechanical properties are used to study the effects in the FE models of interface friction, distal end loading and soft tissue thickness.

Realistic geometric data are obtained experimentally from measurements of external residual limb shape and bones and mechanical properties of residual limb tissues are evaluated from a series of *in vivo* indentation tests. Further finite element models of socket loads are based upon these measured data.

The idealised FE models indicate that the conditions of friction at the interface and distal end-bearing have more dramatic effects upon gross load distribution than limb geometry. Those models based upon measured geometry and properties showed that variations in the socket rectification and in the distribution of mechanical properties of tissues predominated over alignment effects with regard to static pressure distribution.

Acknowledgements

I would like to express my gratitude to all the staff at the Bioengineering Centre and Department of Mechanical Engineering who have helped me with this research work. I would especially like to mention Ms M. Lord and Dr. M. Dewar for their help and suggestions. The advice of Dr R. Corran, Mr A. Crew, Dr S. Dharmavasan, Mr C.D. Greenwood, Mr D. Hurley, Mr P. Jarman, Mr L. Flynn, Mr T. Rodwell, Mr D.Smith and Mr J. Wilkinson was of great benefit to this study.

Table of Contents

page

Chapter 6 : FE models of idealised residual limbs.

Chapter 7 : Experimental measurements on a limb model.

Chapter 8 : FE models using measured amputee data.

Chapter 9 : Summary and strategy for future work.

page

List of figures

page

Chapter 1 : Introduction

Chapter 2 : The UCL Computer Aided Socket Design System.

Chapter 3 : FE models of indentations

Chapter 4 : Experimental measurements of indentations.

Chapter 5 : Evaluation of limb tissue geometry and modulus on an amputee subject.

Chapter 6 : FE models of idealised residual limbs.

Chapter 7 : Experimental measurements on a limb model.

Chapter 8 : FE models using measured amputee data

Chapter 9 : Summary

Appendix A

Appendix B

Appendix C

page

Appendix D

Chapter 1

Introduction.

1.0 Background

The prosthetic socket is the interface between an amputee and his artificial limb; comfort of this component is a major determinant of his 'quality of life'. The total lower limb amputee population in England in 1984 was 51,130 or just over one person in every thousand. Of these 73% were over 60 years of age [DHSS86a]. The average delivery time for a conventional patellar tendon bearing prosthesis was 69 working days, a significant proportion of the remaining life of many older amputees. An average of 3.2 visits per amputee were made to Artificial Limb and Appliance Centres throughout 1984, 1,907 below-knee prostheses were fitted and the total cost of all artificial limbs supplied was £32 m. A 1983 consumer research survey showed that 33% of amputees interviewed complained of a poorly fitting or uncomfortable prosthesis [DHSS86b].

Socket design is specific to the user and must achieve correct fit while providing stable support of the residual limb through those areas of the skin that can tolerate loading. The shape which is able to do this is not simply a model of the residual limb; distortions are incorporated to the limb contours which judiciously encourage loading in certain areas and relieve in others. This shape manipulation process is termed rectification. In socket production, capture of the limb shape, rectification and socket fabrication are essentially hand skills. Better control at each of these stages and a clearer understanding of how rectification affects socket loading are needed to improve the present 'craft-based' system.

In recent years, the use of computers has benefited the measurement, manipulation and manufacture of shapes in diverse fields. Research in lower limb prosthetics has used advanced techniques to investigate amputee gait and prosthetic alignment. The prosthetic industry has recently introduced modular artificial limb systems with associated mass production technologies. The first true attempts to introduce computer aided design / computer aided manufacture (CAD/CAM) techniques, however, have focussed on the production of sockets.

In the early 1980's, Foort and Saunders of the University of British Columbia (UBC), Vancouver began a project to develop a system for the computer aided design of prosthetic sockets for below-knee amputees [SAUNDERS85]. The aim was to custom design sockets of the widely used patellar tendon bearing type using numerical

manipulation of shape data rather than rectification on physical models of residual limbs.

The Bioengineering Centre at University College London (UCL) were also committed to the introduction of automated techniques for socket production. Early projects developed RAPIDFORM, a semi-automatic drapeforming machine [DAVIES85], and later MASTERFORM, a purpose-built carving machine [LAWRENCE85]. These machines were used in a collaborative trial with UBC to replicate the prosthetic shapes designed by their system.

After some experience with the Vancouver software, a pilot study was started at UCL to explore a different CAD philosophy. Initial results were encouraging and development continued with a series of patient trials. During the early months, software was modified to establish a suite of programs which were thereafter evaluated in a more comprehensive patient study. To date, results show the UCL system to be as successful as traditional methods as far as can be evaluated subjectively. However, whilst improvements have been made by this system in the consistency and speed of production of socket shapes a scientific basis for socket design is still missing and a computer aided engineering (CAE) study has been made in a first step towards a better understanding of the rectification process.

The author's involvement in the development of the UCL CAD system and this CAE study are the main topics discussed in this thesis.

1.1 Design and manufacture of the patellar-tendon bearing socket.

Design

Socket design aims to transmit supporting loads, enable the amputee to control his prosthesis and provide proprioceptive feedback. The patellar tendon bearing (PTB) socket, designed by Radcliffe and Foort [RADCLIFFE61], is the basis for the design of the majority of below-knee sockets fitted in the United Kingdom.

The main feature of the PTB socket is the patellar bar - an inward bulge which fits against the patellar tendon midway between the distal edge of the patella and the tibial tubercle. A large proportion of the vertical load on the socket is borne at the bar; clinical

experience has shown that the skin covering the tendon is able to tolerate relatively high loads. Flexibility of the underlying tendon provides better 'shock-absorption' during gait than would result at a bony site.

Any tendency of the limb to move back from the patellar bar is counteracted by pressures at the rear. These equilibrating pressures are promoted by another inward bulge, the 'popliteal depression', which gives the posterior tissues an initial compressive strain prior to loading. Pressure is similarly encouraged in the 'fleshy' areas to the medial and lateral sides of the tibia, mainly to provide mediolateral stability.

The areas described have, in general, a relatively thick layer of soft tissues covering the bone structure and small movements of the socket wall with respect to the limb during gait therefore are less likely to produce high strains and stresses. Another site where significant load is borne is at the medial tibial condyle. Although this is covered by a thin layer of soft tissue, the flaring of the tibia presents a large area at the right inclination to support vertical loads.

The locations of these pressure tolerant areas are shown by 2 views of a right limb in figure 1.1 (a).

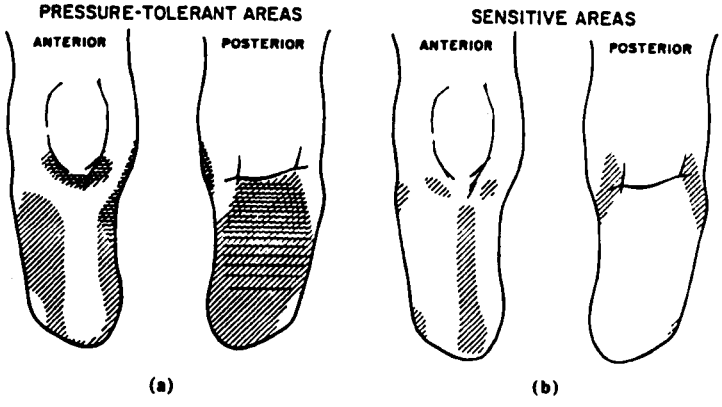

Figure 1.1 - Pressure tolerant/sensitive areas of the residual limb. (after Radcliffe & Foort, 1961)

At the pressure sensitive areas of the residual limb, the socket is contoured away from the limb surface. These areas are generally where a thin layer of soft tissues

covers a bone and high stresses arise more easily. This is especially true where there are prominences such as at the head and cut end of the fibula, the sharp crest of the tibia and the anterolateral and anteromedial aspects of the tibial condyles. These are shown in the anterior view of figure 1.1 (b). At the rear, the tissues covering the hamstring tendons are prone to pinching between the posterior brim of the socket, which is trimmed away here to permit knee flexion, and the tendons themselves, which become tensed during this flexion.

The distal end of the residual limb presents a large area which might be thought suitable to support vertical forces but frequently scar tissue prevents this. Another factor which may make it unsuitable for high loading is the concentration of stress caused by the underlying cut bones. For the majority of residual limbs distal end bearing is prevented.

Although the areas shown in figure 1.1 (b) are usually termed 'pressure sensitive' in prosthetics, the loads which may damage the skin and underlying tissues may be in the form of direct normal pressure, shear forces acting tangentially to the surface of the limb or a combination of these. A high magnitude, coupled with prolonged duration, of normal pressure on body tissues has been shown to restrict blood flow and retard local metabolism [KOSIAK58]. Shearing forces have also been found destructive [ROAF76]. A combination of pressure and shear has been shown to be especially harmful [BENNETT79]. There is evidence too that cyclic pressures of low magnitude can be harmful [BRAND75].

In the original PTB design, a rigid shell made of glass reinforced plastic was used which incorporated the contours described. The rigid shell was lined with a closed cell polymer foam material, Kemblo, which deforms locally to redistribute loads and 'even out' peaks. Radcliffe and Foort also recommended total contact between the residual limb and the socket liner. This gives the greatest available area over which to distribute load and yields a pumping action during gait that helps return venous blood and prevent oedema. An additional benefit is that sensory feedback is likely to be improved if the limb can perceive pressures all over its surface.

When the prosthetic foot is off the ground, the artificial limb must be held in place. Cuff suspension was recommended which consists of a wide band, usually of leather, fastened around the residual limb above the knee. The socket is attached to this cuff by straps at the sides and these must be long enough to permit the polycentric knee to have

unrestricted flexion/extension but must avoid excessive slack which may cause an undesirable piston action. Cuff suspension is still the most commonly used suspension system in England and Wales.

Variants of the original design

The main deviation from the original PTB design has been in the method of suspension. An important area to react mediolateral moments is absent with the cuff suspension system. These moments can cause instability of the knee and, for short limbs especially, support here is important. In the alternative supracondylar system, the socket walls are high on the medial and lateral sides and wrap closely over the femoral condyles to provide suspension and mediolateral knee support. With pliable plastic sockets, the flexibility of the socket material is sufficient to permit the side extensions to expand and thus allow the knee joint into the socket. Sockets made of stiffer materials require wedge inserts on the medial side to 'lock' the condyles in. The majority of sockets fitted in Scotland and the USA use the supracondylar suspension system. The KBM socket is a German variant of this.

The supracondylar/suprapatellar suspension system has, in addition to high mediolateral walls, a high anterior wall which fits closely over the patella. This provides anteroposterior stabilisation of the knee, especially at toe-off, which reduces the tendency for the knee to hyperextend. The anterior wall may also provide an additional load bearing area. A drawback, however, is that the brim is often cumbersome, for example, when kneeling.

Other variations on the original design relate to liners and limb 'socks'. A number of different closed cell foams are currently used as liner materials. Unfortunately all of these undergo permanent deformation with age which restricts their useful life. Pelite is the most commonly used material in the UK. Wool, nylon or cotton 'socks' also improve socket comfort. Woolen socks are able to redistribute loads like foam liners, but are too frequently used to make up for an oversized socket. The main function of nylon socks is to reduce friction during gait by providing an interface between the residual limb and socket that is relatively free to slide. Cotton socks, to a limited extent, combine these functions and are better absorbers of perspiration. If regularly changed, limb socks can improve the 'microclimate' of the socket, reducing the bacteria which accelerate tissue damage.

The use of flexible sockets has recently gained acceptance, especially in the USA. These have an outer frame of a stiff plastic or composite material and a flexible inner

shell in contact with the residual limb or limb sock. Direct loading of the limb by the frame occurs only in the rectified supporting areas, leaving the flexible shell relatively free to distort elsewhere during gait. Although their use has been more widely exploited for above-knee prostheses, improvements have been noted in the brims of below-knee versions [SCHUCK86] and in the ability to assess these clear sockets [FISHMAN87].

Manufacture

The manufacture of below-knee sockets may be separated into four stages. These are casting of the residual limb, manufacture of a plaster positive from this cast, rectification of this positive and, finally, manufacture of the socket using the positive cast as a former. An outline follows of the method currently used by prosthetists at Roehampton.

Prior to casting, the residual limb is covered with a thin nylon sock upon which locations of anatomical features are 'mapped' in indelible pencil. The patella, patellar tendon, fibula head, tibia and hamstrings are typical features identified. When this mapping is complete, plaster of paris bandages are wrapped over the limb and sock. Approximately 15° of flexion at the knee is used during casting to emphasise the anatomical features.

As the plaster starts to set, the prosthetist encourages the limb cast into a shape more suitable for load bearing (figure 1.2). The thumbs are used to indent by the patellar

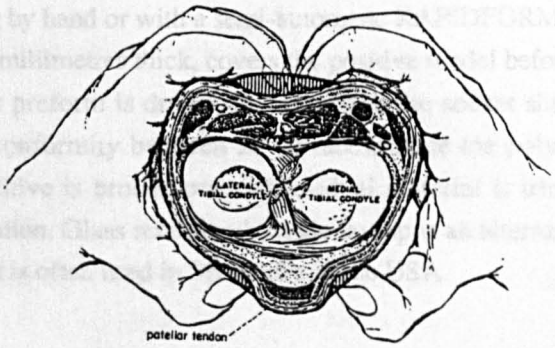

Figure 1.2 - Adjustment of limb shape during casting.
(after Radcliffe & Foort, 1961)

tendon while, at the rear, the other fingers press into the popliteal tissues, which mainly consist of the gastrocnemius. The prosthetist uses his subjective judgement and adjusts the contouring of the plaster wrap according to the 'stiffness' properties of the tissues sensed manually. Thus a degree of rectification is introduced at the casting stage. The cast is removed when fully set.

A positive model is then prepared by pouring plaster mix into the wrap cast. The map marked by the prosthetist becomes imprinted on this model. It is usually at this stage that an axis is established within the prosthetic shape. Before filling with the plaster mix, a mandrel is positioned within the wrap cast. The orientation of the prosthetic shape relative to this mandrel is maintained throughout rectification and socket fabrication and eventually fixes the 'bench' alignment which determines the initial set-up of the socket on the artificial limb. Radcliffe and Foort recommended tilts to the vertical, in both the sagittal and frontal planes, which tend to cause flexion and adduction at the knee in flat footed stance. How these tilts are interpreted seems widely open to individual preferences.

When the wrap cast has been cut away from the plaster positive it is ready for rectification. This is a sculpting process in which material is removed in those areas where pressure is to be applied and added where high pressure is undesirable. Rasps and files are used to create the depressions and new plaster is built on in smooth patches which raise the surface.

Final manufacture of the hard shell socket is commonly achieved in England and Wales by drapeforming by hand or with a semi-automatic RAPIDFORM machine. The Pelite liner, typically 7 millimetres thick, covers the positive model before a pre-heated polypropylene sheet or preform is drawn down to form the socket shell. Vacuum is applied to encourage conformity between all surfaces. Once the polypropylene has cooled, the plaster positive is broken out and residual material is trimmed away to complete socket fabrication. Glass reinforced plastic lay-up is an alternative method of socket manufacture that is often used in Scotland and the USA.

Assessment

Once finished, the socket is assembled with the other limb components and must be assessed in the fitting room before it can be issued. Here the prosthetist sets the final alignment and can then properly judge the fit of the socket by discussing its comfort with the amputee and by studying the residual limb for signs of potential damage. If the

fit is not completely satisfactory, small changes can be made by removing material from the liner or occasionally by glueing in an additional patch. If the socket fit is very poor, the entire manufacture process must be repeated.

The alignment - the position and orientation of the prosthetic components relative to one another - affects both the kinematics and kinetics of amputee gait and significantly influences socket comfort. Subjective evaluation of gait is used and limb components are adjusted to compensate for any gait deviations.

The kinematic problem is to give normal appearance throughout the gait cycle. This criterion is not satisfied for some amputees who can often be seen to scuff their feet on swing through, sway their upper body or have an excessively wide walking base. In satisfying kinetic criteria attempts are made to minimise the moments produced by the coupled actions of the ground reaction forces and those applied by the residual limb. This must be done for any stage of the gait cycle and while standing. Figure 1.3 shows the effect of an inset of the foot at an instant during the gait cycle. Here the socket loads have been resolved into vertical, medial and lateral components.

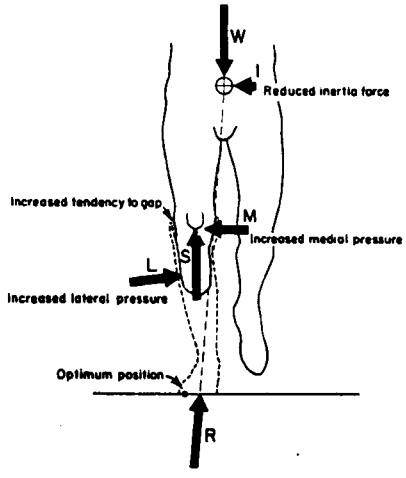

Figure 1.3 - The effect of a foot inset upon socket loading.
(after Radcliffe & Foort, 1961)

Good alignment will enable ambulation that is economical of effort, while allowing higher interface pressures only in those pressure tolerant areas where support is most needed. Prosthetic alignment has been the subject of much investigation. Zahedi et al.

have described parameters by which alignment may be defined and have identified ranges of these parameters which provide acceptable alignment [ZAHEDI86]. Other investigators have studies the effect of alignment changes upon measured kinematic [HANNAH84] and kinetic [WILSON79] data. An objective means of providing satisfactory alignment in the fitting room has yet to be found.

Medical factors

The majority of residual limbs can be accommodated using the standard procedures described above since most have broadly similar shape and function. This can be explained in terms of similarities in the causation and surgical techniques used for amputation. The vast majority of amputations are due to peripheral vascular disease (63.7% in the UK in 1986) [DHSS86a] or diabetes (20.2%) and a long posterior skin flap is widely used in surgery for these and other cases.

The lower limb amputee population in England is presently divided roughly equally between below- and above-knee cases. As medical and surgical techniques improve an increase in the proportion of below-knee amputations, preserving the natural knee function, is expected. This appears to have been the trend in the USA - since 1965 the ratio of above to below-knee amputations has been reversed from 70:30 to 30:70 [KAY75].

For several days after amputation, residual limbs usually contain significant oedema. As healing progresses, oedema generally diminishes and the limb volume is reduced. Many surgeons recommend that amputees be up out of bed and walking on a temporary prosthesis at the soonest possible date. By traditional methods, however, early supply of a temporary prosthesis is difficult and this may need replacing frequently as the volume reduces to a stable state.

In summary, below-knee socket design is founded upon a basic application of biomechanical concepts and the craft-based manufacturing processes are slow and too often unsuccessful. Conventional production methods allow no objective feedback since shape information is lost when wraps and rectified positives are destroyed and there is therefore no logical path which may be followed to improve fit consistently. Since a number of different technicians may be engaged in producing any prosthesis and there are few quantitative standards to work to, communication of an amputee's needs can easily be misconstrued. On an international, and even national level, there is much 'flexing' of the basic guidelines by which prostheses are produced. The lack of accurate quantitative techniques means that skills are obtained slowly and training

requires much hands-on experience. There is a worldwide shortage of trained prosthetists.

1.2 Potential advantages of CAD/CAM in prosthetics.

Computers are being used increasingly to aid the design and manufacture of durable goods. A product typically may evolve firstly with an idea which is rapidly modelled and viewed graphically. The aesthetics of this design may be assessed and an analysis may be performed to test its functionality before a physical prototype is produced. In the case of a mechanical component, the latter stage of assessment may be a stress analysis of the component in use.

In manufacture, numerically controlled machines under the supervision of a computer may produce those components of the product with complex geometry. Industrial robots may perform simpler, repetitive process with great precision. The above description may invoke an image of the automotive industry but the processes may equally apply to the production of modular prostheses in appropriate economic circumstances. Advantages of this type of CAD/CAM implementation are mainly in the speed of design and manufacture and in the control of quality and cost.

Some prosthetics components, essentially the socket and cosmesis, require custom design. The implementation of CAD/CAM technologies for these articles will differ from the above description and this is described fully in subsequent sections of the thesis. A number of potential advantages of numerically based design and manufacture techniques, however, may be identified immediately.

A closed-loop system of production may be employed in which quantified changes are made to an initially unsuccessful trial design to work iteratively towards improved fit. Shape data may be stored and retrieved with ease so that a successful fit may be reproduced repeatedly. Sockets may be produced more rapidly which will improve care and allow the prosthetist more time with the patient for assessment and fitting. With more rapid production, a clearer link may exist between design and assessment and this will be especially of benefit during training. In addition, the chances will be lessened of a poor fit occurring because of the longer-term time-dependent variations of limb

shape. Improvements made in socket productivity and prosthetic training may in turn provide economic benefits.

1.3 Introduction of CAD/CAM systems into prosthetics.

Prior to the development of the UCL computer aided socket design (CASD) system only Saunders and Foort of UBC, Vancouver had produced a computer based system for designing lower-limb sockets. The UBC software uses a limited number of limb measurements to scale a 'reference' PTB socket shape to provide a reasonable socket design. Thereafter, interactive modifications are made to the shape on-screen to produce the final fit. Sets of measurements are taken with calipers and tape-measure. More sophisticated devices appropriate for limb measurement were unavailable at the time of development.

Anteroposterior and mediolateral measurements at the knee are used by the software to scale the proximal part of the reference socket in cross-section and length before anteroposterior and circumferential measurements distal of the knee joint, at one inch intervals, are used to 'taper' the scaled reference shape. The tapering measurements are taken with tissues under compression from a suspension casting system. Final modifications, where patches of material are added or removed to improve fit, are made via an interactive graphics display which can produce wire frame models and plots of cross-sections.

In numerical terms, the 'scaling' and 'tapering' operations are transformations of the reference shape which is stored as a set of cylindrical polar coordinates. The patches are added to the transformed shape by superimposing displacements onto the coordinate data. These are generated using bi-beta functions which have zero magnitude and gradient at their boundaries. This system has been commercially available since 1986.

A prototype CAD/CAM system for above-knee sockets has also been reported [NAKAJIMA82]. The philosophy used by this group was quite different from that of Saunders and Foort since measurements of the full surface of the residual limb were to be used by the design software. The surface was to be defined by radial measurements taken from a positive limb cast which were spaced axially 20 mm apart and at angular intervals of 9° around the measurement axis. A mathematical surface was to be fitted to these data using Bezier type functions. A number of design algorithms were to be

explored, based upon statistical analyses of the differences between limb shapes and conventionally designed socket shapes. Parameters which were to be examined were ratios of the radii, circumference and cross-section of the rectified and unrectified shapes. To permit these comparisons, an axis was to be set on each shape with respect to four anatomical landmarks - three around the knee and one at the distal end. In the final system, it was envisaged that the design algorithms would be able to transform the mathematical surface representing the residual limb into a socket shape. No further publications have been found which indicate whether this prototype ever became a reality.

Algorithms used by both of these systems deal only with shape information and, by assuming that some degree of standardisation is possible, transform one set of shape data into another. Regardless of how 'intelligent' these transformation processes are made, if they are based upon external shape data alone they will yield a unique socket for a given limb shape. Comfort, which depends primarily upon the loads at the interface between the residual limb and socket, cannot be guaranteed because the underlying structure of limb will affect these loads. A better understanding is needed of how damaging interface loads arise before significant improvements in CAD systems can be assured.

1.4 Evaluation of interface loads.

Interface loads may be measured or they may be predicted using analytical models. A review follows of research in these and related areas.

1.4.1 Measurements

A number of investigators have measured normal interface pressures on below-knee sockets whereas no measurements of shear loads have been found in the literature.

The effects of liner materials on peak pressures measured at 4 sites during walking have been observed [SONCK70]. 'Kulite' solid state transducers were used. Pearson et al. used 'Kulite' transducers 3.2 mm in diameter at 4 locations on 10 subjects to measure normal pressures during standing and walking [PEARSON73]. The mean bodyweight of the subject group was 776 N. Pressures have been measured during

walking in groups of subjects wearing lined or unlined sockets [MEIER73]. Capacitance type transducers 20 mm in diameter were used which were stated to have a 'bench test' accuracy of ±20%. Isherwood used welded PVC bags filled with water, which were connected to a silicon diaphragm transducer, to measure pressures in a lined socket at 6 sites [ISHERWOOD78]. The subject's bodyweight was 753 N. The measurements areas of Isherwood's devices were large - between 17 and 58 cm^2. The main results from these investigations are tabulated in figure 1.4.

Investigators:	Sonck et al.		Pearson et al.		Meier et al.		Isherwood	
Test conditions:	Walking (with liner)	Walking (no liner)	Standing	Walking	Walking (with liner)	Walking (noliner)	Standing	Walking
Measurement site:								
Patellar bar	290	270	98	216	194	232	64	304
Lateral tibial condyle	128	90	78	120	127	251	39	50
Medial tibial condyle	131	166	38	41	51	97	34	61
Distal anterior tibia	193	504	78	284	123	127	-	-

Figure 1.4 Table of published interface pressure measurements in below-knee sockets.

(Values are in kPa)

In a research environment, the use of pressure transducers is a cheap and relatively simple way of evaluating normal interface loading. These devices are being made smaller, thus reducing errors due to averaging effects over the measurement area as well as those introduced by curvatures of the loaded surface.

The main practical disadvantages of taking pressure measurements in the clinic are twofold. Firstly, each subject requires an experimental socket in which transducers must be carefully mounted and this will, most probably, not become a service socket. Secondly, assuming that pressure peaks may occur anywhere at the interface, they are not easily located by transducers which can only measure pressures at discrete locations.

Sheet materials, containing a range of ink-filled capsules which rupture under various levels of load, have been used to provide a continuous image of load distribution over a number of areas of the body surface. These cannot be calibrated to

measure socket interface loads, however, since pressure and shear, or combinations thereof, are registered. Their use in prosthetics is infrequent; probably because similar qualitative information of direct relevance to tissue damage is freely available to the prosthetist by observing skin discolourations on the limb.

In addition to the practical complications of locating and measuring peak pressures in the clinic, the usefulness of such data to a CAD/CAM system is questionable. It is reasonable to state that a socket found to be causing an unacceptably high pressure at a particular location must be redesigned and that relief in the 'problem area' will reduce this pressure, but the amount of relief needed and its precise shape and location remain unknown. An iterative trial-and-error method of design, pressure measurement and redesign is impractical. Far preferable is to be able to predict the distribution of interface loads in advance of fabrication and this is only possible with an understanding of the mechanics of loading of the residual limb by the socket.

1.4.2 Pre-requisites for modelling socket loads.

An analytical model of a residual limb supported by a socket, which is capable of predicting interface loads, will require information regarding the geometry and mechanical properties of the socket and the residual limb tissues.

The socket

In Chapter 2 it will become evident how measurements of socket shape are obtained. Below-knee sockets made at the Bioengineering Centre are made of polypropylene (Young's modulus approximately 1.2 GPa) and have wall thicknesses between 3 and 7 mm. These sockets are designed to be rigid. Pelite is used exclusively for the manufacture of socket liners in the Bioengineering Centre. An approximate modulus, obtained from tests which compressed discs of this material, is 350 kPa.

The limb tissues

The tissues which make the residual limb are now described briefly. A section through an asymptomatic leg shows how the limb tissues are distributed. In a residual limb, wastage of the muscles is usual which reduces their volume. Pathological studies have shown that with lack of use muscle fibres may be replaced by fat and fibrous tissue [GUYTON71].

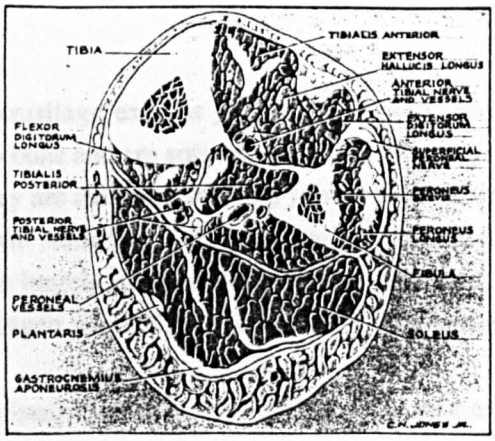

Figure 1.5 - Section through the leg
(after Slocum, 1949)

For the purposes of the current study, the limb tissues are separated into bones and 'soft tissues'. The soft tissues shown in figure 1.5 are mainly skin, muscle and fat. Tendon, ligament and cartilage are also included in this category.

At the outer extreme of the section lies the skin. This comprises epidermal and dermal layers. The epidermis itself is a layered structure with dead cells at the surface which form a hard protective layer. The thickness of the epidermis is mostly of the order of 0.1 mm but may be greater at such locations as the palms, soles and knees. The dermis contains a network of fibres of collagen and elastin. The collagen fibres are stiff in tension and have high strength; in skin, they have a 'zig-zag' appearance which straightens when extended. The elastin fibres, as their name suggests, are able to sustain fairly large elastic strains. Surrounding this fibrous mesh is a matrix of protein polysaccharides, proteoglycans, which is often termed the 'ground substance'. The dermis averages between 1 and 2 mm thick. The subcutaneous tissue is a continuation of the dermis; however, a more widely spaced fibre mesh exists here which contains fat cells. The thickness of the fatty, adipose, tissue layer varies with body location.

The muscles are arranged in fibres, which themselves may be subdivided into microscopic filaments, and are enclosed by sheaths. Another sheath, the epimysium,

encloses the whole muscle. Blood vessels and nerves are distributed through the muscles.

Tendon, ligament and cartilage exist at joints and do not appear in figure 1.5. Tendons connect muscle to bone and are soft connective tissues which contain densely packed collagen fibres. They are therefore stiff and strong. Ligaments connect bone to bone and are more compliant since fibres are less regularly arranged. Cartilage at the knee joint, for example, is largely made up of proteoglycans and water which are covered with a mesh of collagen fibres. This is suitable for withstanding high loads.

The bones are the prime tissues through which forces are transmitted in the body and thus they have evolved as stiff structures. Published values of compressive and tensile moduli for the tibia fall in the range 1.2 to 1.4 GPa [YAMADA70, EVANS73]. The compact bones such as the tibia and fibula are made up of many units which surround vascular channels. These units are themselves made up of sheets of bone tissue. The outer surface of all bones is covered by a layer of fibrous tissue, the periosteum.

The larger blood vessels and nerves pass between the tissues described.

Measurement of limb tissue geometry may be accomplished in a number of ways. The external limb shape may be sensed using various tactile or optical devices and radiographic, or other, scanning techniques may provide images which show the geometry of underlying tissues. This subject is discussed further in Chapter 5.

A means to measure and characterise the mechanical behaviour of the limb tissues is less readily identified. The literature shows that the most popular noninvasive approach for measuring the compressive properties of soft tissues has been to use an indenting tool to measure a load versus deflection response. Few authors have been able to use these data other than for qualitative comparisons. Of interest in these publications are observations about the measured responses, their time-dependence and the practicalities of their measurement.

Some early investigators indented soft tissues in attempts to identify variations in mechanical properties due to factors such as age, sex and the presence of oedema or obesity. Kirk and Kvorning [KIRK49] duplicated an apparatus of Schade [SCHADE12] to study skin and subcutaneous tissues. The apparatus measured the deflections of an indenter, loaded with a dead weight, into the anterior aspect of the tibia. Deflections were logged over a 2 minute period following the application of load

and 'instantaneous' and 'creep' components of deflection were identified. Differences were observed between groups of old and young subjects; the younger group demonstrated larger deflections of both type. Tests were repeated three times in succession at the same location and the magnitudes of both components of deflection were found to be greater in the first than in subsequent tests. Another study demonstrated a greater compliance of skinfolds in females than in males [CLEGG66].

A study by Hickman et al. measured the response of skin and subcutaneous tissues at the ear lobe and anteromedial aspect of the tibia [HICKMAN66]. Loads were applied by round discs of various diameters and deflections of these were measured. One series of tests measured deflections 15s after a step pressure, in a range between 0.7 and 27 kPa, had been applied. Tests on the ear lobe of an asymptomatic subject showed that relatively low pressures produced engineering strains in excess of 25%. Above this strain the tissues exhibited a much stiffer response. A series of ramp tests demonstrated the existence of hysteresis in the ear lobe tissues.

Creep tests were also performed which involved the application of a step pressure followed by a period of constant pressure loading. Strains occurred rapidly over the first few minutes of loading and continued, although at a much reduced rate, for a test period of 3 hours. Similarly, when load was removed a large proportion of the strain was recovered rapidly but strain remaining after this was recovered more slowly. In oedematous tissue, a loss of initial elasticity and slower rates of creep and recovery were observed; however, the opposite effects were found in obesity.

Other tests counted the flow rate of radiosodium injected into the blood to show the effects of loading upon blood flow. A nominal pressure well above the capillary pressure of 3.3 kPa was found necessary to seriously impair blood flow in the forearms of asymptomatic subjects. Circulatory recovery was found to precede the delayed viscoelastic recovery from the effects of applied pressure.

Another apparatus was produced which used a force transducer and a LVDT to measure loads and deflections of both spherical and flat indenters [ZIEGERT78]. Responses were recorded at three sites on the anteromedial aspect of the tibia of a number of asymptomatic subjects. A nonlinear load versus deflection response was obtained; although, this became linear above loads of about 13 N. The indenter geometry for this test is not described. Creep test data also were obtained by applying a dead weight load and measuring deflections for 5 minutes. The response consisted of curves 'whose slope approaches zero after about four minutes'. At the end of the first measurement period, an equal increment load was applied and a rapid displacement

again occurred; however, this did not increase significantly with time. Further tests preconditioned tissues by applying a constant indenter load for 5 minutes and found that the load versus deflection response of these tissues was near-linear. The gradient of the response was assumed to be a representative tissue stiffness. Measured stiffnesses varied by up to 70% between sites on any given subject and by up to 300% between subjects at equivalent sites. Results from tests taken at the same site at least 24 hours apart were repeatable within 20%.

Indentation tests on skin and subcutaneous tissues have shown behaviour to resemble that of viscoelastic solids. The mechanism of the time-dependent deformation is not fully understood; some authors have postulated theories to explain it.

Hickman et al. proposed that deformation caused by applied normal pressures contains an elastic and a viscoelastic component [HICKMAN66]. The former was comprised of elastic strains within the fibrous matrix and compressive and shear strains in the ground substance. These deformations were thought to distort the capillaries and larger vessels, thus reducing blood flow. Since a large proportion of the applied load is carried by the fibrous matrix and ground substance, however, the full magnitude of the applied pressure is not transmitted to the blood. The viscoelastic component of the deformation was felt to be due to flow of the ground substance under the action of stress gradients. This gradually causes further distortion of the vessels and hence a further reduction in blood flow. The rapid recovery of blood flow upon unloading was attributed to the recovery of the larger elastic component of deformation.

Ziegert and Lewis emphasised the importance of extracellular fluid and assumed the skin and subcutaneous tissues at the anterior aspect of the tibia to resemble an elastic membrane covering a porous elastic material filled with a viscous fluid [ZIEGERT78]. It was felt that the elastic membrane does not act as a major load-carrying member. They attributed an initial creep response to the outflow of this fluid under low loads whereas, with all the fluid displaced, the porous structure acts in a nearly linear-elastic fashion. Guyton states that a small portion of interstitial fluids are free to flow but that the major portion is held tightly by hydrated substances [GUYTON71].

Oomens et al. [OOMENS87] also use the analogy of a sponge filled with fluid, when describing the ground substance, and emphasise its importance in compression. They postulate that nonlinear time-dependent behaviour in compression is due to distortions of the pores of the 'sponge' which cause increased resistance to outflow of

the interstitial fluids. Lanir [LANIR88] has attributed this increased resistance partly to osmotic pressures.

Measurements of the load versus deflection response of indentations offer no direct indication of stress-strain relationship for the indented material. Some authors, however, have analysed stress and strains beneath indenters theoretically.

An analysis of the stresses within an elastic material was performed which combined classical linear-elastic theory and a variational approach [BENNETT71]. Homogeneous, isotropic behaviour was assumed for a continuous layer of material resting on a rigid base. A solution in two dimensions only was considered in which an indenting beam was assumed to extend infinitely normal to the plane of interest. Compressive and shear [BENNETT72] stresses were analysed beneath beams of various geometry. The predicted compressive stresses beneath the beam varied only with depth into the layer, not with the distance across the beam. These stresses fell rapidly with distance from the edge of the beam. The maximum predicted shear stresses were located at or beyond the edge and as the ratio of the beam width to layer thickness was reduced shear stress was found to increase. The general distributions of compressive and shear stresses predicted by the theory were confirmed experimentally by measuring deformations of a grid marked on a section of silicone gel. The measured strains were used to calculate the stress distribution once the material properties of the gel had been established [BENNETT73].

The equilibrium of an infinite elastic layer indented by a rigid axisymmetric indenter has also been considered [HAYES72]. The elastic layer was assumed isotropic, homogeneous and rigidly restrained on its underside and deformation was assumed frictionless. Indentations using hemispherically-tipped indenters (figure 1.6) were considered and these were represented mathematically by a mixed boundary value problem which satisfied the equations of linear-elastic theory. The aspect ratio, d/h, of the material beneath the indenter was identified as an independent variable which described indentations. Increasing d/h was found to decrease the indentation for a given applied load. This is expected since a larger radius of curvature of indenter tip will produce a larger contact area, Πa^2 (figure 1.6). Maximum compressive stresses were calculated on the axis and these diminished asymptotically to zero outside the contact region. Shear stresses were zero on the axis and reached a maximum near the circumference of the contact region before diminishing to zero outside.

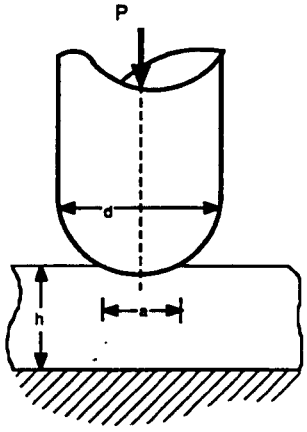

Figure 1.6 - Indentation of an elastic layer by a round-tipped indenter.

Finite element (FE) models have been created of similar indentations by round-ended indenters of various curvature [BRUNSKI80]. Models were produced of indentations into a layer of skin 2 mm thick, having a Young's modulus of 2.76 MPa, which covered an 18 mm thick layer of fat and muscle with a modulus of 0.162 MPa. Both materials were assigned a Poisson ratio of 0.49. Indentations were made up to 10% of the total thickness of the tissue layers. Vertical stresses calculated at the surface were concentrated on the axis when the indenter tip was hemispherical. Where the tip radius of curvature was larger, and the end was therefore flatter, peak stresses were nearer the circumference of the contact region. Maximum Von Mises stresses were found to be higher with the more pointed indenter and high stress regions were located near the contact radius in the skin and on the axis just below the skin. With the flatter indenter, high Von Mises stresses were located near the rigid base in the softer layer.

In a thesis, Schock presents results of indenter tests on an excised section of skin, subcutaneous fatty tissue and muscle of a Yorkshire pig [SCHOCK81]. Pig skin has been used in a number of biological studies due to the similarities between its structure and that of human skin [WINTER76]. Values of compressive modulus were obtained using measurements of engineering strains beneath the indenter of up to 50% and stresses predicted by a finite difference (FD) model. Lower moduli had previously been obtained from uniaxial compression tests on *in vitro* specimens of the tissues. In the latter tests, differences in the stress-strain states at two levels of load were used to calculate a 'tangent modulus'. Engineering strains were of the order of 40-60%. No

other publications on *in vitro* uniaxial compression tests have been found. Results of Schock's tests are summarised in figure 1.7.

Tissue:	Indentation test	Compression test
Skin	420	80
Adipose tissue	150	50
Muscle	340	120

Figure 1.7 - Estimated compressive modulus of excised pig tissues.
(after Schock, 1981. Values are in kPa)

The stress contours produced by the FD model were generally similar to those predicted by Brunski's FE model with round-ended indenters. A model of a flat-ended indenter identified highly concentrated compressive and shear stresses around the edge.

In a second series of indentation tests, a grid was marked on the *in vitro* specimens. Measurements of grid displacements were used to calculate the distribution of compressive strain beneath indenters. Differences between distributions from flat and round-ended indenters were similar to those shown in the compressive stress distributions predicted by the FD models.

The literature reviewed has shown mostly observations of stress distributions and only Schock has offered a stress-strain relationship for soft animal tissues in compression. A great deal of research has been performed to find stress-strain relationships for various soft tissues in tension and, to a lesser extent, torsion. These studies have mostly taken measurements from *in vitro* specimens of separate tissues which have been assumed homogeneous. Skin has received most attention. The methods of analysis and assumptions used are of more interest to the current project than the actual expressions derived to describe behaviour.

Human skin in uniaxial tension has been shown by many investigators to be capable of sustaining large strains and to have a nonlinear load versus extension response. Some empirical studies have yielded mathematical stress-strain relationships [KENEDI64, RIDGE64, FUNG67]. The nonlinearity of load versus extension, with an initial lax phase which stiffens to a near linear response, has been attributed largely to the straightening and reorientation of collagen fibres [KENEDI65].

Finite strain theory is appropriate for the analysis of large deformations and has been used by some investigators. In general terms, these studies assume tissue behaviour to approximate that of a continuum and aim to find expressions for the strain energy per unit volume in specimens as a function of the priniciple extension ratios. A full development of the theory used appears in [GREEN60] and more concisely in [SAUNDERS64]. An exponential form of strain energy function has been used to describe large uniaxial extensions of cat skin [VERONDA70]. Both compressible and incompressible behaviour were assumed and results using the former assumption were superior. Other exponential forms have been produced for soft tissues in uniaxial tension assuming isotropic, incompressible [GOU70, DEMIRAY72] and orthotropic [TONG76] behaviour. Muscle fibre in torsion has also been studied assuming isotropic, incompressible behaviour [SNYDER72].

Some studies have assumed the structure of individual fibres to have a particular configuration and mechanical analysis of the simple structure proposed has yielded an expression of the load-extension relationship for each fibre. This expression is then extended to give a stress-strain equation for a fibrous network. Parameters, which are dependent upon the material properties and geometry of each fibre, are evaluated by fitting the derived equation to experimental data. This technique has been used for skin with a model based upon the stretching of collagen fibres [RIDGE64] and, more recently, for a number of different collagenous tissues [DECRAEMER80a, MANSCHOT86].

Attempts to define the behaviour of soft tissues more fully have incorporated time as an independent variable. The viscoelastic behaviour of human skin is demonstrated by the existence of hysteresis, stress relaxation and creep phenomena [BARBENEL78]. Studies have mainly used stress relaxation and oscillating strain tests in one or two dimensions and have attempted to produce a phenomenological mathematical description of viscoelastic behaviour. The general theory used is described in [LOCKETT72]. Logarithmic relationships between applied stress and time have been formulated to describe stress relaxation tests on skin [BARBENEL73] and mesentery [FUNG72]. Parameters within these relationship, however, vary with the level of applied strain. Linear functionals which relate stress to strain *history* have been expanded into infinite series of integrals to represent nonlinear behaviour [GREEN57]. This form of relationship has been fitted to data from human skin [DALY66], aorta [SHARMA76], collagen fibres [HAUT72], ligamentum nuchae [JENKINS74] and tympanic membrane [DECRAEMER80b].

In vivo assessment of the compressibility of separate tissues is difficult since deformations in three dimensions must be measured. Measurements made *in vivo* should not overlook the fact that specimens generally are not isolated structures and that there may be an exchange of blood or interstitial fluids with the surrounding tissues. *In vitro* testing is also difficult since fluid loss is likely. Many analyses of separate tissues have assumed incompressible behaviour and it would appear that body tissues are practically incompressible. Hydrostatic pressures cause little or no deformation; the human body is capable of tolerating a pressure of 1655 kPa deep under water [CHOW78]. Deviatoric stresses are found to have far more effect; a uniaxial pressure of less than 6.7 kPa has been found to induce pathological changes [HUSAIN53].

It is generally accepted that skin is anisotropic [KENEDI65]. Observation of the fibres within the tissue structure have helped explain this directional dependence [FINLAY69]. Muscle fibres and collagen fibres within tendon are aligned specifically to give tissues with strength in a preferred direction. Nevertheless, isotropic behaviour is often used as a first approximation to analyse stresses and strains in soft tissues.

An interesting practical point raised in the literature is that in the first few cycles of loading of a fresh *in vitro* specimen of skin, the hysteresis effect progressively reduces to a stable state; a phenomenon termed preconditioning. Usually, only preconditioned specimens are considered mechanically stable for testing. Preconditioning has been explained as an irreversible reorientation of fibres which, *in vivo*, will not be removed until the subject is free to move and apply normal physiological stresses and strains [STARK71].

Finite strain and viscoelastic analyses have been used to produce relationships which describe the behaviour of a number of soft tissues under well-controlled conditions of tension and torsion. No general relationships exist to describe a triaxial stress state. Were such relationship to exist, assumptions regarding the mechanical interaction between tissues would still be required to model *in vivo* loads.

1.4.3 Existing models of tissue deformations.

As well as the indenter model mentioned, a few other problems relating to body support have been tackled using the FE method .

A FE program was written to model a buttock of a sitting person [CHOW78]. Solutions were obtained using a 33 element axisymmetric mesh, applying loads incrementally to produce a nonlinear solution. A value of 15 kPa was used for the Young's modulus of a homogeneous buttock tissue layer which covered a rigid bone. The Poisson ratio was 0.49. The importance of Von Mises stresses was emphasised since these indicate the degree of deformation in an incompressible material. A number of loading mechanisms were proposed and it was found that peak Von Mises stresses were smallest when the applied pressure distribution was most uniform and applied shear forces were minimised. A model of the buttock supported by a flat, frictionless interface calculated maximum Von Mises stresses to be on the axis next to the rigid bone and the authors commented that this corresponds with clinical findings since pressure sores frequently are initiated beneath the skin. The load versus deflection response of the bone in this model was compared with a response measured on a physical model which used a wooden bone and a tissue layer made of a gel. Rough agreement was obtained for small deflections; however, a greater stiffening in the physical model caused the two plots to diverge.

The plantar tissues of the foot have been modelled using a FE analysis [NAKAMURA81] and a FE model has aided the design of skin flaps in surgery [LARRABEE86]. Other analyses of stiffer biomechanical structures, mainly bones and prosthetic implants, have applied FE theory. A review of some of these appears in [HUISKES82].

The only FD study of tissue deformations found in the literature is the axisymmetric indenter model of Schock.

1.4.4 Strategy for a limb model.

The residual limb is made up of a number of different tissues and is clearly inhomogeneous. The individual tissues themselves are not made of homogeneous materials and are mostly anisotropic. The mechanism of recoverable tissue deformation

may vary as increasing loads are applied. Deformations are time-dependent. In compression, time-dependence may be due to a proportion of intercellular fluids which are free to disperse.

A great deal of research will be needed to obtain precise results from a mathematical model of a loaded limb. In the current project, assumptions are made about tissue behaviour so that a 'first generation' model may be produced. In formulating this model, the main objective is to build a qualitative impression of the parameters which have the greatest influence upon interface loads. Areas can thereby be identified for future investigation so that improved results may be obtained. Another objective is to furnish a means by which mechanical measurements of limb tissues may be taken in a normalised form. In the near future these measurements may be used by an improved CASD system to base socket designs upon a fuller description of the residual limb.

Due to the complex geometry and mechanical properties presented, techniques which may be used to model interface loads are scarce. The FE and FD methods, however, appear to be possible candidates. These are numerical techniques by which solutions to complex differential equations may be obtained using computers. Each has its pros and cons.

The FE method is capable of defining complex geometry in the form of a mesh of elements. Complex boundary conditions also may be modelled. A large number of commercially available FE packages exist which have the flexibility to define and analyse a wide range of problems. The main drawback is that the technique is best suited to linear analyses. In the FD method, a grid is used to represent the domain of the problem. Boundary conditions may be defined which apply all along the boundary rather than at discrete nodes and solutions to nonlinear problems may be more accurate than by FE methods. Time-dependent problems are well suited to solution using FD analysis; however, solutions to equilibrium problems are generally computationally less efficient than by the FE method. Another drawback is that definition of boundary conditions, especially for boundaries with irregular geometry, is complex. No general purpose FD packages exist.

In the current project, the FE method is favoured for 3 main reasons. Models may be generated and amended for different geometry, loads or boundary conditions with relative ease using bought-in software. Secondly, realistic geometry and boundary conditions may be used in the analyses. Lastly, since no exact mechanical properties

are known for soft limb tissues, assumptions about stress-strain relationships must be made. In a first generation model which assumes a linear constitutive law, a major benefit of FD analysis, therefore, will not be gained.

Precise values of predicted interface loads appear to be unlikely in a first generation model; however, it is hoped that FE models using idealised material behaviour but realistic geometry and boundary conditions will provide a foundation upon which improved models may be built. The assumptions that are made to idealise the material behaviour are that the soft tissues are locally homogeneous, i.e. that inhomogeneous effects 'even-out' at a given section through the soft tissue layer. Similarly, anisotropic effects shall be assumed negligible. It will also be assumed that the mechanism of tissue deformation is unchanged at all strains and a linear constitutive law is obeyed. By collecting mechanical data using controlled strain rate and by modelling static loads only, time-dependence shall be assumed to have uniform effect all over the limb. The assumption of linear and purely elastic behaviour of soft tissues may at first appear gross; however, it has been proposed that the nonlinearity and time-dependence under the action of uniaxial stresses is due mainly to a limited dispersion of fluids. In a total contact socket, it is an objective to apply pressure all over the limb surface and avoid the large gradients of pressure which may cause significant fluid dispersion.

1.5 Concurrent developments

A number of relevant studies have been reported since starting the current project.

In the area of shape design, above-knee socket and shoe insole shapes have been produced using a commercial CAD system [VANDERLIN86]. The UBC software development has continued and currently 9 reference shapes are available. This has extended the family of shapes that may be generated [SAUNDERS88].

Two FE studies of socket interface loads have also been reported. An FE package, ANSYS, has been used with the aim of 'predicting the loaded shape of an amputee's residual limb' [KROUSKOP87a]. This model is for the above-knee case and applies a standardised load distribution to the FE mesh which represents the soft limb tissues. The external geometry of the limb was sensed 'live' with the amputee subject standing while a force-sensitive probe was used to take radial measurements, lightly touching the limb at several points over its surface. Shape capture with this apparatus typically

takes 6 minutes. The idealised bone structure was located within the soft tissues using ultrasonic measurements and formed a rigid boundary for the FE mesh. Values of the mechanical properties of the soft tissue were obtained from measurements using an ultrasonic transducer which monitored motion within the limb tissues when subjected to vibration [KROUSKOP87b]. A linear viscoelastic analysis was used to calculate weighted average values of elastic modulus from scans through the tissue layer. Tissue density and the amplitude and frequency of the cyclic displacements of the limb tissue were variables in the analysis. The Poisson ratio and the five values of modulus used in the FE models are not given; however, in describing the ultrasonic system values of 6.2, 35.8 and 108.9 kPa are quoted at a site in which the states of muscle tension are given as 'relaxed', 'mild' and 'maximum' respectively. The applied load distribution was produced from pressure measurements in a number of sockets using a pneumatic transducer array.

The displaced mesh from this analysis was assumed to describe a comfortable socket shape and nodal coordinates were used to create a data file which was input to a numerically controlled router for subsequent manufacture of the socket shape. To date the manufacture of two sockets by this method has been reported by the group.

A FE model of a below-knee limb has also been described [CHILDRESS87]. Limb geometry was obtained from multiple computed tomography (CT) scans which were digitised on a tablet. Measurements of load versus deflection response were taken from a probe which indented the limb tissues through ports in the wall of an experimental socket. Corresponding responses were predicted by a linear finite element model of the limb which represented the soft tissues as a homogeneous layer. The soft tissue modulus used in this original FE model was adjusted according to comparisons between the measured and predicted responses and a value of 60 kPa consequently was assigned to all tissue elements in the final model.

Pressures at seven sites, predicted by the analysis, were compared with measurements on the experimental socket. A piezo-resistive diaphragm pressure transducer was used. Models of two subjects were created and predicted pressures were in the ranges 0 to 90 kPa and 0 to 300 kPa. The respective ranges of measured pressures were 0 to 110 kPa and 0 to 60 kPa. The latter of the two subjects was not distal weight bearing. Pressure at the patellar bar for this subject was predicted to be 300 kPa; the measured value was 80 kPa. This discrepancy was attributed to the inability of the transducer to measure local pressure concentrations and better correlation was found elsewhere; predicted and measured pressures in the popliteal area were 60 and 80 kPa respectively.

1.6 Scope of the present study.

In this chapter, design philosophy and fabrication methods for below-knee socket production have been introduced. In **Chapter 2**, the system developed at UCL to automate these processes is described.

As part of a CAE study of limb/socket interface loading which aims to improve the fundamental understanding of socket loading, estimates of the mechanical properties of soft limb tissues were required. FE models are presented in **Chapter 3** to provide theoretical data of the load versus deflection response of indenters pressed into an elastic layer. In **Chapter 4**, experimental results are presented from indentation tests on an engineering material whose mechanical properties were readily evaluated. A study presented in **Chapter 5** estimates values of a tissue modulus by comparing measured responses, from indentations into residual limb tissues, with responses predicted by the FE models. An idealisation of tissue behaviour is used to permit this comparison and an assessment is made of the consequences of the assumptions used. Measurement of the geometry of the limb tissues is also discussed.

Models of a residual limb were then used to predict the distribution of loads at the interface. In initial models discussed in **Chapter 6**, limb geometry and mechanical properties are idealised to study interface loads using a number of assumed geometric configurations and interface conditions. Measurements of interface pressure on a physical models are presented in **Chapter 7** for comparison with the pressures predicted by these FE analyses. The culmination of the CAE study is a series of FE limb models based upon the measured geometric and mechanical data and these are presented in **Chapter 8**.

In **Chapter 9**, the main findings of the current project are summarised and suggestions are made for future models.

Chapter 2

The UCL Computer Aided Socket Design System.

2.0 Introduction.

Following attempts to improve consistency and productivity in the manufacture of prosthetic sockets the Bioengineering Centre developed its own CAD system for custom-designing below-knee prosthetic sockets. The author was involved with this project from the outset and was solely responsible for the measurement, rectification and system management software and contributed to the overall system design as part of the small research team.

Essential stages of socket production.

In conventional socket production, the casting stage provides a map of anatomical features a measure of limb geometry and an indication of tissue 'deformability' while incorporating some distortions to the limb shape. During rectification, the prosthetist uses the map, together with his subjective judgement of the compliant properties of the limb tissues, to decide what changes to make to the cast shape. Many socket fabrication processes are used which follow various guidelines to encourage conformity of surfaces and provide a stable shape and a durable socket.

For the purposes of a CAD/CAM system, these processes may be separated into data collection, modelling of shape data and automated socket manufacture. The data collected may include the internal and external geometry and mechanical properties of the limb tissues. Modelling may use one of several possible mathematical techniques to alter limb shape data to produce a suitable socket shape. Then, a number of possible automated processes may be used to manufacture sockets.

The CAD part of the system is the central concern of this chapter. For the CAM aspects, many commercially available computer-controlled machines are capable of producing a physical positive shape; more efficient socket manufacture may be possible with purpose-built machinery. The manufacturing system used at the Bioengineering Centre is briefly described.

2.1 Philosophy of the system.

The philosophy adopted for CASD at the outset largely dictates how the measurement and modelling processes must be performed. Two main schools of thought have emerged.

The first, as used by the UBC system, is based upon the principles that all limbs have broadly similar structure, are therefore accommodated by sockets of broadly similar shape and that the full 'family' of these shape may be produced by varying a limited number of geometric parameters on a 'reference' shape. An analogous approach had been used for the quadrilateral above-knee socket; another of Foort's designs which is widely used [FOORT63]. The 'quadrilateral' shaping is introduced at the brim of the socket and a range of re-usable brims now exist which are selected according to anteroposterior and mediolateral measurements below the hip joint and are adjusted for a close final fit. A similar philosophy is used by fashion shoe manufacturers where lasts of each shoe size contain dimensions of a reference last in fixed proportions.

An alternative CASD philosophy is to accept conventional practices and automate the measurement and rectification processes. In this case, measurement of the full limb surface is necessary. Any tissue loading at the time of measurement, however, will change the limb shape and measurements should be under controlled loads or with tissues unloaded. Objective measurements of tissue compliance may also be used. Rectifications must be correctly positioned according to each amputee's anatomy or, if legitimate, in standardised locations relative to a number of reference points. It is unclear how prosthetists take account of the individual characteristics of limbs when rectifying limb models. If these changes are quantified, however, it may be possible to correlate their shape and size with measurements of anatomy and mechanical tissue properties.

The latter philosophy was favoured by the Bioengineering Centre since early versions of the UBC software were not flexible enough to produce sockets for a wide range of limb types without a large amount of interactive modification and further scaling parameters were desired to extend the 'family' of available socket shapes. Mimicking conventional techniques was considered more likely to produce a successful fit since the underlying anatomical shape is present in each socket; the rectifications are relatively small distortions to this shape. This was also thought to be a more flexible, stepwise approach for gaining a better understanding of socket design.

The measurement of tissue properties has been mentioned above; however, the development of systems to evaluate these data was considered to be a long term objective and, for the interim, it was decided to base CASD upon shape data alone. Research to evaluate tissue properties is presented in Chapters 3 to 5.

Since shape data alone was to be used for CASD, other philosophical considerations were in the areas of shape representation and adjustment. Prosthetic shapes may be represented by a large number of discrete surface coordinates which locate nodes at the corners of facets to make up a 'surface mesh'. Alternatively a continuous, mathematically defined function may be used to approximate a surface within a given tolerance. Storage of coefficients of mathematical functions rather than a large number of coordinates is more efficient. and surface continuity can be guaranteed on mathematical surfaces. Smoothness of a mesh must be checked, point-by-point, by visualising the surface or using a mathematical checking algorithm. Mathematical modelling techniques including bi-beta , Bezier or B-spline surfaces may be applicable in prosthetics.

In general, adjustments made to mathematical models are more elegant than surface meshes. Adjustments to mathematical surfaces may be affected by altering a small number of surface parameters whereas distortions to a mesh must be made with point-by-point relocation. While the use of mathematical modelling is seen as an eventual objective for shape representation and adjustment, it was decided to concentrate initial efforts on the development of measurement and rectification software using simple mathematical algorithms working with the 'surface mesh' approach.

2.2 Capture and storage of shape data.

Since the philosophy adopted for the UCL CASD system was to base socket designs on the measured external shape of the limb, a system was needed which was capable of capturing this shape data with sufficient accuracy in an acceptable time period and storing it in an accessible format.

Prosthetic shapes have cylindrical topography and it is convenient to take measurements with shapes rotated about their long axis. A regular surface mesh of polar coordinates may be built up if measurements are taken at fixed intervals of both

angular and axial displacement. In the UCL CASD system, each surface mesh is represented by a regular grid of radial measurements which are stored in data files. Figure 2.1 shows a measurement grid and introduces the terms 'slice' and 'strip' which respectively denote sets of points that have the same axial or angular coordinate.

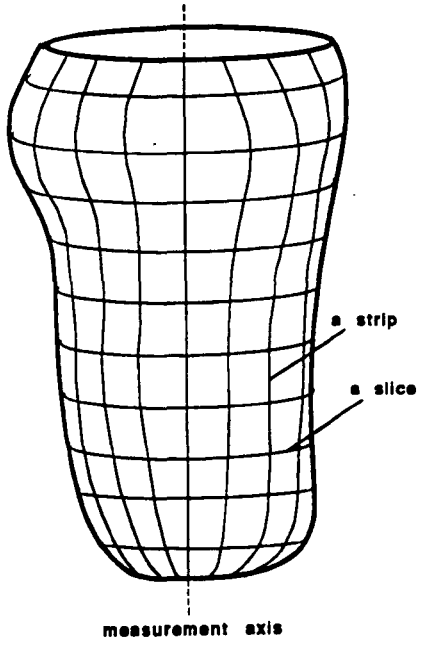

Figure 2.1 The measurement grid

In each data file, radial values only are stored and these are arranged in sets which each define a slice. The slices of data are ordered along an axis whose positive direction runs from the distal to proximal end. The points in each slice are ordered according to a left-handed screw rule.

The number of discrete measurements needed to define a surface to a given accuracy depends largely upon the shape of the surface. The spacing of these data determines the size of data sets and the accuracy with which surfaces are described. Large sets of data may require long periods to process and storage limitations may be reached rapidly. Carving with an angular interval of 5° and axial pitch of 1/4" was satisfactory for early carving of Vancouver sockets. In trials using an angular interval of 10°, the resultant loss of definition of shape was considered tolerable. This density of measurement yields data sets of typically 1500 radial values which are stored in ASCII data files approximately 10 kBytes in size.

Since no acceptable measurement apparatus was available at the time, one was developed at the Bioengineering Centre. Deformations due to the measurement device are to be avoided and non-contacting techniques such as Moire fringe measurement, grid projection, line triangulation, silhouetting, sonar, microwave, X-ray or magnetic resonance imaging methods are preferable. No 'off-the-shelf' apparatus which employed these methods was available at the time however. Contacting methods including probing under controlled contact load, automated measurement of positive casts and automated measurement of wrap casts were considered as alternatives. A device for measuring plaster casts and wraps was chosen since the technology for this was simplest and the expected lead time shortest.

The pilot 'digitising' system used a potentiometric measuring device and an existing lathe in which to position prosthetic shapes. This is illustrated in figure 2.2.

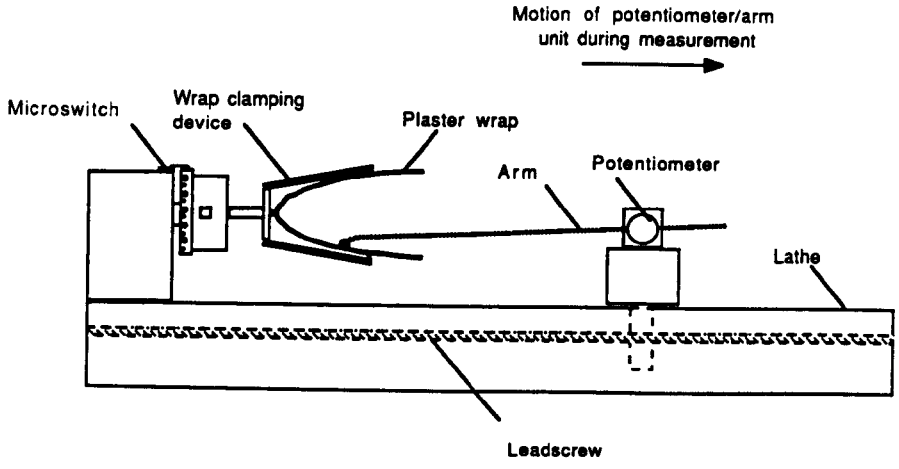

Figure 2.2 - Layout of the pilot measurement system.

Radial measurements of the shapes are sensed from the position of the tip of an arm mounted on the shaft of a rotary potentiometer. The output voltage from this potentiometer is directly proportional to the angular position of the shaft. Neglecting the small error involved over the range of movement of the arm, it is assumed that the vertical displacement of the tip of the arm also produces a proportional voltage. Using an analogue to digital converter (A to D) card, voltages representing radial measurements are logged by a PDP-11 computer. To improve accuracy limited backlash gears are used to amplify the motion of the arm.

Measurements of plaster shapes are taken along a helical path, which is followed by a wheel at the tip of the arm, as the shape is rotated and fed along the lathe bed. To fix the angular interval at which measurements are taken, a circular acetal plate is attached to the chuck. Around the edge of this plate 36 rivets protrude which are used to operate a microswitch mounted above them. As each rivet passes this switch, therefore, a pulse is applied to another channel of the A to D board indicating that a measurement is to be taken. Under the control of a FORTRAN measurement program, this pulse triggers the sampling of the A to D channel connected to the arm potentiometer.

Prior to measurement, the arm is calibrated by digitising the output voltage of the potentiometer at two known radii. From these two points a linear relationship is established within the computer program and this is used to convert the digitised voltages into radial measurements. A further transformation uses linear interpolation between successive revolutions of the helix to create sets of radii lying at fixed intervals of axial displacement, i.e. slices. Linear interpolation has proven adequate for all unrectified shapes where no steep contours generally exist. For rectified shapes measurements are collected 'slice by slice'. The measurement program finally calculates the volume of the shape. This has proven useful in monitoring the development of residual limbs and is especially of benefit in the period immediately following amputation, where limb volumes are not stable.

A point of reference on the measured shapes is needed so that corresponding points on the surface of the plaster and in the measured data may be located. A mid-patellar tendon reference point was arbitrarily chosen and this is identified by marking in all plaster wraps a point midway between the tibial tubercle and the distal edge of the patella. The position of the reference point along the length of plaster shapes is established by a rule on the lathe and is entered into the measurement program for inclusion in a header in the measurement data file. Digitisation of plaster wraps commences at the distal end from a datum strip which passes through the reference point. Three inches proximal of the reference point measurement ends.

Since producing the pilot apparatus, a number of improvements have been incorporated. The current system uses optical incremental encoders to sense the rotation of both the chuck and the arm of a purpose-built device. The pulses output from these encoders are applied to a pair of decoder/counter chips which are addressed via a parallel interface by an IBM PS/2 microcomputer which runs a PASCAL measurement program. The number contained by the arm decoder/counter chip is analogous to the

output voltage of the potentiometer of the pilot system. By monitoring the progress of the chuck the measurement program again controls the position at which radial measurements are collected.

Other recent developments which can provide limb shape data include an optical system also developed at the Bioengineering Centre [SMITH86]. This uses digital processing of silhouettes to create radial data. In another system a laser line is projected onto the limb surface [FERNIE85]. The contour shown by this line is observed by a number of offset cameras and its location in space is calculated by a computer program.

2.3 Shape visualisation.

Large sets of numerical data that can be stored and manipulated by computers are interpreted by humans with great difficulty. To enable rapid visualisation and checking of the prosthetic shape data graphical output was required. Plots of cross-sections or wire-frame models may be misinterpreted. Grey-scale shaded images are more easily recognised. Displays which rotate shapes in real time can enhance perception; however this generally will require expensive computer hardware and was thought unsuitable for the system.

Using a library of graphical routines, written by Dr A.M. Wray of the Department of Mechanical Engineering, UCL, a program was written to create three dimensional 'solid' graphical views . Figure 2.6 (a) shows a pair of views of a socket designed by the UCL CASD system. The viewing program sets the positions of a viewing point and a point light source and each image is built up facet-by-facet. The brightness of the grey shade used to fill each facet is determined from the dot product of the vector normal to the facet with the vector pointing from the light source to the centre of the facet.

2.4 Shape rectification.

To rectify measured shapes and produce a suitable socket shape, a set of algorithms were required which may be used to imitate the shape transformation effected by a prosthetist when he sculpts a plaster positive. These changes in shape may be quantified by taking measurements of unrectified and rectified shapes, thereby defining a radial change at each point on the measurement grid. This grid of changes is termed a rectification grid.

Average Rectification Grid

To write a computer program capable of making typical rectification changes to a measured shape an 'average' rectification grid was needed. The development of this average grid is fully documented elsewhere [DEWAR85]. Briefly, however, an average rectification map was produced from photographs of a number of plaster positives, produced by conventional means, upon which rectification areas were marked. In this way, the locations of rectification regions were standardised. The average map was divided into proximal and distal portions (figure 2.3) since it was based upon measurements from limbs of various length.

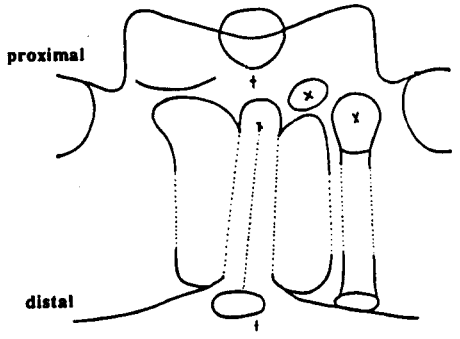

Figure 2.3 The average rectification map.

To establish an average rectification grid, the average map was projected onto a number of measured plaster positives. Within the boundaries of the average map, a prosthetist made his usual changes. The rectified shapes were remeasured and, by subtracting from each radial value the corresponding measurements on the unrectified shapes, a number of rectification grids were obtained. In order to average grids of

different length, a program was written which 'stretched' each grid to the longest length encountered. The stretching algorithm created extra slices of data in the region along the tibial shaft, where the boundaries in the average rectification map are approximately parallel and stretching causes negligible distortion (figure 2.3). The extra data were produced using linear interpolation between points on adjacent slices at suitable locations along the 'stretchable' region. Data in all of the stretched rectification grids were averaged to create a unique average rectification grid for the prosthetist.

Rectification Program

The average rectification grid, in the form of an ASCII data file, is stored on the hard disk of a computer and is read by the PASCAL rectification program each time a socket is designed. Slices of rectification data are located relative to the measurement data about the mid-patellar tendon reference point. To facilitate the numerical rectification process the average rectification grid was rearranged into distinct regions. This is shown in figure 2.4 where the radial changes are plotted relative to a datum on each slice. The rectification data are ordered with the most proximal slice at the top and with the reference strip marked 0°. Data for the lateral side appear on the right.

Working down the limb with figure 2.4, region 'D' applies rectifications to the proximal portion. The number of slices in region 'C' is changed according to the length of limb and partly overlays the changes made by region 'D'. Region 'B' adds rectification distally and 2 slices of measurement data at the distal end, not shown in figure 2.4, are left unchanged (region 'A').

In conventional rectification, the distal end is built up by about 3/8". The algorithm found most successful to reproduce this creates 2 extra slices of raw measurement data again using linear interpolation. These slices are added between 1 and 2 inches from the distal end where residual limbs are generally approximately cylindrical and this 'stretching' causes little distortion.

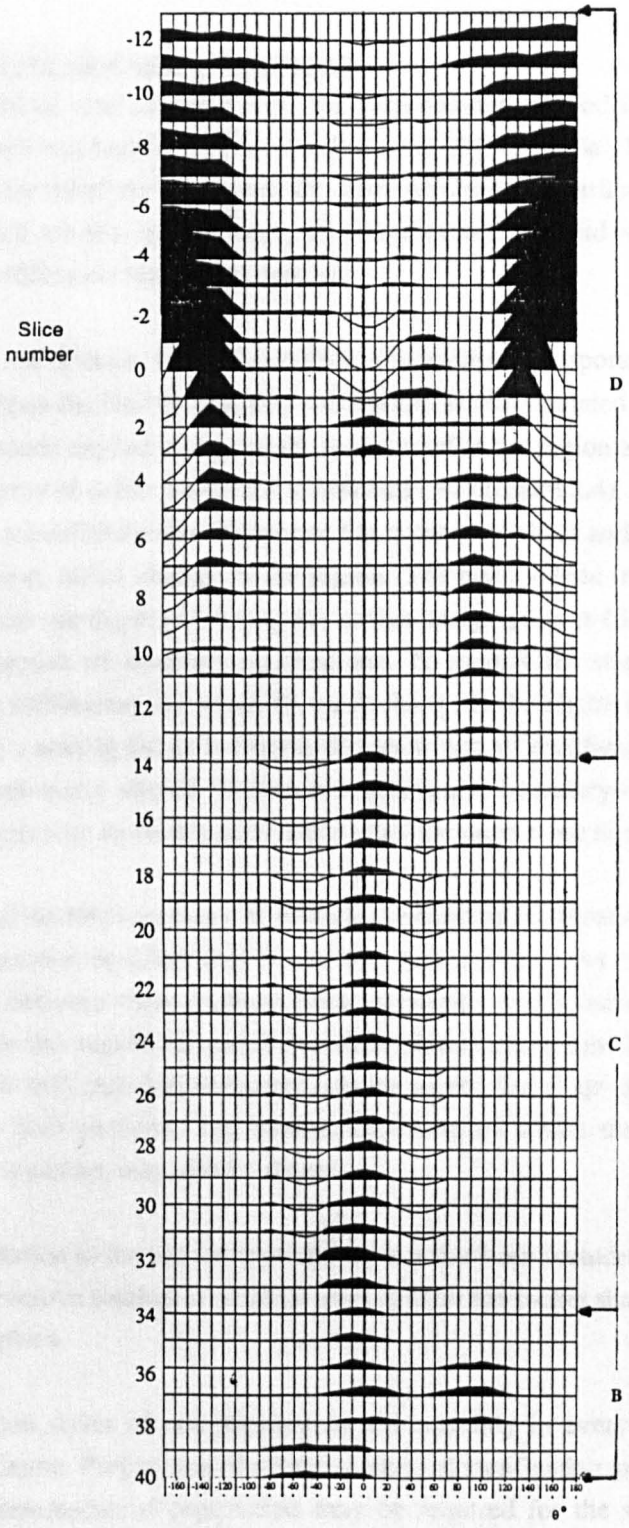

Figure 2.4 - The average rectification grid.

Modifications to the standard rectification grid

During the initial trial of programs, the requirement to modify the standard rectification pattern was found desirable in a few cases [DEWAR86a]. In most of these cases, merely 'extra relief' or 'extra pressure' were required at a particular anatomical feature. In a small number of instances, the rectification map did not fit well and relocation of a rectification 'patch' was needed.

To cater for the former type of problem, the author incorporated within the rectification program the facility to scale rectifications within bounded regions. In this process, rectifications applied, for example, to the patellar bar region are defined by a rectangular sub-array of points within the rectification grid (figure 2.4). The boundaries of this sub-array are defined within a separate file in terms of slices and strips, as is the location of the peak radial change in the region. The peak values in each of the 9 'modifiable' regions are displayed during the socket design process (figure 2.6 (f)) to express the magnitude of standard rectifications. To modify the standard, the user enters a value, in millimetres, by which the peak change in the region is to be altered. Using this value, a scaling factor is determined by which all rectification data in the region are proportionally altered. Within the rectangular boundary of each region, scaling is performed only on rectification data having the same sense as the peak value.

Three additional modifications may be made to the standard rectification. Every radial dimension in proximal or distal portions of the socket shape may be modified. A transition region between these portions exists between 1 and 2 inches distal of the reference point. In this region, the radial modification reduces to zero linearly and the radial modification may therefore be tapered into the unmodified shape or modifications may be made to both portions. The number of slices, by which the length of the measured data is stretched, may also be altered.

Recently, a solution to the second type of problem has been included, whereby the user may add or remove patches of material anywhere on the socket shape with the aid of interactive graphics.

The rectification styles of two prosthetists are currently in everyday use at the Bioengineering Centre. Preparation of a large number of rectification grids to cater for the individual preferences of prosthetists may be required for the system to gain widespread acceptance in the profession.

The rectification programs were originally developed on a Digital PDP-11/73 minicomputer and have since been transferred to run on an IBM PS/2 microcomputer.

2.5 Shape carving and socket production.

The facility to carve prosthetic shapes was available at the start of the project using the MASTERFORM CNC machine [LAWRENCE85], which was purpose built at the Bioengineering Centre. This had produced acceptable positive casts designed by the Vancouver CASD software. In this machine, 3 degrees of freedom are controlled by stepper motors in order to carve the prosthetic models from plaster blanks which have the shape of a frustrum of a cone. A helical tool path is used. Two of the degrees of freedom position the cutting tool longitudinally and radially, the other is the rotation of the blank about its axis of symmetry. The PASCAL carver program transforms slices of shape data into tool displacements and these data are sent, via an RS-232 serial line, to the carver's own microcomputer which is interfaced to the stepper motor control board.

Although radial data is measured using a 1/4" axial pitch, an improved surface finish on carved positives has been achieved by interpolating between slices of data to create carving files of 1/8" and 1/16" axial pitch.

New carving machines [CRAWFORD85,CRAWFORD86] and cast materials [JARMAN85,JARMAN86a] have since been developed. Research has also been undertaken to carve the internal socket surface directly [DEWAR86b].

To produce a socket, a carved plaster model is covered with a Pelite liner and is used as a former in a RAPIDFORM machine [DAVIES85]. In this process, a polypropylene 'preform' is heated in an oven at a controlled temperature for a controlled time after which it is automatically drawn over the plaster cast and pulled in to the correct shape under vacuum.

2.6 Shape alignment

So far no mention has been made of the alignment of prosthetic shapes in the CASD system yet the numerical rectification process will only work correctly with data presented about consistent axes which coincide with those used to define the rectification grid. Rectifications are improperly located and socket shapes distorted if radial changes are made to coordinate data about different axes.

In conventional socket manufacture, axes are fixed on prosthetic shapes to provide an initial 'bench' alignment which sets the position and orientation of the coupling to which other limb components are attached and therefore the alignment between the residual and artificial limb. The bench alignment is commonly set in 2 stages where a 'neutral' axis is first defined. This is frequently set by eye relative to plumblines which bisect the views of the shape in both the sagittal and frontal planes. To produce the bench alignment from this neutral position, the shape is tilted by a few degrees in both of these planes.

While the use of an inclined 'bench' axis is an essential part of prosthetic practice, it is undesirable for the purposes of the CASD system because an eccentric axis may require bulky carving blanks and result in large out of balance forces during carving. In preference, the neutral axis is chosen and this was fixed on all shapes when defining average rectification maps and grids using the conventional procedure. When wraps are presented for subsequent socket design, however, it is inconvenient to have to set the neutral axis manually and a software solution was used.

This solution takes the form of a number of PASCAL procedures in the early part of the socket design program which, prior to rectification and carving, reorientate data which are measured about a roughly central axis. Figures 2.5 (a) to (f) show, step-by-step, how the realignment to a consistent neutral axis is accomplished.

Figure 2.5 (a) is an orthographic view in the sagittal plane of a plaster wrap which is positioned relative to a vertical neutral axis. The axis of measurement in this view, however, is inclined to the vertical and therefore neither are measured slices horizontal nor measured strips vertical. The mid patellar tendon reference point lies on the bold outline which represents the silhouette of the wrap. The origin of the left-handed cylindrical polar axes lies on the most distal slice measured.

The radial data are first transformed into coordinates about a right-handed Cartesian set of axes, as shown in figure 2.5 (b). The positions of the centres of area of the reference slice and the slice 1.5 inches from the distal end are found. These centres will not coincide exactly with the centres of horizontal reference and distal slices; however, error in their positions are small if the measurement axis is roughly central.

The origin of the Cartesian axes is next shifted to the centre of area of the reference slice (figure 2.5 (c)). The distances, in the y- and x-directions, between the centres of area and the shifted z-axis are used to calculate angles ψ and ϕ respectively and, by rotating the Cartesian axes through ψ about the x-axis and then through ϕ about the y-axis, the z-axis becomes coincident with the neutral axis (figure 2.5 (d)). In this view, however, the slices of discrete data are not horizontal nor do the strips lie in vertical planes.

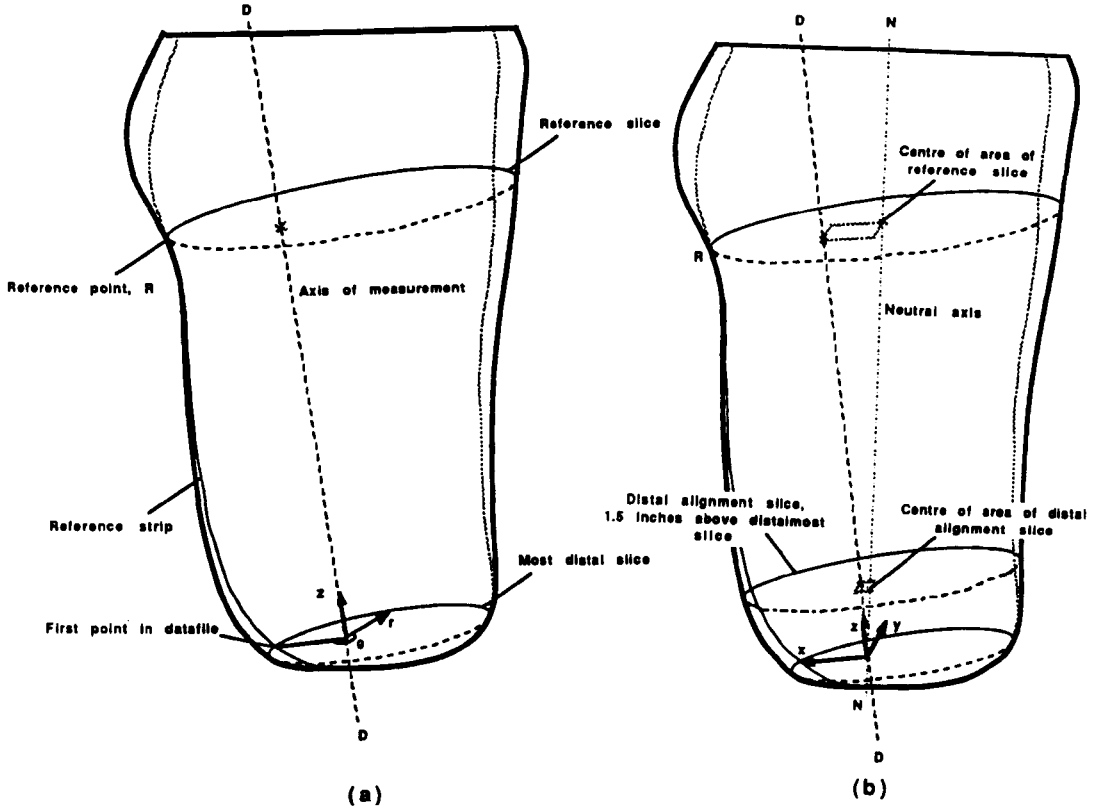

Figure 2.5 - Axes used during software alignment of measured shapes.

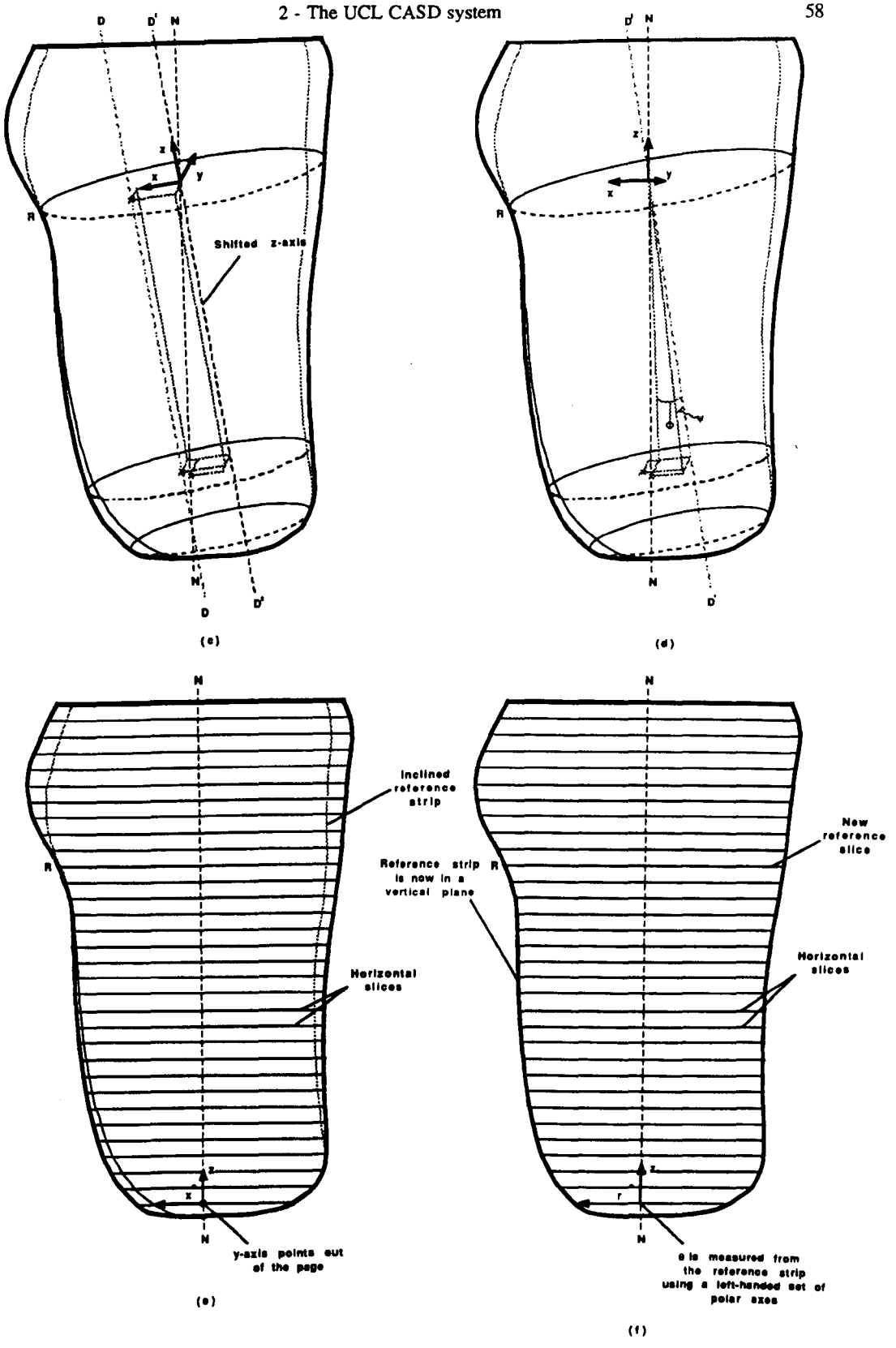

Figure 2.5 (continued) - Axes used during software alignment of prosthetic shapes.

New data in horizontal slices are found using linear interpolation between Cartesian points on each inclined strip. The strips in this view, however, still do not lie in vertical planes (figure 2.5 (e)). The Cartesian data, therefore, are transformed into cylindrical polar data and further linear interpolation is used between points on the horizontal slices to find data at regular angular intervals from a new reference strip and thereby produce strips in vertical planes (figure 2.5 (f)).

The linear interpolation used on the convex prosthetic shapes tends to reduce radial values and thus overall volumes. This error is not considered significant, however, and reduces volumes typically by only 0.75%. Early trials showed the location and form of rectifications applied using this axis to be acceptable and these alignment procedures remain in the current software. In the future, more sophisticated interpolation algorithms are to be used to enable the realignment of complex shapes; however, these may become redundant if a 'mathematical surface' approach is adopted.

Since positive casts are carved on a neutral axis, a purpose designed jig was produced at the Bioengineering Centre to provide the tilts to the socket shape to give a suitable 'bench' alignment [JARMAN86b].

2.7 The system management program

In its early form, the CASD software existed as a series of separate programs in which keyboard commands directed the measurement, design and carving processes. Records of work were kept manually. For use outside a research environment, normally by end users with little computer literacy, there was a need for the system to be simpler to use and more self-managing than this.

Mouse-controlled menu selection successfully provides a 'friendly front-end' to a wide range of computer software and a system management program using this format was written which contains the original CASD software as subprograms. For any patient the CASD system may be used to create several sets of measurement and socket data. Details are needed of how and when measurements were taken together with information relating to the design of sockets, i.e. the measurement and rectification grid used and the modifications made. In addition, some information relating to personal

details of each patient is useful. It is convenient to have all of the above details 'to hand' so, for example, a prosthetist can, when designing a new socket, remind himself of the date when a measurement was last taken of the patient's residual limb. While using the system, therefore, a prosthetist may require access to data previously stored in files on a patient's own floppy disk and an easy means of reaching these data during any CASD process was desirable.

A card index type of system is a familiar method of keeping records and the system management program was written to emulate this on screen using the purpose-written graphics library. Four sets of cards are presented to the user which relate to PATIENT, SOCKET, MEASUREMENT or RECTIFICATION details and the mouse may be used to select the 'tab' of one of these to bring it into view (figure 2.6 (b) to (e)). Since modifications relate only to individual standard rectification grids, details of these are contained within the set of RECTIFICATION cards. The locations of the bounded modification regions, together with changes made to a standard grid, are displayed in schematic views on screen (figure 2.6 (f)).

While the 'tabs' of the file cards may be selected to view the patient's prosthetic and personal details, the measurement, viewing, design and carving processes are all controlled from a menu box which is situated in the bottom right-hand corner of the screen. It is hoped that the management program is sufficiently intuitive and time saving that prosthetists will be attracted to the use of CASD.

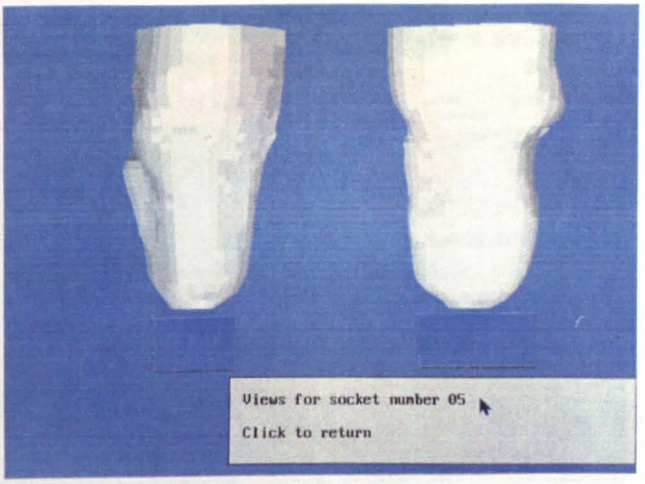

(a)

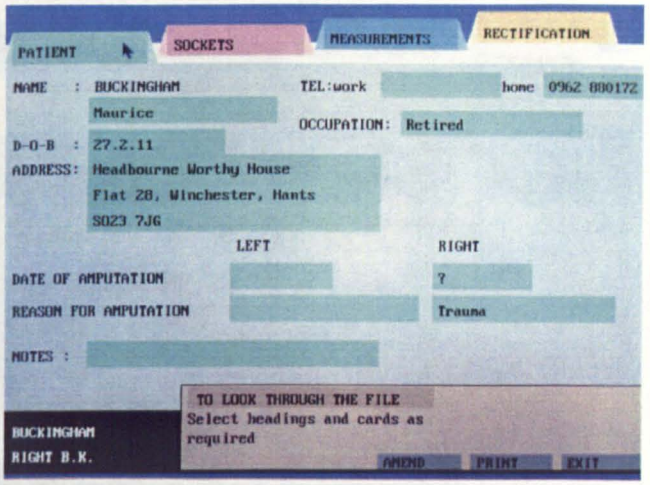

(b)

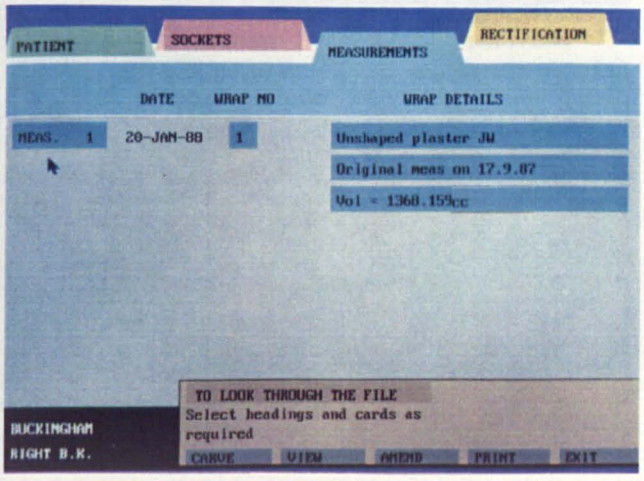

(c)

Figure 2.6 - Graphical displays of the UCL CASD program.

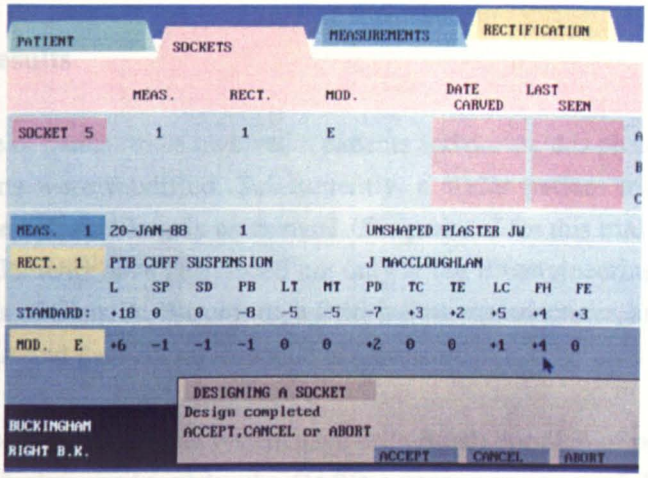

(d)

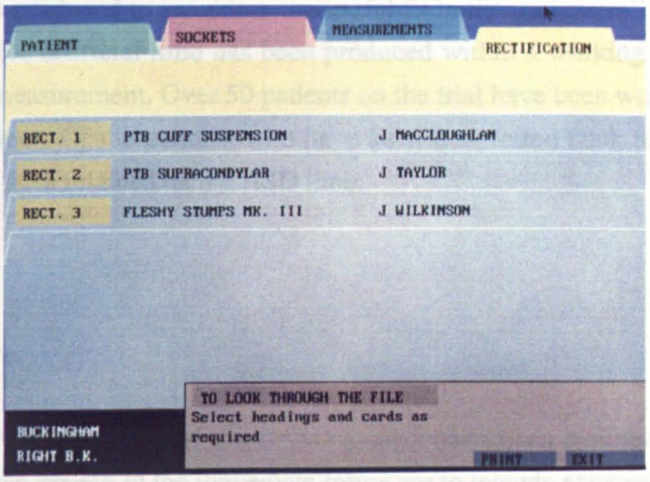

(e)

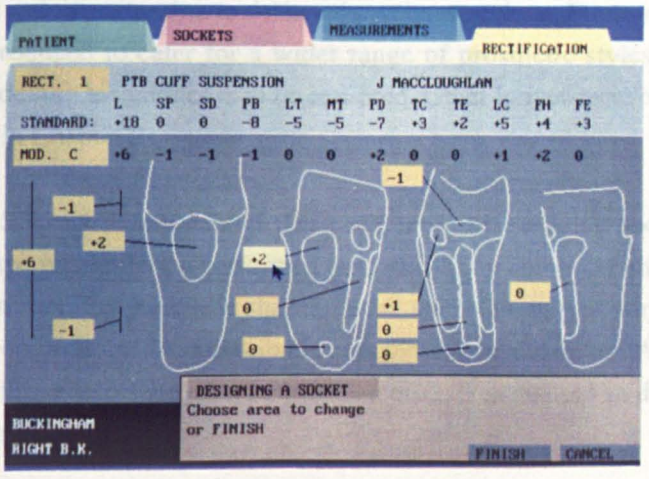

(f)

Figure 2.6 (continued) - Graphical displays of the UCL CASD program.

2.8 Clinical results

The initial phase of patient trials involved 8 patients and during this phase the CASD computer programs were modified. Subsequently, a wider patient trial has been undertaken with the software largely unchanged. The protocol for this trial is described in [DEWAR86c]. Patients have been fitted not only at the Bioengineering Centre but also at the premises of Chas. A. Blatchford, a British limb manufacturer, and at centres in Sweden, the USA and the Federal Republic of Germany.

To date, 92 limbs designed by the system have been fitted. For 48% of patients fitted at UCL, the first design produced by the CASD system was successful. The mean number of sockets produced to provide a successful fit in the trial overall is 1.7. In 18 cases, a comfortable artificial limb has been produced within a working day starting from a new limb measurement. Over 50 patients on the trial have been wearing CASD limbs for over a year. Of the patients who have been transferred back to the normal limb service, 81% have retained their CASD limb.

2.9 The future.

Many of the future objectives of the CASD project have been mentioned already. Developments to the system in the immediate future are to include enhancements of its graphical aspects and the extension to design above knee sockets. Further rectification grids are to be produced to cater for a wider range of prosthetic styles. The use of mathematical modelling techniques is to be explored. Other longer-term objectives are discussed further in Chapter 9.

The UCL CASD has demonstrated that acceptable below-knee sockets can be designed with shape manipulation performed numerically by computer and experience has been gained in handling prosthetic shapes. A full understanding of why a particular shape produces a comfortable load distribution is still missing however. A CAE study, which aims to improve upon the present understanding, is presented in the remaining chapters of the thesis.

Chapter 3

FE models of indentations.

3.0 Objective.

A FE model of a residual limb loaded by a prosthetic socket requires a description of the stress-strain relationship for the limb tissues. There is a dearth of information describing the mechanical properties of soft tissues; however, it appears that stress-strain relationships are not simple. For the current project, an idealisation of tissue behaviour is used and it is assumed that the stress-strain relationship may be defined in terms of a compressive modulus. To obtain values of tissue modulus, theoretical plots are prepared of the load versus deflection response of a rigid indenter forced into an idealised tissue layer. The predicted response is then compared with a measured response from indentation tests and from this comparison a modulus is evaluated. It is assumed that this modulus will provide good approximations when used in a FE model of socket loading.

The objective of the work presented in this chapter is to predict indenter responses using the FE method.

3.1 Accuracy of FE analyses of large compressive strains

To provide a perspective to the relative accuracy of the FE method for analysing large deformations of elastic materials a solid cylindrical specimen of unit height, h_o, and diameter, d_o, is considered. Two analyses which use the FE method are compared with the exact solution for the case where the original height of the specimen becomes half of this value, h_f, under the action of uniaxial, frictionless compressive loading. The specimen is shown in figure 3.1.

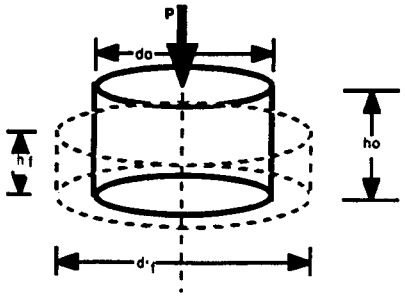

Figure 3.1 - Compression of a cylindrical specimen.

The specimen is made of a material which is homogeneous, isotropic and incompressible and which obeys a linear constitutive law. The constant of proportionality, E, between stress and strain is usually defined in terms of engineering values and is a constant, the Young's modulus, only for small strains. For this material, however, E is the constant of proportionality between **true** values of stress and strain and is valid for any stage of deformation. In this large displacement problem, although a linear stress-strain relationship between stress and strain, the relationship between strain and specimen height is nonlinear.

The exact solution is obtained using the true stress and true strain definitions

$$\sigma = \frac{P}{A} = \frac{P}{\frac{\pi}{4} d^2} \qquad - 3.1$$

and

$$\delta\varepsilon = \frac{\delta h}{h} \qquad \Rightarrow \varepsilon = \ln\left(\frac{h}{h_o}\right) \qquad - 3.2$$

where A, d and h are instantaneous values of the cross-sectional area, diameter and height. At any stage of deformation the equation

$$\sigma = E\,\varepsilon \qquad - 3.3$$

relates the stress to the strain.

By introducing the Poisson relation between the lateral strain in the diameter, ε_d, and the axial strain in the height, ε_h,

$$\varepsilon_d = -\nu\,\varepsilon_h \qquad - 3.4$$

where ν is the Poisson ratio, an expression for the diameter, d, at any instant is

$$d = d_0 \frac{d}{d_0} = d_0\, e^{-\nu\,\varepsilon_h} \qquad - 3.5$$

Rearranging equation 3.1 and substituting equations 3.3, 3.2 and 3.5 yields an expression for the load required to compress the specimen to a height, h_f, which may be written

$$P = \frac{\pi}{4} d_f^2 \sigma = E \frac{\pi}{4} d_f^2 \varepsilon_{h_f} = E \frac{\pi}{4} d_0^2 \left(\frac{h_f}{h_0}\right)^{-2\nu} \ln\left(\frac{h_f}{h_0}\right) \qquad -3.6$$

Since the cylinder is made of an incompressible material $\nu = 0.5$ and the load required to compress it to a height of 0.5 units is found to be -1.089 load units. The **engineering** stress required to cause this strain is obtained by dividing this load by the original cross-sectional area and is -1.387 units.

A simpler analysis, such as is used by linear FE models, neglects the lateral straining of the cylinder and use is made of engineering values of stress and strain. The following relations are applied :

$$\sigma = \frac{P}{A} = E \varepsilon \qquad - 3.7$$

where P is the applied force and A is the original cross-sectional area and

$$\varepsilon = \frac{h_f - h_o}{h_o} \qquad - 3.8$$

where ε here is the engineering strain. Substituting equations 3.7 and 3.8 into equation 3.3 and rearranging gives

$$P = E \frac{\pi}{4} d_0^2 \frac{h_f - h_0}{h_0} \qquad - 3.9$$

The force required for the compression is calculated to be -0.393 load units using this equation. This corresponds to an engineering stress of -0.5 units.

Accuracy of FE solutions may be improved if a simple iterative method is used where the analysis is divided into a number of incremental steps of deformation. This has been used by a number of investigators to study idealised tissues behaviour

[NAKAMURA81, CHOW78]. It will now be shown that this, unfortunately, cannot yield the exact solution.

If an increment of load, ΔP, is considered which increases the applied stress on the specimen and deforms it to a shorter shape with a larger cross-sectional area, an expression for ΔP is

$$\Delta P = A\,\Delta\sigma + \sigma\,\Delta A \qquad - 3.10$$

This may be rewritten in terms of strains as

$$\Delta P = A\,E\,\frac{\Delta h}{h} + E\,\varepsilon\,\Delta A \qquad - 3.11$$

Substitution of the strain and area terms for terms of specimen height, followed by differentiation yields

$$\frac{dP}{dh} = \frac{E\pi}{4} d_0^2 \left(\frac{h}{h_o}\right)^{-2\nu} \left(1 - 2\nu \ln\left(\frac{h}{h_0}\right)\right) \qquad - 3.12$$

in the limiting case where ΔP tends to 0.

Equation 3.12 may be integrated to give the expression

$$P = \frac{E\pi}{4} d_0^2 h_0^{2\nu} \left[\left(\frac{1}{2\nu\, h_0^{2\nu}} - \frac{1}{2\nu\, h_f^{2\nu}}\right) + \left(\left(\ln\left(\frac{h_f}{h_0}\right) + \frac{1}{2\nu}\right)\frac{1}{h_f^{2\nu}} - \frac{1}{2\nu\, h_0^{2\nu}}\right)\right] \qquad - 3.13$$

for the force required to compress the cylinder to a final height, h_f. This may be reduced to the same form as equation 3.6.

In the original equation, 3.10, used to derive equation 3.13, the first term on the right hand side represents that part of the increment of load which increases, by $\Delta\sigma$, the stress over the instantaneous area. The second term calculates the part of the load which produces an increase, ΔA, in the area of the specimen at the current level of stress.

Iterative FE solutions may use linear theory and treat each increment of deformation as a completely separate problem where the final, displaced, geometry from one

iteration becomes the initial geometry of the next. The FE program therefore calculates a new system stiffness matrix prior to each iteration (see Appendix A). If the load increments used in this type of solution are made very small, the result might be assumed to tend to that given by equation 3.13. In these solutions, however, the modelled structure is assumed free of stress at the start of each iteration. The second term on the right hand side of equation 3.10, therefore, is assumed to have zero value throughout the iterative process. If load increments in an iterative solution are made very small, P may tend to a 'best' value found using the first part of the right hand side of equation 3.13 - i.e. the equation

$$P = \frac{E\pi}{4} d_0^2 h_0^{2\nu} \left(\frac{1}{2\nu h_0^{2\nu}} - \frac{1}{2\nu h_f^{2\nu}} \right) \qquad - 3.14$$

Analysis of the problem of the incompressible cylinder using this equation finds P to be -0.785 load units, some 28% lower than the exact answer and corresponding to an engineering stress of -1.0 unit.

Greater accuracy *can* be achieved by FE analysis for problems where the strain-displacement relationship is nonlinear. In these analyses, displacements are referred to the mesh in its undeformed state and Green's strain tensor is used [ZIENKIEW71]. This gives rise to a stiffness matrix which is a function of nodal displacements. An iterative method is used to obtain the nonlinear solution. With the software used for the current project, this form of solution is restricted to a limited number of element types. Furthermore, some of the models presented in the thesis require boundary conditions to vary during deformation and an iterative modelling process is suitable.

The magnitude of the error in equation 3.14 increases primarily with the magnitude of the applied strain but is also affected by the Poisson ratio of the material. The sensitivity of this error to these factors is demonstrated by figure 3.2 which has been generated using the second part of the right hand side of equation 3.13. If the engineering strain applied to the incompressible cylinder is only -25% the error of the 'best' iterative solution becomes 13%.

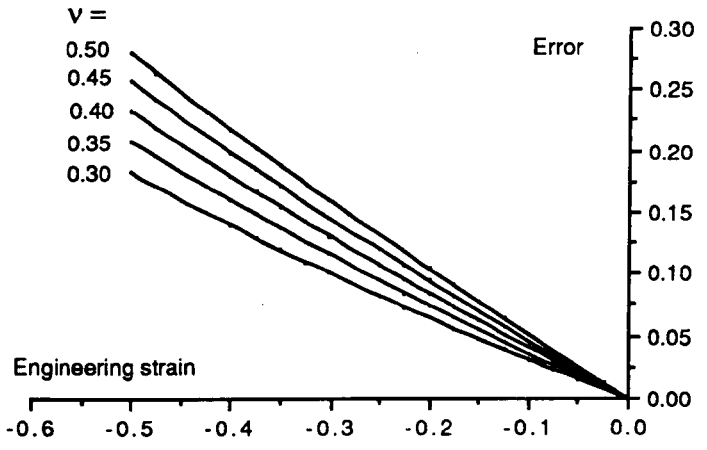

Figure 3.2 - Error in 'best' iterative FE solutions of uniaxial compression.

Equation 3.14 has been formulated on the assumption that the steps of strain used to calculate the applied load are infinitessimal, however computer solutions will use finite increments of strain. The choice of the size of increment to use is a compromise between the desired accuracy and the cost in computer time.

Convergence of iterative solutions to the continuous function described by equation 3.14 was studied. A PASCAL program was written which used equation 3.9 to calculate the applied load required to cause increments of deformation to the cylinder. After each increment, geometry was redefined before the next load increment was calculated. Solutions were obtained using 1,2,5,10,100 and 1000 equal increments of a total applied engineering strain of -50%. Figure 3.3 shows the relationship between cumulative applied load and specimen height calculated by of each of these runs.

As expected, solutions converge towards a unique curve as the number of increments is increased. The run using 1000 steps of strain follows the curve described by equation 3.14 within 0.09% whereas the analysis performed in 10 steps produced a maximum error of 8.6% at -50% strain. Another run took 10 steps to calculate the applied load necessary to produce an engineering strain of -25% and the result was only 3.1% below the 'best iterative' answer.

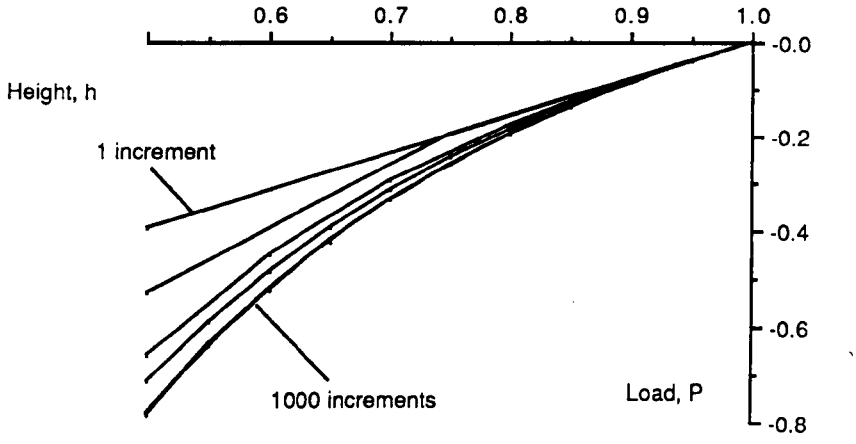

Figure 3.3 - Effect of the number of increments used to calculate uniaxial compressive loads using an iterative FE analysis.

A shortcoming of FE analysis is that completely incompressible materials cannot be modelled. This arises out of the existence of the terms (1-2ν) in the denominator of each term of the stress-strain matrix (see Appendix A). A division by zero is required to model a material with a Poisson ratio of 0.5 and the solution breaks down. With near-incompressible materials, the size of this term approaches zero, the solution becomes unstable, and rounding errors may be significantly magnified.

To study the effect of the value of Poisson ratio upon the load versus height response of the cylinder under frictionless uniaxial compression plot have been produced. In figure 3.4 values of Poisson ratio in the range 0.3 to 0.5 have been used in the exact equation 3.6 to calculate the compressive loads.

To cause an engineering strain of -50%, the magnitude of the compressive load required for a material with a Poisson ratio, ν, of 0.45 is 6.7% lower than that with a Poisson ratio of 0.5. At a strain of -25% the corresponding difference is 2.8%.

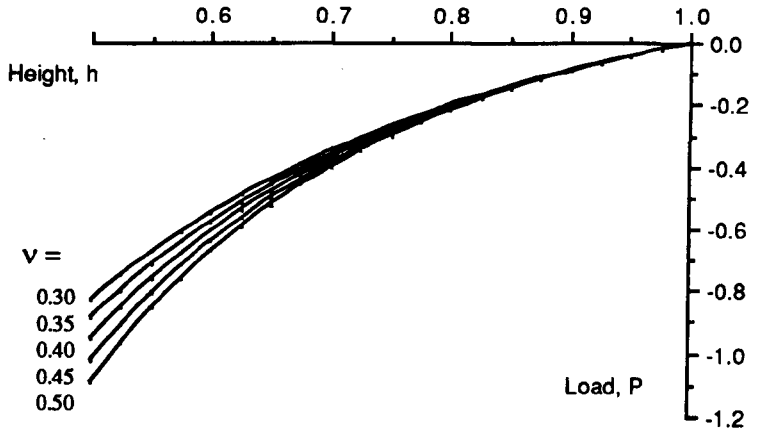

Figure 3.4 - Effect of Poisson ratio upon uniaxial compressive loads.

This section has identified some of the pitfalls of using FE analysis to predict compressive loads which cause high strains. The approach used in the current project, however, is to compare a measured indenter response with a response predicted by FE models of the indentation process. A modulus used in these FE models, which produces a predicted response that correlates well with the measured response, may be appropriate for use in further FE models which contain similar strains, e.g. models of socket loading. It is clear from this section that moduli evaluated in this way may not be the real constants of proportionality between stress and strain and may therefore be inappropriate for general use.

3.2 The FE method used

Software

A review of FE packages most commonly used in the United Kingdom (PAFEC, ANSYS and NASTRAN) revealed no significant leader in terms of all round capabilities. Since there was no obvious benchmark test at the outset and since limitations of software are frequently not encountered until complex functionality is required, a full assessment of each package was thought unrealistic and PAFEC, available at UCL and recommended by other users, was chosen. The PAFEC FE

package is a suite of programs capable of defining and analysing problems of stress analysis, heat flow and dynamic behaviour in one, two or three dimensions.

The first step of the analytical process is to assemble into a data file a series of modules of text which describe the problem. In the stress analyses discussed hereafter nodal geometry, element topology, boundary restraints and material properties are the main details which define a mesh of elements to represent the object modelled. Loads and/or prescribed displacements may be applied at any of the nodes using additional modules. With problems thus defined, further information is incorporated into the data file to control the analysis. In this way, the user elects for an iterative solution, an axisymmetric solution, stress calculation or other optional methods of analysis.

Figure 3.5 shows a very simple PAFEC data file which may be used to produce iterative solutions for the problem of uniaxial compression of a cylinder. In this exceptional case one element only is used.

The completed PAFEC data file is used by individual programs of the package which divide the analysis into a number of tasks or PHASEs. These include checking of element geometry, numbering of degrees of freedom within the mesh, calculation of element stiffness matrices and their incorporation into a system stiffness matrix and solution for nodal displacements or reactions. After each phase of the analysis, results are written to text files.

The definition of problems and interpretation of results is facilitated by the PIGS graphical package which integrates with PAFEC. As a preprocessor, PIGS is useful for checking mesh data and the location of restraints and loads. When postprocessing results, the stress contour and deformed mesh plotting facilities were found most useful.

An basic outline of the theory used by PAFEC appears in Appendix A.

```
TITLE MODEL FOR UNIAXIAL COMPRESSION OF SOLID CYLINDER
CONTROL
FULL.CONTROL
AXISYMMETRIC
LARGE.DISPLACEMENTS
PHASE=1,2,4,6,7,9
CONTROL.END
C THIS MODEL USES A SINGLE ELEMENT
NODES
NODE.NUMBER X Y
1,0.0,0.0
2,0.0,0.5
3,1.0,0.0
4,1.0,0.5
ELEMENTS
NUMBER ELEMENT.TYPE PROPERTIES TOPOLOGY
1,36200,11,1,2,3,4
MATERIAL
MATERIAL.NUMBER E NU
11,1.0,0.45
RESTRAINTS
NODE.NUMBER PLANE DIRECTION
1,1,1
3,2,2
DISPLACEMENTS.PRESCRIBED
NODE.NUMBER DIRECTION DISPLACEMENT.VALUE
3,1,-0.5
4,1.-0.5
INCREMENTAL
STEP.LIST
10,10,10,10,10,10,10,10,10,10
END.OF.DATA
```

Figure 3.5 - PAFEC data file for uniaxial compression of a cylinder.

Mesh design

A finite element mesh suitable for accurate stress analysis has a concentration of elements where stress gradients are high and few elements in low stress regions. In the areas where elements are concentrated, discontinuities of stresses across element boundaries can be kept small. The coarse parts of the mesh are desirable to reduce the size of the FE solution and because a large number of elements in areas of low stress may cause very small terms in the stiffness matrix and rounding errors may result. In some cases the aspect ratio of elements with respect to the applied strain may influence the accuracy of results.

To design each mesh for the models presented in this thesis, a number of trial meshes were used to identify general stress pattern and these were refined appropriately. Convergence to a unique solution is the objective of this design process and trial meshes can be evaluated in a number of ways. PAFEC calculates nodal

stresses for each element in a mesh. For example, in a 2-dimensional mesh up to 4 stress may therefore be calculated at any one node. In the models presented, convergence was detected using linear analyses by checking the differences between calculated stresses at nodes to assess the continuity of stress within a mesh. A coarse FE mesh was gradually improved and solutions were assumed to be converging when discontinuities of stress became a small and were barely effected by further refinement.

3.3 Flat-tipped indenters.

A series of models was produced first of indentations into an idealised tissue layer by cylindrical indenters with a flat tip (figure 3.6(a)).

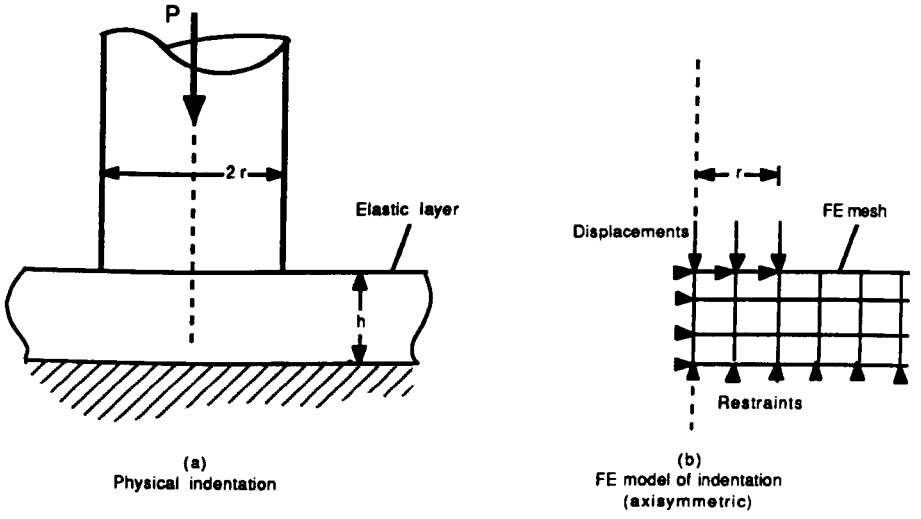

Figure 3.6 - Indentation by a flat-tipped indenter.

The tissue layer is assumed to be elastic, homogeneous, isotropic and nearly incompressible. The bone that this layer rests upon is assumed to be rigid, flat and continuous. The interface between the bone and soft tissue is assumed frictionless.

A number of geometric configurations were represented by varying the ratio of the indenter diameter, d, to the layer thickness, h, - i.e. the aspect ratio of the material beneath the indenter. Ratios of 1.0, 2.0, and 4.0 were modelled.

The indentation considered may be modelled simply and efficiently by prescribing vertical displacements to nodes on the upper surface of the mesh of elastic elements. Figure 3.6 (b) shows the modelling procedure. Displacements equal to half the layer thickness were used. At the interface between the elastic layer and the rigid base, nodes were permitted to move only horizontally. All models discussed in this chapter used a layer thickness of 1 unit, and set the indenter diameter according to the ratio d/h. In the figures presented, units of millimetres and Newtons are used; however any consistent set of units may be applied.

Unit modulus (i.e. 1 MPa) was used for the material. The inability of FE theory to model incompressible behaviour has been discussed; PAFEC suggest that the maximum value of Poisson ratio that will yield accurate answers is 0.45 and this was used.

A number of trial meshes were used to produce final models for each aspect ratio. Details of the mesh design process are presented in Appendix B.

The stresses calculated from linear analyses of the final meshes were used by PIGS to produce the stress distributions shown in figure 3.7. This shows the Von Mises stresses for the part of the elastic layer beneath the indenter.

The linear models discussed use a single step displacement and thus predict a linear load-displacement response. To predict the stiffening that will result from geometric changes in the elastic layer, iterative PAFEC runs were used with 10 increments of engineering strain each of -50%. It should be noted that the surface nodes with prescribed displacements were restrained from horizontal motion as they moved down in these models. No relative motion took place, therefore, between the modelled indenter and the elastic layer and a 'totally rough' interface existed. The calculated indenter responses with each aspect ratio are shown in figure 3.8. The iterative solutions used were unable to sum incremental stresses.

Iterative frictionless models are less easily devised. If horizontal motion of the interface nodes is permitted, the lateral straining of the elastic mesh causes the elements beneath the indenter to 'widen' as they 'shorten'. The nodes of these elements thus become spread out and the prescribed displacements, which are assigned to these nodes, act over a larger area. The effect is to model an indenter which increases in area as deformation progresses.

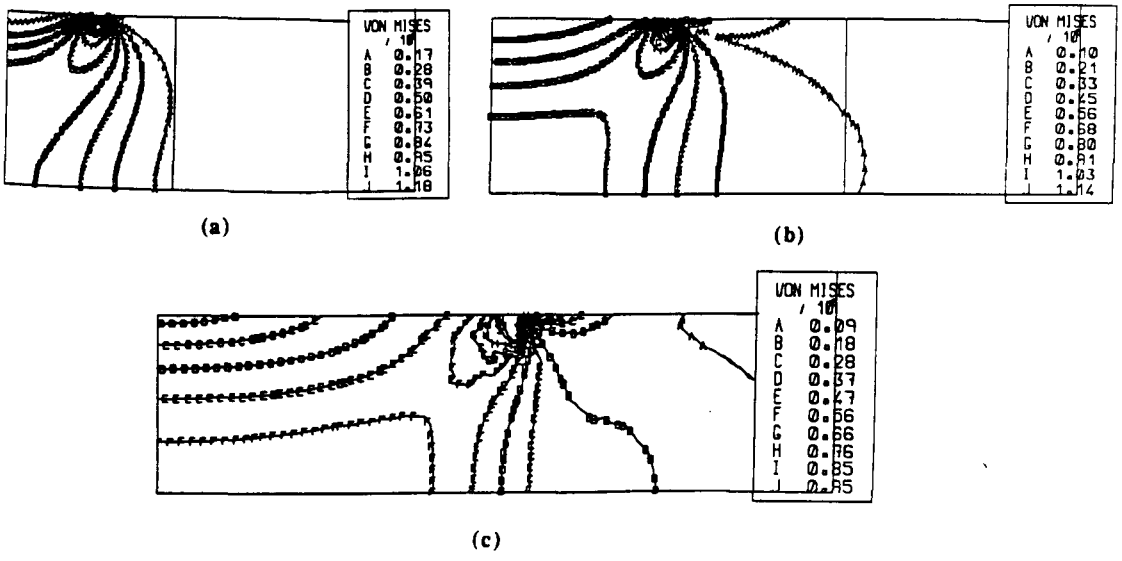

Figure 3.7 - Distribution of Von Mises stress beneath flat-tipped indenters.

(a) d/h=1.0.

(b) d/h=2.0.

(c) d/h=4.0.

To overcome this problem and enable the deformed material to 'slide over' the tip of the modelled indenter, some modifications to the iterative solution method were necessary and computer programs were written for this purpose. In these runs, the nodes in contact with the indenter were free to move horizontally. After each increment of deformation, however, the mesh geometry was updated by a PASCAL program which added nodal coordinates and displacements and checked the positions of the displaced interface nodes. Restraints were then removed from any nodes which were radially displaced from the indenter axis by more than 2% of the intended indenter radius. With new boundary conditions established, another increment was run and the process was repeated to the desired total indentation.

Using the procedure described, plots were produced of applied indenter load versus displacement and these appear in figures 3.8 along with the response predicted by the 'totally rough' models.

Plots of nominal stress (applied load divided by indenter area) versus nominal strain (indenter displacement divided by original layer thickness) for each aspect ratio appear in figure 3.9.

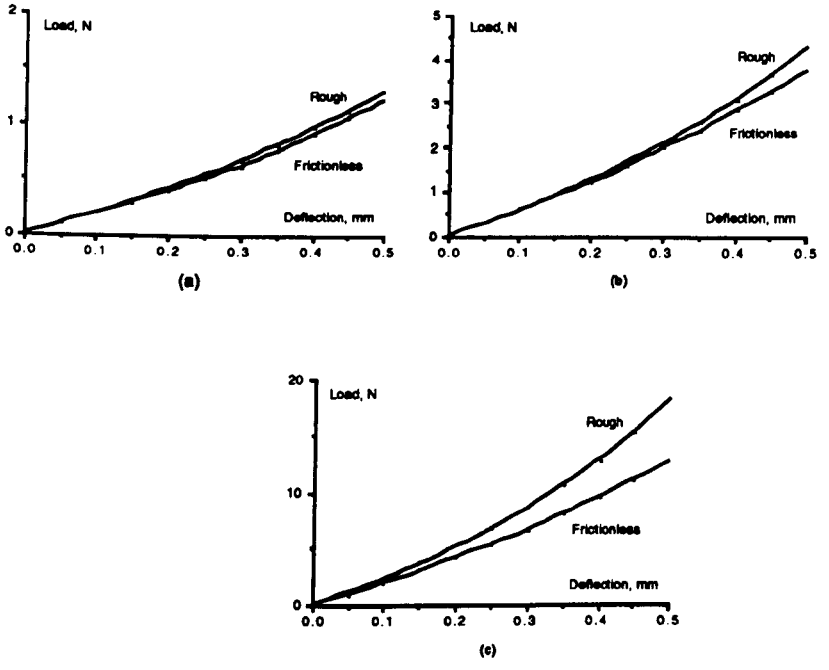

Figure 3.8 - Load versus deflection response of flat-tipped indenters

(a) d/h=1.0.

(b) d/h=2.0.

(c) d/h=4.0.

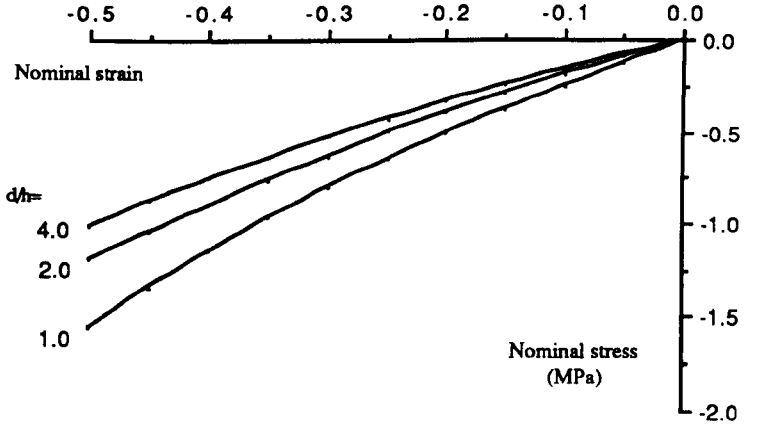

Figure 3.9 - Nominal stress versus strain for flat-tipped indenters.

The model using flat indenter was approached warily; behaviour of theoretical solutions at the sharp edge of the indenter is uncertain. A similar 2-dimensional problem has previously been considered [TIMOSHENK34] in which figure 3.6 (a) may represent a transverse plane of an infinite beam resting on an elastic layer. The local pressure, p, applied to the layer is given by

$$p = \frac{\sigma_{nom}}{p\sqrt{r^2 - x^2}}$$

where x is the horizontal distance from the centre of the beam and σ_{nom} is the applied nominal stress. At the edge of the beam, infinite pressure is predicted and the solution fails. The FE analysis appears to have predicted reasonable indenter loads; however, discontinuities of stress existed at the edge due to the exceptional boundary conditions here. At the edge node, in even the finest meshes used with d/h=2.0, the difference between the calculated principle compressive stresses was 78% of the peak value. Due to uncertainties about the influence of the edge, alternative models were created which did not produce such high stress concentrations.

3.4 Round-tipped indenters.

The second type of indenters modelled were also cylindrical but had hemispherical tips. Values of the ratio of indenter diameter, d, to layer thickness, h, equal to 1.0, 2.0 and 4.0 were again used to represent different geometries. Indentations were to a depth equal to half the original layer thickness.

In these models, the contact area at the interface is an additional geometric variable; however, the 'contact radius' is dependent only upon the aspect ratio, d/h, and the level of strain for a given material. In a further model with an aspect ratio of 0.5, the total indentation was only 25% of the layer thickness since with larger indentations the contact radius may be independent of the applied strain.

A description of the mesh design process for each aspect ratio appears in Appendix C.

The models used to test trial meshes simply forced the upper surface of the elastic mesh to conform to the hemispherical shape of the indenter. To obtain distributions of Von Mises stresses these models were re-run; however, in the repeat runs prescribed displacements were not included at those nodes which had previously been forced to adhere to the indenter surface. These nodes were detected by the sense of the reactions calculated in the original runs. The Von Mises stress distributions for aspect ratios of 1.0, 2.0 and 4.0 are shown in figure 3.10.

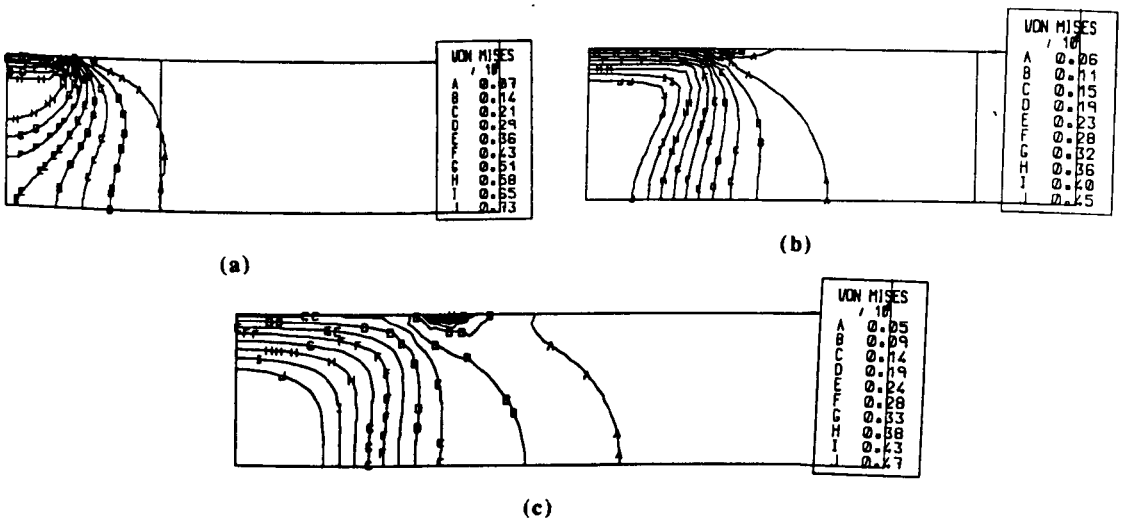

Figure 3.10 - Distribution of Von Mises stress beneath round-tipped indenters.

(a) d/h=1.0

(b) d/h=2.0

(c) d/h=4.0

The linear models used to create the stress contours permitted no horizontal motion of the interface nodes.

An iterative frictionless model was able to redefine geometry and boundary conditions as deformation progressed. In these models, all nodes on the bottom surface of the mesh were displaced upwards (figure 3.11). Nodes on the upper surface were initially free to move but were restrained when they were judged to be in contact with the indenter. Boundary conditions were checked between each of 10 or more increments of displacement to detect contact.

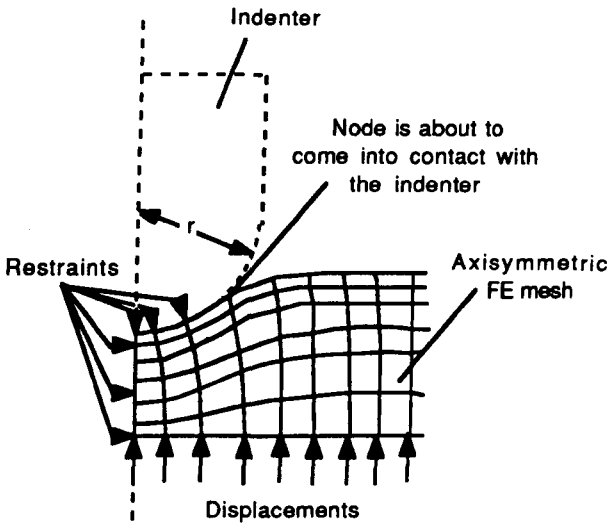

Figure 3.11 - Modelling of round-tipped indenter.

The upper surface nodes were judged to be in contact when they were separated from the indenter surface by a distance of less than 2% of its radius of curvature. Once nodes were found to be within this distance, restraints were applied. Contact nodes were restrained in a radial sense with respect to the static centre of curvature of the indenter tip and thus frictionless sliding at the interface was modelled. The total vertical load reacted by the indenter restraints was equivalent to the load applied by an indenter moving downwards with the same displacement as the upward movement of the bottom surface.

The cumulative indenter load is plotted against the displacement in figure 3.12 for models with each aspect ratio.

Figure 3.13 shows corresponding plots where load has been normalised by the cross-sectional area of the indenter (nominal stress) and indenter displacement has been normalised by layer thickness (nominal strain).

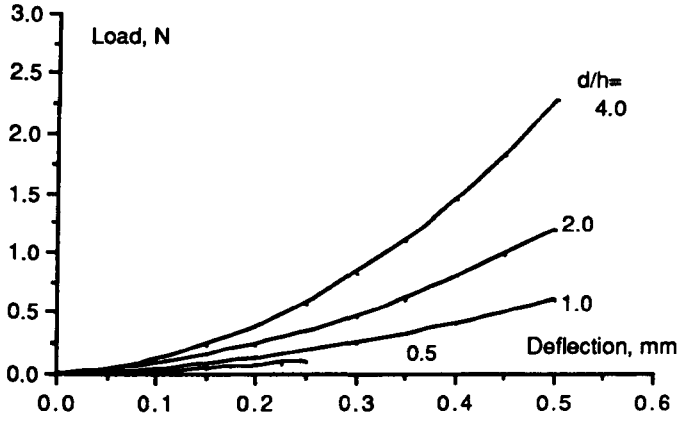

Figure 3.12 - Load versus deflection response for round-tipped indenters

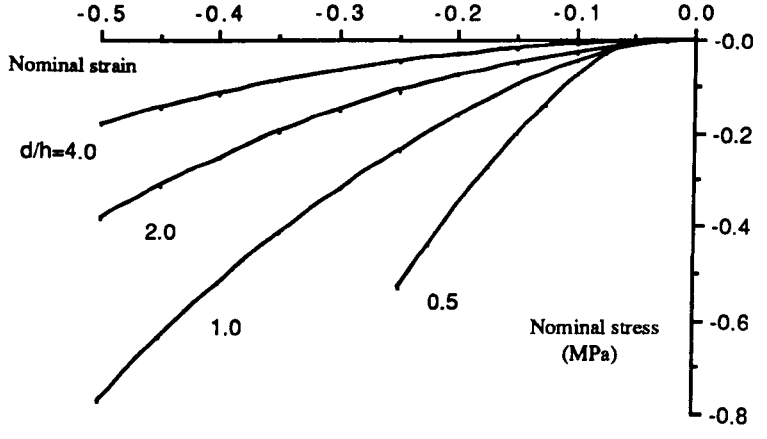

Figure 3.13 - Nominal stress versus strain for round-tipped indenters

3.5 Discussion of results.

In the flat indenter models with a frictionless interface, the gradient of plots of nominal stress versus strain from the iterative FE models was found to increase as the aspect ratio of the material beneath the indenter decreased. The nominal stress required to cause a nominal strain of -50% with an aspect ratio of 1.0 was over 1.5 times that where d/h was 4.0. The increase is probably due to the greater influence of the surrounding material which is not under the direct stress of the indenter but must undergo compatible straining.

If it is assumed that the models predict the response that would be obtained experimentally, it can be seen that a simple interpretation of experimental data may produce misleading values of Young's modulus, E. The case is considered where nominal strains of -50% are applied. If a 'best fit' straight line is fitted to the plots of nominal stress versus strain (figure 3.9) and a value of E is calculated from the gradient of this line, estimates of the modulus will be greater than in reality. The error of estimates reduces as d/h is increased; the estimates of E which correspond to d/h equal to 1.0, 2.0 and 4.0 are approximately 2.8, 2.2 and 1.9 times the true value of unity.

For each aspect ratio modelled, the applied stresses predicted by the 'totally rough' models were greater than in the frictionless models, as expected. The deviation between plots under the two interface conditions became more apparent as d/h was increased, also as expected.

In the round-tipped indenter models, the effect of aspect ratio upon the predicted stiffness was more noticeable than with the flat indenters. In the case where d/h was 1.0, the nominal stress which produced a nominal strain of -50% was 4.4 times that where the ratio was 4.0.

Plots of nominal stress versus strain from these models were more nonlinear than in the flat indenter models, presumably because of the effect of the increasing contact area as indentation proceeds. The initially rapidly changing slope of each plot 'flattens out'. This may be because the rate of increase of the contact area with respect to indenter deflection reduces as the indenter presses into the material.

If it is again assumed that these plots predict experimental results correctly, estimation of a value of modulus is difficult due to nonlinearity. If a straight line is fitted to data, estimated values will be largely dependent upon the range of strain over which measurements are taken.

In section 3.1, analyses of frictionless uniaxial compression were used to evaluate the accuracy of FE solutions. Since stresses are uniform in this mode of deformation the exact analysis is readily derived. It was shown that iterative FE solutions may deviate from exact solutions by a significant amount, especially where high strains exist. Errors which are due to assumptions of the FE method used, restrictions on computer time which limit the size of increments used and the inability of the FE method to model incompressible materials all tend to cause these solutions to underpredict loads. At an engineering strain of -50% the error may be approximately 43% if it assumed that its constituents are linearly related. At an engineering strain of -25% the corresponding error is approximately 19%.

For the indenter models, it might be assumed that, as in the case of frictionless uniaxial compression, indenter loads will be underpredicted by an amount which depends primarily upon the magnitude of the stresses and strains in the material. For the near-incompressible materials modelled, deformations will largely be due to deviatoric rather than hydrostatic stresses and thus the magnitude of the Von Mises stress may be an indicator of the size of these errors. Since the stress distribution beneath the indenters was nonuniform, however, errors may vary throughout the material and it is difficult to estimate the accuracy of these FE models. For this reason, an experimental approach to test the models was felt necessary to justify further use of the theoretical results obtained in the work of this chapter.

Chapter 4

Experimental measurements of indentations.

4.0 Introduction.

In the previous chapter, FE models have been used to calculate the load versus deflection response of indenters forced into continuous layers of an elastic material. For the iterative FE analysis used, it was predicted that the applied stress required to cause a given strain will be underestimated. By taking specimens of an engineering material with mechanical properties similar to those assumed in the FE models, comparisons of measured and predicted responses may allow variations in the magnitude of this underestimate to be explored.

4.1 Experimental technique.

A Zwick model 1474 testing machine was used to measure applied loads and deflections. In a recent calibration test this machine was found to measure loads within one percent, even at the lower end of its load capacity which was used during these tests. Deflections were measured using Zwick's 066210 extensometer. The specification for this module gives the error limits as ±1% and, in a test which measured the free deflection of an indenter in space, the drag force it applied was not detectable.

The part of the experimental set-up which required most attention was the selection of the test material and preparation of specimens. In the finite element models, the elastic material possessed a linear relationship between true stress and true strain and was homogeneous and isotropic. The models employed a Young's modulus, E, of unity; however, by multiplying the modelled loads or stresses by an appropriate value of E other 'theoretical' curves may be prepared for any 'linear' material which is nearly incompressible. A material with a stiffness comparable to that of soft lower limb tissues was sought, however, since a physical model of a residual limb was to be manufactured for work presented in a later chapter and it was felt that experimental experience with such a material would be useful. A compressive modulus of the soft limb tissues in the region of 100 to 200 kPa was estimated from nominal stress versus nominal strain responses in a series of pilot indenter tests at a number of sites on the legs of an asymptomatic subject. The use of rubbery materials was thought most likely to approximate the near-incompressible behaviour modelled.

Uniaxial compression tests were used to evaluate the Young's modulus and Poisson ratio of a number of materials. Cylindrical specimens were placed upon a flat perspex plate which rested on the base of the machine. Loads were applied by a similar plate rigidly coupled, via a threaded studding, to the load cell which was mounted on the crosshead of the machine. Applied load versus deflection responses gave values of Young's modulus whereas the Poisson ratio was calculated using measurements of the specimen diameter from marks on the compressing plate at a various levels of applied strain.

Some open and closed cell foams were found to have sufficiently low stiffness but these exhibited little lateral straining and were in general nonlinear, probably due to effects of the voids that they contain. All rubbers and elastomers tested showed good linearity but were mostly rather stiff. A room temperature vulcanised (RTV) silicone elastomer (Dow Corning Q3-3320) was found to have suitable mechanical properties and was used for all physical models of soft tissues discussed in this thesis. The main advantage of this type of material is that the base and catalyst mixture used to produce each batch may be poured to mould specimens of all shapes and sizes. Preparation involved the mixing of the two components (base to catalyst 20:1 by weight) followed by degassing in a vacuum chamber for a full half hour. Throughout the degassing process the container holding the highly viscous mixture was agitated vigorously to help expel air. Early specimens which did not undergo this process were of inconsistent modulus and exhibited nonlinearity of true stress versus strain. A disadvantage was that not all of the specimens could be prepared in a single batch since the volume was limited of the base/catalyst mixture that could be degassed at one time and slight variations existed between batches.

For indentation tests on Q3-3320 specimens, cylindrical indenters with flat or round tips were manufactured from extruded acetal. Indenters of both type were made with diameters of 15, 20 and 25 mm. The flat ended indenters were turned on a lathe and the edges were left sharp on machining, the rounded indenters had hemispherical tips and were manufactured using a ball turning tool. These all screwed directly into the coupling of the test machine's load cell.

Elastomer specimens for the indentation tests were cylindrical and a number were prepared to evaluate various aspect ratios of the material beneath the indenter, d/h (indenter diameter divided by layer thickness). These were formed in moulds with

diameters of 102 mm. After curing the thickness of specimens was checked with digital calipers and in each case was within ±0.2 mm of the expected value.

Once the test apparatus had been checked for 'play' some of the phenomena were investigated which were considered likely to introduce measurement errors. These were friction at the interfaces, viscoelasticity and age-hardening of the elastomer and the effects of temperature variations of the specimens.

For a qualitative assessment of frictional effects, a series of tests observed the magnitude of uniaxial compressive load versus deflection response of a specimen of Q3-3320 under a number of interface conditions (Figure 4.1). The aspect ratio (diameter divided by height) of the specimen was approximately 4, its thickness was 20 mm. In test (a) the specimen was compressed between dry perspex plates whereas in tests (b) and (c) the interface between the specimen and the compressing plates was lubricated with KY jelly, a medical lubricating jelly, and a light oil respectively. In test (d) the interface was roughened by placing sheets of 720 grit abrasive paper between the specimen and the compressing plates.

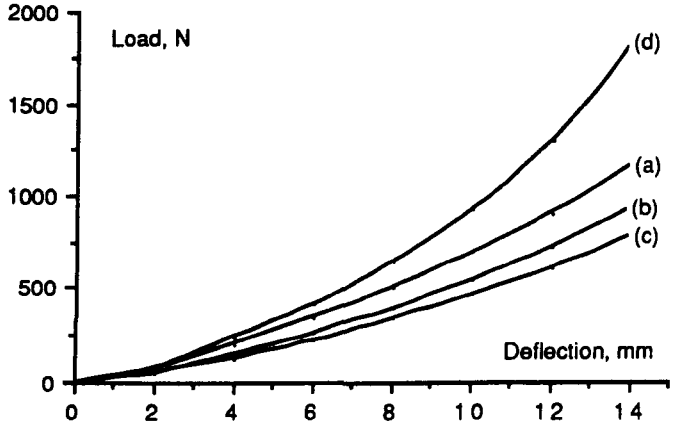

Figure 4.1 - Effect of interface conditions upon measured compressive loads

(a) dry perspex plates.

(b) KY jelly.

(c) lubricating oil.

(d) abrasive paper.

These results show that care must be taken if frictionless conditions are assumed in experimentation since a roughly 50% increase in applied load was required to cause a nominal strain of -0.5 when lubrication was omitted. Other tests showed that compression between plates made of perspex required slightly lower loads than with plates of steel or polypropylene. Lubricating oil was used in all tests discussed in this chapter.

The rate of applied straining of Q3-3320 was found to have a small effect on experimental measurements. Figure 4.2 is a plot of the load versus deflection response of an indentation test using a round-tipped indenter. Data from tests at strain rates of 0.2, 0.02 and 0.002 s^{-1} are shown.

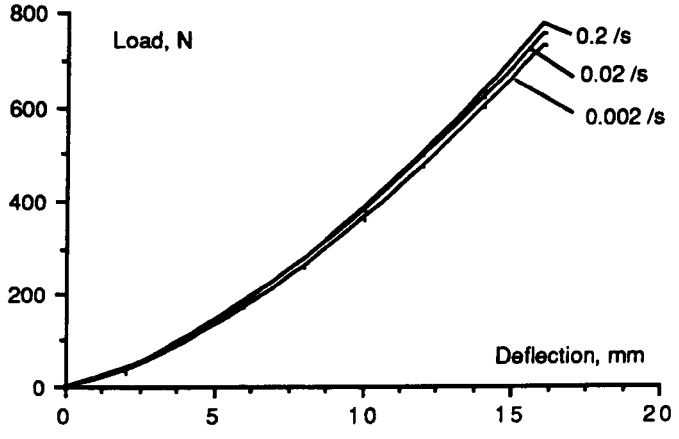

Figure 4.2 - Effect of strain rate upon indenter loads for Q3-3320 elastomer.

A difference in the loads required to cause a given strain of the order of only 6% exists across this wide range. The speed of the crosshead movement of the Zwick machine may be controlled and a nominal strain rate of 0.05 s^{-1} was used in all tests presented within this chapter.

Low viscoelasticity in the elastomer was also demonstrated by stress relaxation tests. Figure 4.3 is a plot of the applied indenter load versus log(time) for a test involving constant strain rate (0.05 s^{-1}) loading followed by stress relaxation at a fixed strain due to a hemispherical tipped indenter.

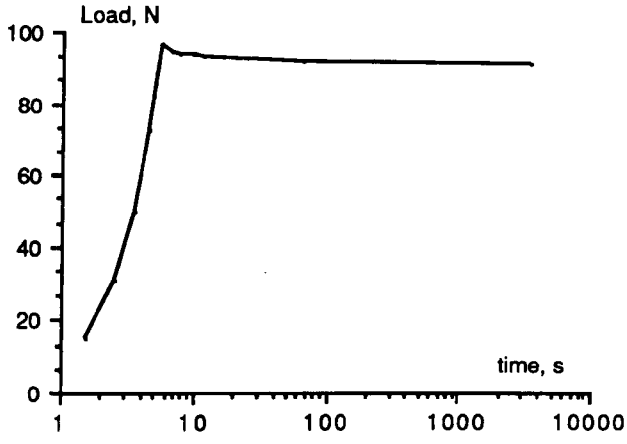

Figure 4.3 - Stress relaxation in Q3-3320 elastomer.

Other stress relaxation tests at various levels of final applied strain showed the ratio of the peak load after ramp straining to the 'fully relaxed' load to always be roughly 0.95. The low viscoelasticity of the elastomer was important in tests presented later in this thesis (see Chapter 7).

Once specimens had been allowed to harden for over a week, results from both uniaxial compression and indenter tests were reproducible under different prevailing room temperature conditions.

4.2 Uniaxial compression tests.

In order to evaluate the Poisson ratio of the elastomer, simultaneous measurements of the diameter and height of specimens at a number of levels of uniaxial compressive strain were used to calculate lateral and axial extension ratios. The natural logarithms of these quantities are true strains and are plotted in figure 4.4 for a typical test. The straight line which fits these data best has a gradient of -0.48.

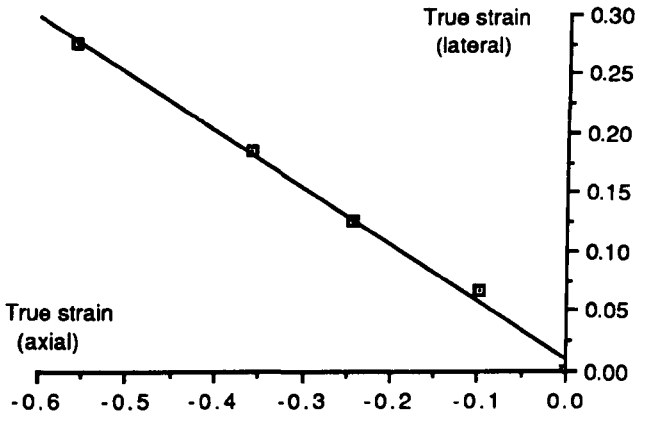

Figure 4.4 - Axial versus lateral strain in Q3-3320 elastomer

To evaluate the compressive modulus of the elastomer results from uniaxial compression tests on two specimens made from different batches of Q3-3320 are used. Specimen (a) had an initial diameter of 102 mm and initial thickness of 40 mm. Specimen (b) had initial diameter of 64 mm and initial thickness of 18 mm. Figure 4.5 shows plots of engineering stress vs engineering strain calculated from the raw test data for these two specimens.

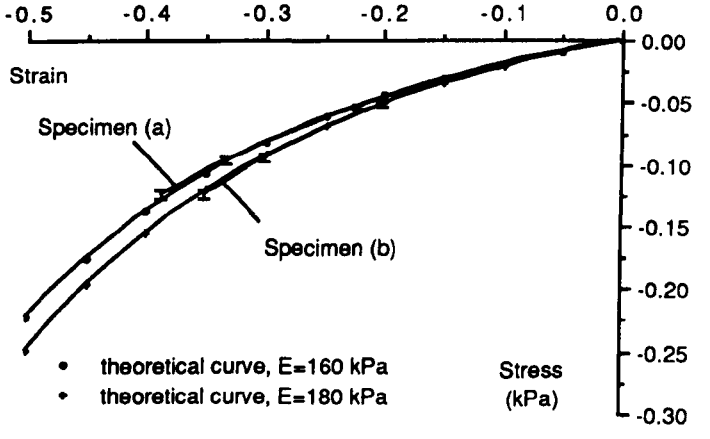

Figure 4.5 - Engineering stress versus strain for Q3-3320 elastomer in uniaxial compression.

On repeated testing, allowing at least 4 minutes between each run, the variation in the applied load necessary to cause a given engineering strain was found to be no more than 4% and this is represented by error bars on each curve. Superimposed upon these plots are theoretical curves produced using the 'exact' solution from equation 3.6, which represent the **engineering** stress/strain behaviour for a material which possesses a linear relationship between **true** stress and strain. For specimen (a), close agreement with experimental data was achieved from an 'exact' curve derived using a Young's modulus, E, of 160 kPa whereas a value of E equal to 180 kPa was found suitable for specimen (b). The measured value of ν of 0.48 was used to generate these theoretical curves.

In figure 4.6, the experimental curves from the two specimens appear with a second pair of theoretical curves which are plots of applied engineering stress versus strain calculated from an iterative FE type solution using 10 increments of strain and a Poisson ratio of 0.45. 'Adjusted' values of E equal to 208 and 234 kPa, i.e. 30% greater than the measured moduli, were used to generate the theoretical curves and provide an acceptable fit to the experimental data for the range of measured strains.

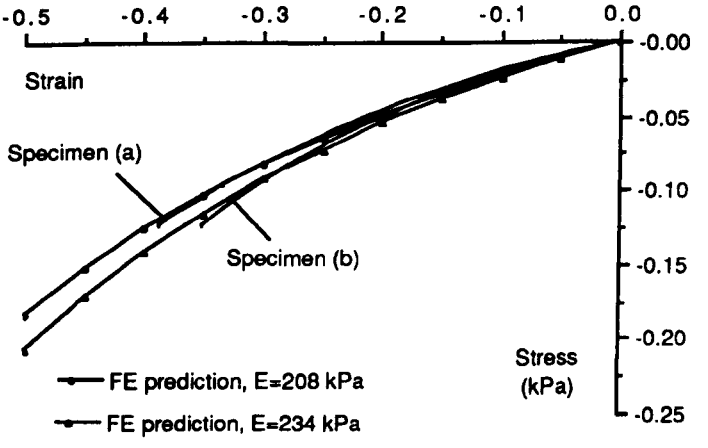

Figure 4.6 - Engineering stress versus strain for Q3-3320 elastomer in uniaxial compression and predicted curves from an iterative FE analysis.

4.3 Flat-tipped indenter tests.

A series of tests using flat ended indenters aimed firstly to show the effect of the aspect ratio, d/h, and secondly to demonstrate the repeatability of experiments when the same value of d/h was represented by indenters and specimens of different sizes.

From the measured load versus deflection responses, nominal stresses were calculated as applied load divided by the cross-sectional area of the indenter. Nominal strains were calculated by dividing the change in thickness on the indenter axis by the original uniform layer thickness.

The first 3 tests used the 20 mm diameter indenter probing into layers of the elastomer which were 5, 10 and 20 mm thick corresponding to aspect ratios of 1.0, 2.0 and 4.0 respectively. Results from these tests appear in figures 4.7, 4.8 and 4.9.

The data presented are calculated from mean values of applied load at a number of levels of strain from typically five tests. Error bars are again included to show the variation between tests. Each plot of normalised stress versus strain using the experimental data appears with two theoretical plots produced from the results of the FE models. The first of these uses the mean value of E of 170 kPa deduced from the exact analysis used on the uniaxial test data. The other curve uses a value of E equal to 221 kPa, corresponding to the mean value of 'adjusted' Young's modulus which had been produced by fitting the iterative FE data from the model of uniaxial compression to the experimental compression data.

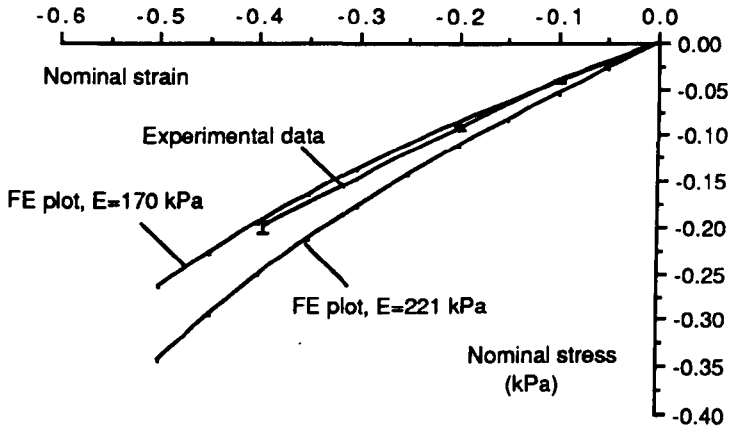

Figure 4.7 - Nominal stress versus strain for flat-tipped indenter, d/h=1.0.

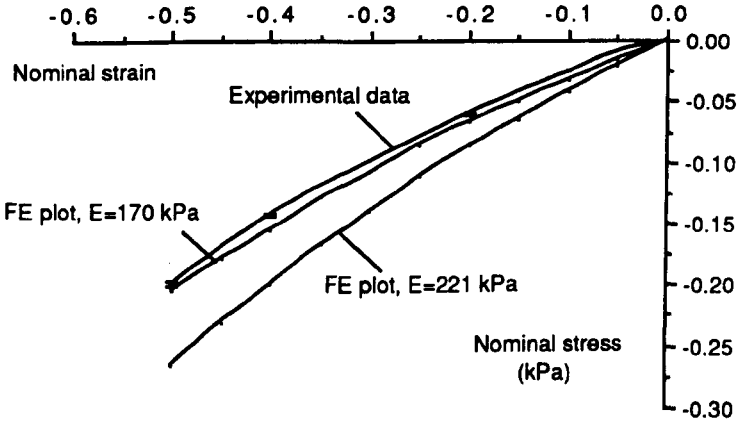

Figure 4.8 - Nominal stress versus strain for flat-tipped indenter, d/h=2.0.

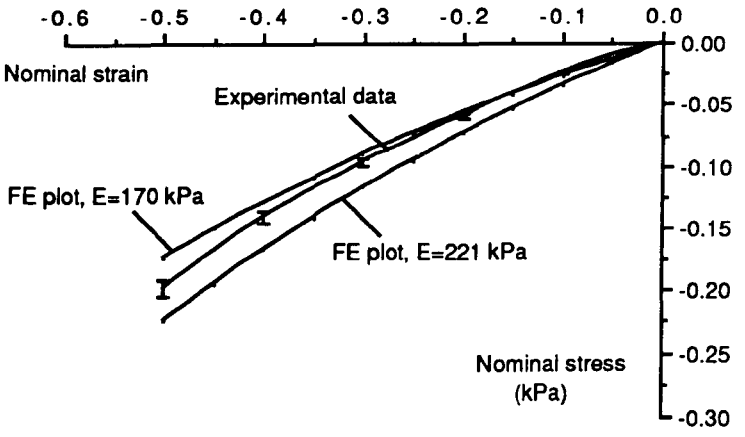

Figure 4.9 - Nominal stress versus strain for flat-tipped indenter, d/h=4.0.

Two further tests used the 15 mm diameter indenter with a 7.5 mm thick layer of Q3-3320 and the 25 mm indenter with a layer 12.5 mm thick. This gave further data for an aspect ratio of 2.0. Plots of normalised stress versus strain for these tests appear in figure 4.10, together with that obtained using the 20 mm indenter.

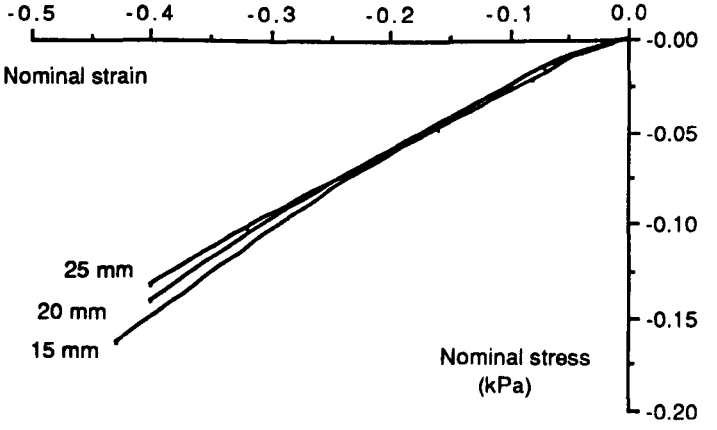

Figure 4.10 - Nominal stress versus strain for Q3-3320 layers of different thickness; flat-tipped indenter, d/h=2.0.

4.4 Round-tipped indenter tests.

Another 5 tests, similar to those discussed in the previous section, used round-tipped indenters to show effects of the aspect ratio and scale of tests. Again plots were obtained of nominal stress versus nominal strain. In this case, however, the nominal stress was calculated by dividing the applied load by cross-sectional area of the cylindrical part of the indenters.In an additional test to set used with the flat indenters, the 20 mm indenter was forced into a layer of elastomer 40 mm thick to give a ratio d/h of 0.5.

Stress-strain plots for these tests appear in figures 4.11 to 4.14, together with theoretical plots generated using the results of the FE models and values of E equal to 170 and 221 kPa.

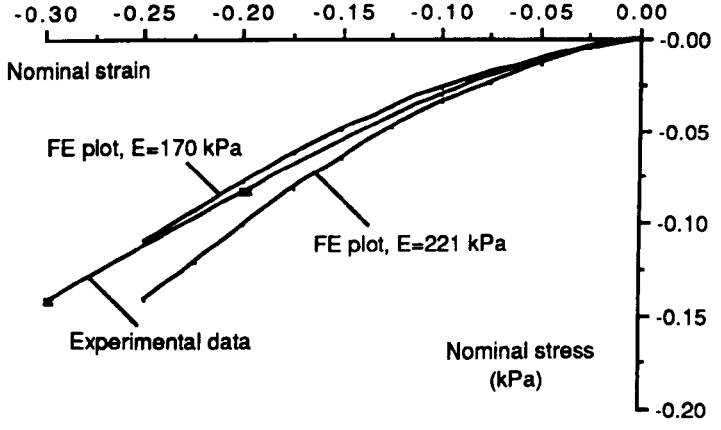

Figure 4.11 - Nominal stress versus strain for round-tipped indenter, d/h=0.5.

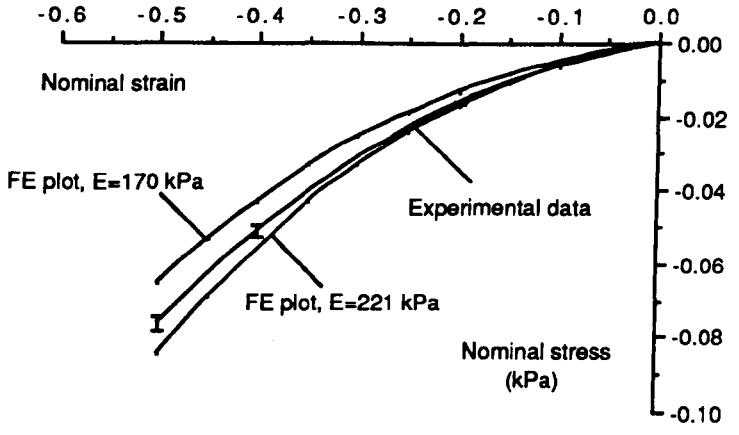

Figure 4.12 - Nominal stress versus strain for round-tipped indenter, d/h=1.0.

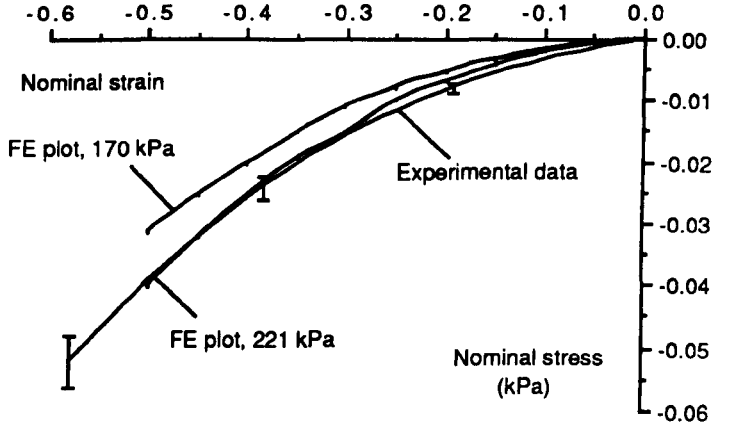

Figure 4.13 - Nominal stress versus strain for round-tipped indenter, d/h=2.0.

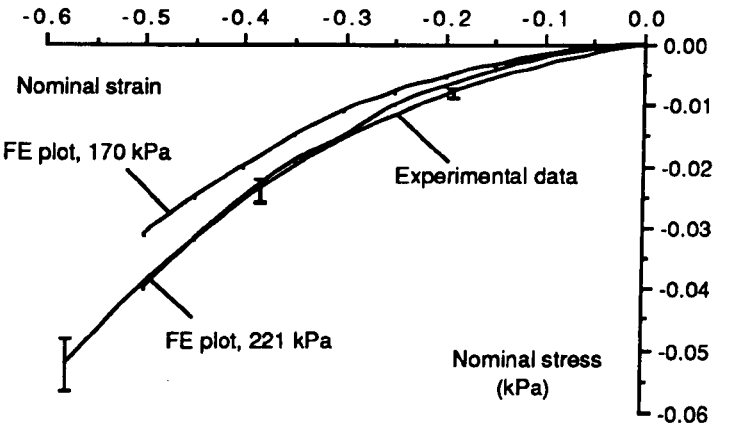

Figure 4.14 - Nominal stress versus strain for round-tipped indenter, d/h=4.0.

Tests, in which the aspect ratio was always 2.0, used 15, 20 and 25 mm indenters with elastomer layers 7.5, 10 and 12.5 mm thick respectively. Figure 4.15 shows stress-strain plots for the data measured.

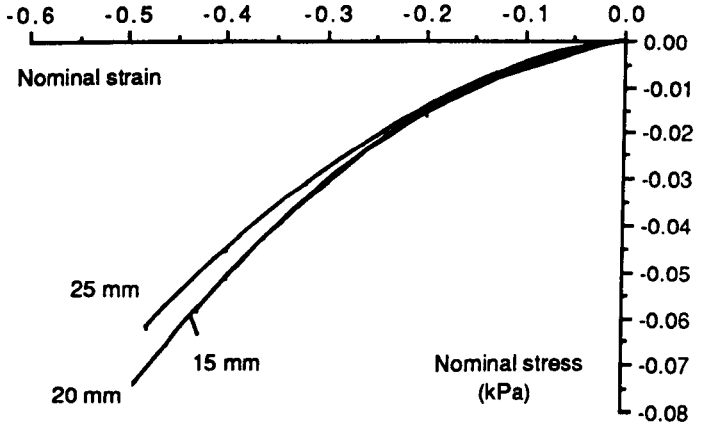

Figure 4.15 - Nominal stress versus strain for Q3-3320 layers of different thickness; round-tipped indenter, d/h=2.0.

4.5 Discussion of results.

Uniaxial compression tests

The shape of the experimental stress-strain plots obtained from the uniaxial compression test data agreed closely with plots generated by an exact theoretical analysis (figure 4.5). This would appear to indicate that the elastomer obeys a linear constitutive law for the range of strains measured. Assuming that Q3-3320 is homogeneous and isotropic, results indicate a mean value of compressive modulus of 170 kPa (±6%) and a Poisson ratio of 0.48.

The 'flatter' theoretical stress-strain curves due to the iterative FE analysis of uniaxial compression are, as expected, unable to follow the experimental plots (figure 4.6). The range of engineering strains measured was somewhat lower than occurred in the models since there was a tendency during testing for the specimens to 'squeeze out' from between the compressing plates at high strains. The 'adjusted' values of E used to generate the iterative FE plots are 30% greater than the exact values. This adjustment was indicated by comparison between plots generated by the exact analysis and the iterative FE analysis for strains in the range 0 to -50%. It was assumed that this adjustment would provide the best fit were data available over this range of strains.

The difference of approximately 12% in compressive moduli measured from specimens (a) and (b) represents the largest difference measured between the four batches used. These variations are thought to be primarily due to small differences in the base to catalyst ratio used, the degree of residual air in the mixtures and the prevailing atmospheric conditions during hardening. Localised variations in the mixture ratio and in the amount of residual air may, in fact, cause variations between specimens made from the same batch. Although there is no maximum thickness recommended by Dow Corning which will allow proper curing of the mixture, some variation in the hardness of the elastomer through the thickness of specimens is thought likely.

The strain rate and temperature at which the specimens were tested were controlled within limits that are expected to cause negligible errors. Despite the use of lubricating oil any remaining effects of interface friction are less easily evaluated. With dry perspex plates the lateral strains are resisted by frictional forces and 'bulging' at the sides is significant. Visual inspection of specimens during compression testing where the interface was lubricated showed little evidence of 'bulging' and this may indicate that frictional effects were very small under these conditions.

Indenter tests

In the flat tipped indenter tests, the trend predicted by the results of the FE models was confirmed experimentally since a reduction in d/h caused an increase in the gradient of the nominal stress versus strain curves.

For each experimental run, plots of nominal stress versus strain agreed more closely with the theoretical curves generated using the exact modulus rather than the 'adjusted' modulus. This would appear to indicate that errors due to the shortcomings of the FE analysis are smaller than in the models of uniaxial compression over the same range of nominal strains; however, during experiments, residual strains were observed if a flat indenter test was repeated in rapid succession. This indicated a component of deformation that was not purely elastic under these conditions; local plastic deformation or creep may have occurred at the edge. If this deformation takes place, a linear stress-strain relationship is not obeyed.

In the round-tipped indenter tests, reducing d/h was also found to cause an increase in the gradient of nominal stress versus strain curves from both experimental and theoretical data.

The experimental plots, however, showed better agreement with theoretical curves generated from FE models using the 'adjusted' value of E equal to 221 kPa rather than the 'exact' value. Thus it would appear that errors in these models are similar in size to those occurring in models of uniaxial compression. The exception to this rule was where d/h was 0.5; however, the experiments in this case departed from the relevant model in two ways. Firstly, the aspect ratio of the specimen differed significantly from that modelled since the manufacture of a large volume of elastomer in one batch was difficult. Secondly, indentation caused the specimen to buckle, its edges curling up off the base of the test machine above strains of about -15%. In all other tests, the elastic layer was at least as wide as was modelled and the surface tension/capillary effects in the lubricating oil under the specimens prevented buckling.

The plots of nominal stress versus strain for tests in which d/h was 2.0 and the indenter size and specimen thickness were varied, show that measured stress for a given strain was larger with thinner specimens. This was true with both types of indenter and would appear to bear out the argument that stiffness of the elastomer layer reduced with distance from the surface and thus thinner specimens are harder. If the differences between these tests were due to frictional effects, an increased indenter size,

and thus contact area, would be expected to increase frictional forces and thus the measured 'system' stiffness. This is contrary to the findings.

In summary, for engineering strains in the range 0 to -50% a value of Young's modulus 30% in excess of the exact value has been used to describe a uniaxial compression test and indentations with a round-tipped indenter with a reasonable degree of accuracy. As a first approximation, it shall be assumed that this modulus will be able to describe behaviour in other models in which primarily compressive deformations occur. The theoretical data from the round-tipped indenter models may be fitted to indentation data from tests on another material and a value of modulus may thus be estimated that is suitable for subsequent use in iterative FE models.

Chapter 5

Evaluation of limb tissue geometry and modulus on an amputee subject.

5.0 Objective.

The aim of the CAE study overall is to create a 'first generation' limb model to identify the key parameters which influence interface loads. The objective of the work presented in this chapter is to obtain a realistic set of data defining the geometry and mechanical properties of a residual limb which may be used in the FE limb model. For the purposes of the current study, the tissues are separated into bones and 'soft tissues'.

To evaluate meaningful average measurements objectively will probably require a study on a large number of amputees and this was unjustified at present. The data collected, therefore, were based upon measurements taken on a single amputee who was subjectively chosen by his prosthetist as 'average'.

5.1 Evaluation of geometry.

In a '2-phase' model, measurements are required of both the external shape of the residual limb and the shape of the bone structure within.

Measurement of external shape has been discussed in chapter 2 in which the digitisation of plaster wraps is described. Although there is inevitably some distortion of the tissues by the plaster bandages used in this process, pressures on the limb due to the cast are expected to be small and experience with the CASD system show it to be reliable as a starting point for socket design. Another reason why this technique was used is that the CASD system fixes a 'neutral' axis to the measured data for subsequent design of sockets. The rectifications, which displace the tissue surface to form the socket shape, are made with respect to this axis. The benefits of this will become more evident when the model is described (Chapter 8).

Measurement of the shape and location of the internal bone structure is more difficult. The most accurate methods are probably computer-aided tomography (CT) or magnetic resonance imaging (MRI). Current machines which employ these techniques, however, require the subject to lie flat during scanning. The distortion to the soft tissues that results will cause the relationship between the bones and the external

surface to differ from that in an upright position. This counteracts the benefits of the accuracy of these methods.

Some investigators have devised algorithms capable of generating full bone shape data from few measurements using a parametric scaling [MILLER80,COOPER86]. None of the publications, however, provide information that is directly useable for current purposes.

To produce the required data, hybrid 'scanning' and 'scaling' technique was used which gathered data from 2 readily available sources. Firstly, a pair of X-rays of the amputee's residual limb were taken in the frontal and sagittal planes and these were used to establish the general dimensions of the bone structure and its location within the limb. Secondly, cadaver bones of approximately correct dimensions were selected and measured using the CASD digitiser. Although there were inevitably some differences between the cadaver bones selected and the subject's own bones it was felt that a realistic set of data could be defined in this way.

The X-rays were taken with the subject in an upright non load-bearing position, wearing a polypropylene 'shell' which was produced in a RAPIDFORM machine. The shape of this shell was defined by measurements taken from a plaster wrap. Magnification was measured by placing a rule in each exposure and was small since a large separation distance was used between the X-ray machine and the subject. The outline of the bones was well represented; however, there was some difficulty in determining the tissue surface. Nevertheless, the bold lines in figure 5.1 show tracings of the bones and tissue surface which are expected to follow the appropriate silhouettes within one or two millimetres. Some gapping was shown between the limb and shell in the X-rays.

To create the 3-dimensional bone data, a skeleton tibia, femur, fibula and patella were first chosen. By comparison with measurements from the X-ray views, these were assembled as a unit using adhesive tape and this unit was mounted in the chuck of the digitising machine on a lockable ball-joint apparatus which permitted both rotation and shift relative to the axis of rotation of the chuck.

The bone unit was measured as a set of radial values taken every 5°, in 'slices' axially spaced 1/4" apart. To check the alignment of these data relative to the external shape data, anteroposterior and mediolateral 'strips' from both data sets were plotted together on a common axis. After a few iterations of measurement and realignment,

reasonable agreement was achieved between these plotted 'views' and those obtained by X-ray.

For the final iteration of measurement, the bone structure was digitised 'slice by slice', i.e. not on the helical path used to measure plaster wraps. Each slice was measured three times and averages of corresponding radii were taken. To 'smooth' these data, a PASCAL program was written which calculated new radii using a running average filter over 9 points.

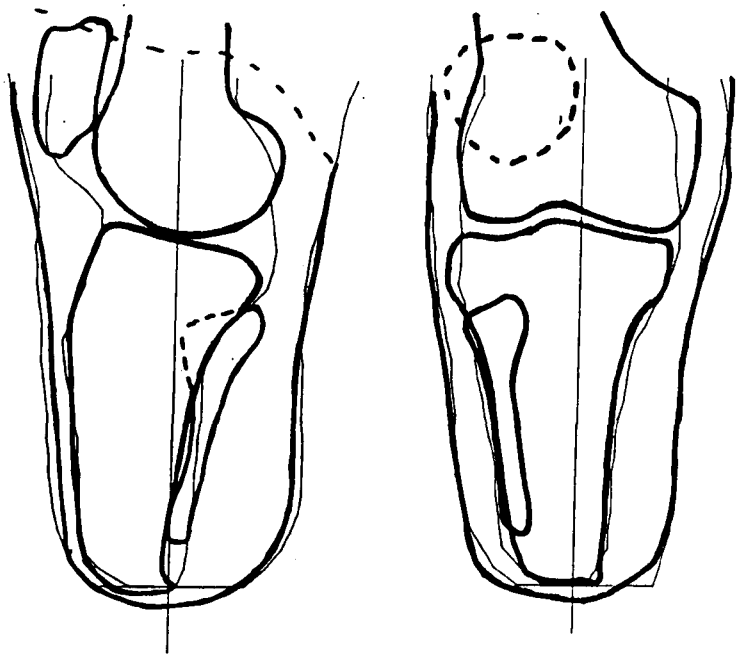

Figure 5.1 - X-ray tracings superimposed upon plots of measured geometry of bone structure and external shape.(scale 1:2.25 approx.)

In figure 5.1, the feint lines are the measured bone and external shape data plotted about a common axis. The PASCAL program which was written to produce these plots calculates the outline of a silhouette strip. For the medial view, this assumes that the anteroposterior plane passes through the reference point on the patellar tendon and the axis of measurement of the bone and external geometry. The maximum dimension of the discrete data in the viewing direction is then calculated for each slice in both data sets to build up the complete silhouette strip. In the mediolateral plane, the silhouette is found similarly, but a perpendicular viewing direction is assumed.

Although deviations exist between the measured and X-ray images in figure 5.1, there are no differences in the thickness of tissues that appear unrealistic. Because the subject's patella, and hence patellar tendon reference point, is externally rotated in the X-ray views, there may be a difference between the viewing directions of the two images and this could account for the deviations seen between the 2 representations of the external surface.

5.2 Evaluation of modulus.

In this section, measurements are presented of indentations into the soft limb tissues of the amputee subject. The test data are used to estimate values of an elastic soft tissue modulus. A series of pilot tests is discussed first which aimed to discover the practical aspects of measuring tissue indentations and to assess the implications of the assumption of time-independent mechanical behaviour.

5.2.1 Pilot tests.

Apparatus

In the pilot test, the Zwick 4074 testing machine was used to measure indenter loads and deflections. Although not ideally suited for *in vivo* testing this is a ready calibrated rig with which strain rate can be controlled and a wide range of loads and deflections can be measured. Tests using this apparatus were somewhat uncomfortable for the subject and therefore only an asymptomatic volunteer was used. The two sites chosen for testing were located at the patellar tendon reference point used by the CASD system and in the popliteal region on the posterior aspect of the limb approximately 100 mm distal of the knee joint. The applied load versus deflection response of the 20 mm diameter hemispherically tipped indenter was used to assess the tissues.

For accurate measurement of indentations into the soft tissues, rigid support of the underlying bone structure is required. This is difficult, however, since supporting loads must be transferred to the bones via soft tissue. In an attempt to minimise movements of the bone structure, the subject's limb was placed upon a polythene bag 'cast' part-filled with plaster of paris which rested on the base of the machine. In this way the

supporting area is large and interface pressures on the underside are low. Deformations of the supporting soft tissues and thus deflections of the bones should also be small.

Measured load versus deflection response

As is commonly experienced with measurements on human subjects, there was a wide variation in results when tests under the same conditions were repeated, despite careful location of the test site and control of the strain rate. Figure 5.2 shows the variation between results encountered in two series of tests on the patellar tendon site.

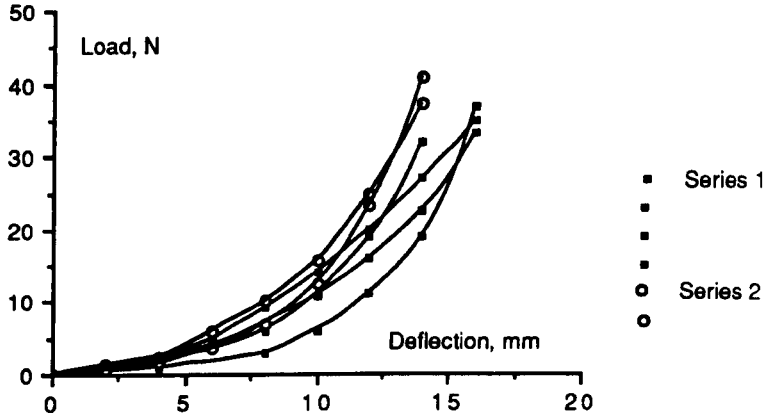

Figure 5.2 - Load versus deflection response of indenter at patellar tendon site.

Prior to each test series, an initial preconditioning procedure applied two load/unload cycles up to the maximum comfortable load. The subject stood up in between the individual tests in a series and took a few paces during a period of approximately two minutes. A constant strain rate was applied in these tests using a crosshead speed of 50 mm/min. The series (1) and (2) of figure 5.2 took place several days apart and thus the longer-term variations between series would appear to be more significant than the short-term variations within a series. This was also true at the popliteal site. For this reason, comparisons made in the pilot tests are between tests performed in a single series. Peak loads in the pilot tests of the order of 70 N were applied. Since this magnitude of load caused discomfort, the maximum load to apply in a test on an amputee was estimated to be approximately 50 N.

Effect of muscle tension

The effect of muscle tension upon the stiffness of soft tissues subjectively appears significant by simply 'prodding' in a muscular area of the body in tensed and relaxed states. An error in measurement of tissue modulus supplied for use in an FE model, therefore, may arise if tension in the muscles differs between taking such measurements and donning and loading a prosthesis.

In practice, a change in muscle activity *during* loading is probable, resulting in a variable tissue modulus. In the first generation model, such complexities are not dealt with; however, the magnitude of the maximum likely errors was evaluated by measuring the indenter load versus deflection response with the subject's muscles in 'tensed' or 'relaxed' states. The tensed states at the patellar tendon and popliteal sites were produced by a voluntary contraction of either the quadriceps or the calf muscles. Results from these tests appear in figure 5.3.

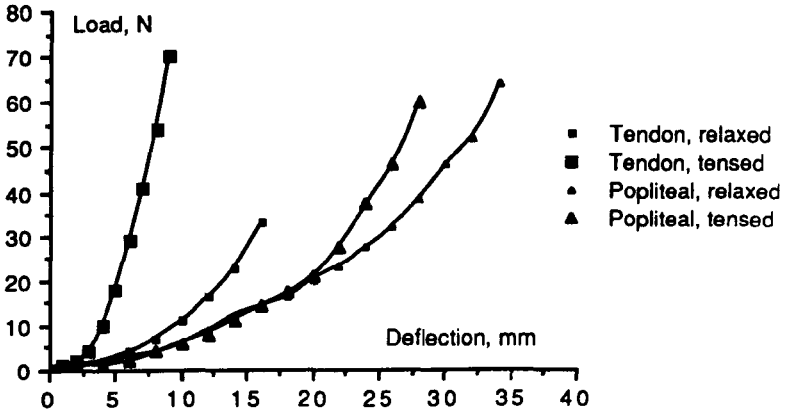

Figure 5.3 - Effect of muscle contraction upon measured indenter response.

Thus tensing of the quadriceps, which in turn produces tension in the patellar tendon, resulted in applied loads up to ten times those required with relaxed muscles. At the popliteal site with contracted calf muscles, a far smaller effect was apparent and occurred mainly in the latter stages of indentation.

Since PTB sockets are designed to bias loading towards the patellar tendon, the overall distribution of interface loads may be greatly affected by the stiffness of tissues in this area. With muscles relaxed the patellar tendon is 'slack'. Contraction of the

quadriceps produces significant movement of the patella proximally before all 'slack' in the tendon is taken up and sufficiently large tensile forces are produced to extend the knee. In practice, there appears no reason for an amputee to tense his quadriceps while donning his socket and, since there is likely to be sufficient 'slack' in the tendon to accommodate the socket contours at the bar, the stiffness during this phase will probably be as described by the 'tendon relaxed' curve. When load-bearing, however, knee flexion is encouraged by socket alignment and this must be resisted by an extending moment. The tendon, therefore, will become tensed to produce this moment and will be subjected to an increasing tensile force as load is borne and the moment increases in magnitude. For the current study, the changing stiffness of the patellar tendon is not modelled. Future work should investigate the sensitivity of results to variations in this stiffness.

Apart from the tensing of the quadriceps to resist knee flexion, stance will generally be maintained using little muscle activity and thus low energy consumption. The state of the other muscles, therefore, is not expected to differ significantly between non load-bearing measurements and standing.

Time-dependence

Viscoelastic tissue behaviour may affect measurements of a response to deformation and may cause loads to vary significantly with time.

The sensitivity of measured stiffness to the applied rate of straining was tested at both sites and figures 5.4 (a) and (b) show results from the patellar tendon and popliteal sites respectively at crosshead speeds of 20, 50 or 80 mm/min.

At both sites a greater dependence of measured stiffness upon strain rate is apparent in the latter stages of deformation and this effect is more noticeable in the popliteal region. For this site and at the patellar tendon, however, applied loads, due to deflections of less than 10 or 8 mm respectively, show little sensitivity to strain rate. If rough estimates of the initial thickness at these sites are respectively 45-60 mm and 18-24 mm, the minimum nominal strains corresponding to these deflections are -20% and -30%. A low dependence of measured stiffness upon strain rate thus appears to exist up to quite high nominal strains for the range of strain rates tested.

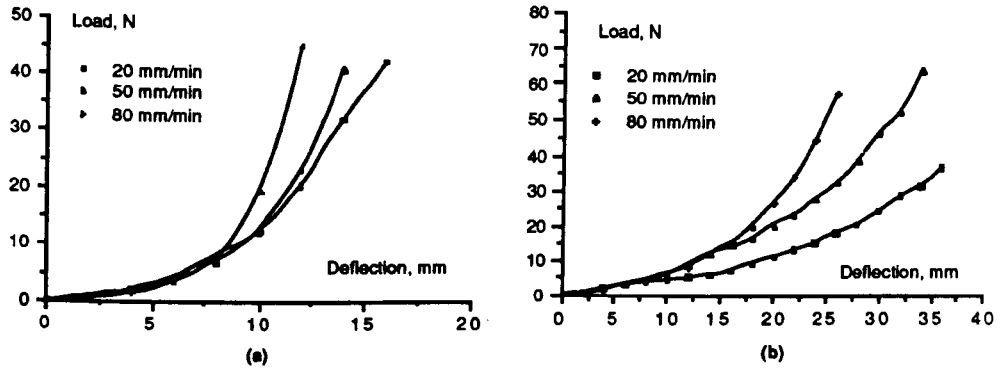

Figure 5.4 - Effect of strain rate upon indenter response.
(a) patellar tendon site.
(b) popliteal site.

For a standing amputee, creep in the soft tissues will probably cause the bone structure to slowly enter further into the socket, under the action of the fairly constant applied load, before fully coming to rest. Stress relaxation may also exist which reduces interface loads; however, this will generally be associated with further creep.

In Chapter 1, hypotheses due to a number of authors have been described which attempt to explain the mechanism of viscoelasticity in soft tissues. The flow of interstitial fluids away from loaded areas is popularly believed to cause the time-dependence. Stress relaxation beneath indenters is readily evaluated and may indicate the significance of time variations of tissue loads. In a comfortable socket, it is proposed that the pressure gradients which may cause fluid dispersion, thereby producing creep or stress relaxation, are lower than those which arise when an indenter is forced into a soft tissue layer by a displacement comparable with socket rectifications. Time-dependent effects observed from indentations into a free tissue surface, therefore, are expected to be more significant than in socket loading.

In the series of tests, stress relaxation was studied by applying strain at a constant rate with an indenter and then holding the strain fixed. The applied indenter load thereafter decayed to a constant value over a period of time. Two parameters were used to characterise this decay. The first of these was the ratio of the constant load, after which no relaxation could be detected, to the peak load which existed at the end of a

constant strain rate indentation. The second parameter was the time taken to reach this steady state.

Several factors were considered likely to influence the relaxation behaviour. These were mainly the location of the test site, the initial rate of applied strain, the magnitude of the peak applied load, the geometry of the test probe used, the stress state in surrounding tissues and the tension in the muscles. The possible combinations of these indicated a large number of tests and therefore only two states were considered for each factor.

These were :-

Location of tissue site:
(a) On patellar tendon
(b) In popliteal area

Applied rate of deflection of indenter:
(a) 80 mm/min.
(b) 20 mm/min.

Peak applied load:
(a) 60 N.
(b) 20 N.

Indenter used:
(a) 20 mm diameter, round-tipped indenter.
(b) 48 mm diameter, flat-tipped.

State of surrounding tissues:
(a) Unloaded.
(b) Loaded.
State of the musculature
(a) Relaxed.
(b) Tensed.

Tests failed in which muscles were tensed voluntarily by the subject since it was found to be impossible to maintain a steady state of tension over the full duration of a relaxation test and therefore only tests with muscles relaxed were performed. For the tests where the surrounding tissues were loaded, the indenter passed through an aperture in a thick steel plate. The plate rested across the limb with weights hung on either end and an estimated nominal pressure of approximately 50 kPa was applied in this way. The diameter of the aperture was 22 millimetres.

As many as possible of the combinations of the above were performed; however, the flat indenter was too large for the patellar tendon site and for tests in which the surrounding tissues were loaded only the narrower, round-tipped indenter was used. These latter tests were only possible at the popliteal site. Figure 5.5 is a tabulation of

the results of these tests. Two or three runs were used to produce the average values of load ratio and relaxation time given in this table.

Test number	Tissue site	Strain rate	Peak load	Indenter geometry	Surrounding tissues	Load ratio (%)	Relaxation time (s)
1	TENDON	LOW	HIGH	ROUND	UNLOADED	55	200
2	TENDON	LOW	LOW	ROUND	UNLOADED	54	175
3	TENDON	HIGH	HIGH	ROUND	UNLOADED	50	205
4	TENDON	HIGH	LOW	ROUND	UNLOADED	64	120
5	POPLITEAL	LOW	HIGH	ROUND	UNLOADED	82	100
6	POPLITEAL	LOW	LOW	ROUND	UNLOADED	95	50
7	POPLITEAL	HIGH	HIGH	ROUND	UNLOADED	78	90
8	POPLITEAL	HIGH	LOW	ROUND	UNLOADED	90	65
9	POPLITEAL	LOW	HIGH	FLAT	UNLOADED	74	175
10	POPLITEAL	LOW	LOW	FLAT	UNLOADED	89	50
11	POPLITEAL	HIGH	HIGH	FLAT	UNLOADED	69	80
12	POPLITEAL	HIGH	LOW	FLAT	UNLOADED	83	70
13	POPLITEAL	LOW	HIGH	ROUND	LOADED	74	170
14	POPLITEAL	LOW	LOW	ROUND	LOADED	77	105
15	POPLITEAL	HIGH	HIGH	ROUND	LOADED	60	160
16	POPLITEAL	HIGH	LOW	ROUND	LOADED	52	165

Figure 5.5 - Results of stress relaxation tests.

From the results, comparison is possible between pairs of tests in which one factor only is changed. For example, variations between tests carried out on the tendon or popliteal sites can be observed by making comparisons between test numbers 1 & 5, 2 & 6, 3 & 7, 4 & 8. In 3 of these 4 cases the load ratio was smaller, i.e. the fall in applied load was proportionally greater, and in every case the relaxation time was longer, for the test on the tendon. The mean load ratio for the tests at this site was 72.5% compared with 86.5% in the popliteal region.

Variations between comparable tests in which the applied strain rate was low or high can also be observed. In 7 out of 8 cases the load ratio was smaller where strain was applied at the high rate. The mean ratio in these tests was 71.8%. Where the lower strain rate was applied, a mean load ratio of 79.9% was measured. The relaxation time was longer in 50% of the high strain rate tests.

Comparisons are also possible between tests in which the peak load was low or high. In 6 of these 8 cases the load ratio was smaller where the peak load was higher and in 7 cases this meant a longer relaxation time. Mean load ratios of 73.6% and 78.1% were measured where the peak load was high and low respectively.

In each of 4 cases where the flat, 48 mm diameter indenter was used, the load ratio was smaller than in a comparable test using the other indenter; however this

corresponded to a longer relaxation time in only 2 cases. The mean load ratio measured with the flat indenter was 78.8% but was 86.5% with the round.

In all 4 comparisons where the state of the surrounding tissues only was different the tests with loaded tissues displayed lower load ratio and longer relaxation time. Mean load ratios with loaded and unloaded surrounding tissue were 65.8% and 86.5% respectively.

The general significance of each factor upon time-dependence was judged from the test data primarily on the proportion of tests in which relaxation effects were greater, i.e. where the load ratio was smaller and the relaxation time longer. The relative magnitude of load ratios was a second indicator of the significance of each factor; measurements of the relaxation time were less accurate than this parameter.

Based on these criteria, it appears that loading of the soft tissues has the most significant effect upon time-dependence. However, where the tissues were loaded, fluid dispersion may have occurred towards the aperture of the loading plate prior to indentation. An 'excess' of interstitial fluid, therefore, may have been present which was slowly dispersed by the action of the indenter.

The type of indenter used also appears significant. It may be that the negative pressure gradient away from the axis of the round-tipped indenter is more effective at forcing the interstitial fluids away during indentation than is the case with the flat indenter. Similarly, more fluid may disperse during the period of the low strain rate tests than with a high rate. In the cases where more fluid remains after indentation, a larger subsequent outflow and hence drop in applied load is expected.

Differences between the time dependence of the two sites was also found significant and this is probably due to the different subcutaneous structures. The influence of the level of applied load upon time-dependence appears to be the least in the factors tested.

From the results, it appears that a modulus based upon a high strain rate indenter test could cause the 'fully relaxed' indenter load to be underpredicted by up to 50%. It must be remembered, however, that this figure has been obtained from a constant strain test. In standing, applied *loads* will be fairly constant. Nevertheless, from the relaxation tests, it is recognised that time-dependence may significantly affect tissue loading and must be more fully assessed in future models. Creep tests on a residual limb contained within a socket may be especially of value.

5.2.2 Indentation tests on an amputee subject.

Apparatus

To take measurements on the amputee subject, an apparatus was produced which was capable of measuring loads and deflections for indentations in an upright non load-bearing position. This was a hand-held tool which was used to force the 20 mm diameter hemispherically-tipped indenter into the limb tissues (figure 5.6). Indentation took place through apertures in the wall of a stiff polypropylene shell which was worn by the amputee and provided the datum from which indenter displacements were measured.

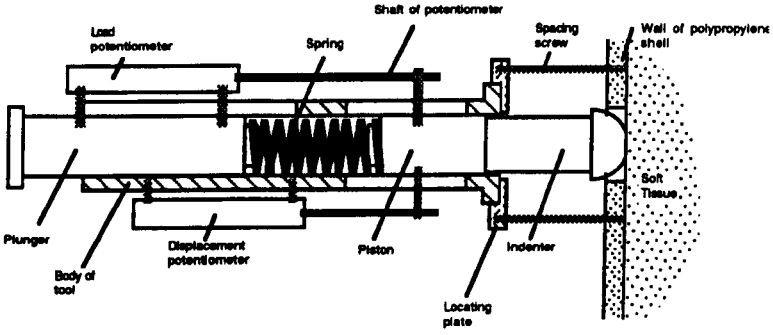

Figure 5.6 - Indenting tool.

(scale 1:2)

The body, plunger and piston of the tool and the locating plate were all manufactured from an acetal copolymer. The indenter screwed directly into the piston. Loads applied to the tissues were measured using the movement of the shaft of a linear displacement potentiometer to gauge the shortening of a spring by measuring changes in the distance between the plunger and piston. Displacements of the indenter were gauged by another linear potentiometer which was fastened to the body of the tool. Since the body was held firmly against the locating plate during indentation, these displacements were measured relative to the polypropylene shell.

A stabilised 5v power supply energised the two potentiometers (Sakae type 13FLP25A, 5kΩ) and the output voltages of these were connected to channels of a Digital ADV-11C analogue to digital converter (AtoD) card in a PDP-11/73 computer.

The polypropylene shell which located each test site was a replica of a measured plaster wrap was made from a thick preform. Distortions of the shell wall were

expected to be very small. The apertures through which the indenter passed were 22 mm in diameter and were located using marks made by the prosthetist on the original wrap. The four sites selected were on the patellar tendon, in the centre of the popliteal pressure region and at the centres of the anterior pressure regions medial and lateral of the tibia. Apertures were drilled by setting the drill bit normal to the surface of the shell by eye. To ensure that the indenter passed through the aperture without interference and that indentations were approximately normal to the surface, a locating plate was rigidly attached to the shell at each site using three spacing screws which threaded into the wall of the shell.

To calibrate the tool, a jig was manufactured from dural and consisted of a locating plate spaced approximately 40 mm above a flat, smooth base.

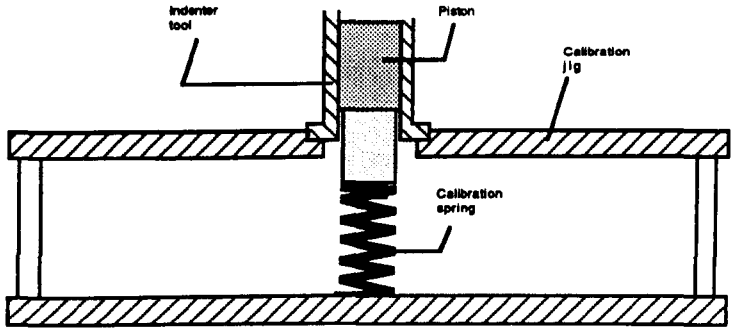

Figure 5.7 - Calibration jig for the indenter tool.

(scale 1:2)

The displacement potentiometer was calibrated using a 10 mm thick spacer placed in the jig. The load potentiometer was calibrated by using the tool to compress a spring of known rate (figure 5.7). The dynamic load calibration procedure was favoured to a dead weight calibration since frictional effects are likely to be similar to those during a test. A light oil was sprayed into the barrel of the tool prior to calibration and testing to give a smooth action of the moving parts and reduce fluctuations in these frictional effects which would yield errors in measured loads.

Test procedure

Calibration and measurement were controlled by a FORTRAN program running on the PDP-11/73. This was linked to a library of MACRO routines, LSILIB (a DECUS product), which specifically controlled the AtoD sampling and converted the 0 to 5 volt range of output voltages to integer values in the range 0 to 4095.

The first task was to calibrate the displacement potentiometer. The program requested that the indenting tool be placed flush against the locating plate of the calibration jig with the indenter resting on the top of the spacer. The output voltage of the displacement potentiometer was then digitised before a second voltage sample was taken with the spacer removed, allowing the indenter to touch the base of the jig. The two integer values were then used to establish the gradient and intercept of a linear relationship between digitised voltage and indenter displacement and this was used to calculate subsequent deflections. The linearity of this relationship over the full range of motion was verified with a test program which permitted digitised values to be compared with displacements measured with a dial gauge.

To calibrate the load potentiometer, the indenter was replaced by a spacer and this rested on a calibration spring of known rate which had been placed on the base of the jig. The program sampled the voltage of the displacement potentiometer continuously every 10 ms until load was applied to the plunger and a deflection of the spacer, by 0.1 mm, was detected. Thereafter, both potentiometers were sampled simultaneously, at the same rate as before, while the plunger of the tool was forced downwards compressing the calibration spring. Displacements were calculated from the raw digital data and these were multiplied by the spring rate to give applied loads. A regression algorithm was then used to give a linear relationship between the applied load and the output voltage of the load potentiometer from a least squares fit.

Measurement of loads and deflections took place after an estimate was entered into the program of the maximum comfortable indenter deflection from two or three preconditioning indentations. At the start of tests, the tool was placed against the locating plate with the indenter just touching the skin. As the plunger was pushed, the program repeatedly logged the displacement potentiometer until a measured deflection of 0.05 mm indicated that indentation was starting. Both potentiometer voltages were then sampled simultaneously every 50 ms and the digitised values were used to calculate loads and displacements. Measurement terminated when the estimated maximum comfortable indentation had been reached.

To check the rate of straining during tests, rough estimates of the initial tissue thickness at each site were used to calculate the rate of indentation corresponding to a target strain rate of $0.05s^{-1}$. The mean rates of indenter deflection over the two halves of each test were calculated from the data and, if either of these rates departed by more than $\pm 30\%$ of the target value, data were rejected. If the data were acceptable, these were written to a file.

Before using the procedure described above for *in vivo* testing on the amputee subject, a number of validation tests were carried out on layers of elastomer (Q3-3320) and data were compared with results obtained using the Zwick 4074 machine. Agreement was within a few percent over the range tested.

Results

Load and deflection measurements from 4 tests on the amputee subject at each of the 4 sites are shown in figures 5.8 (a) to (d).

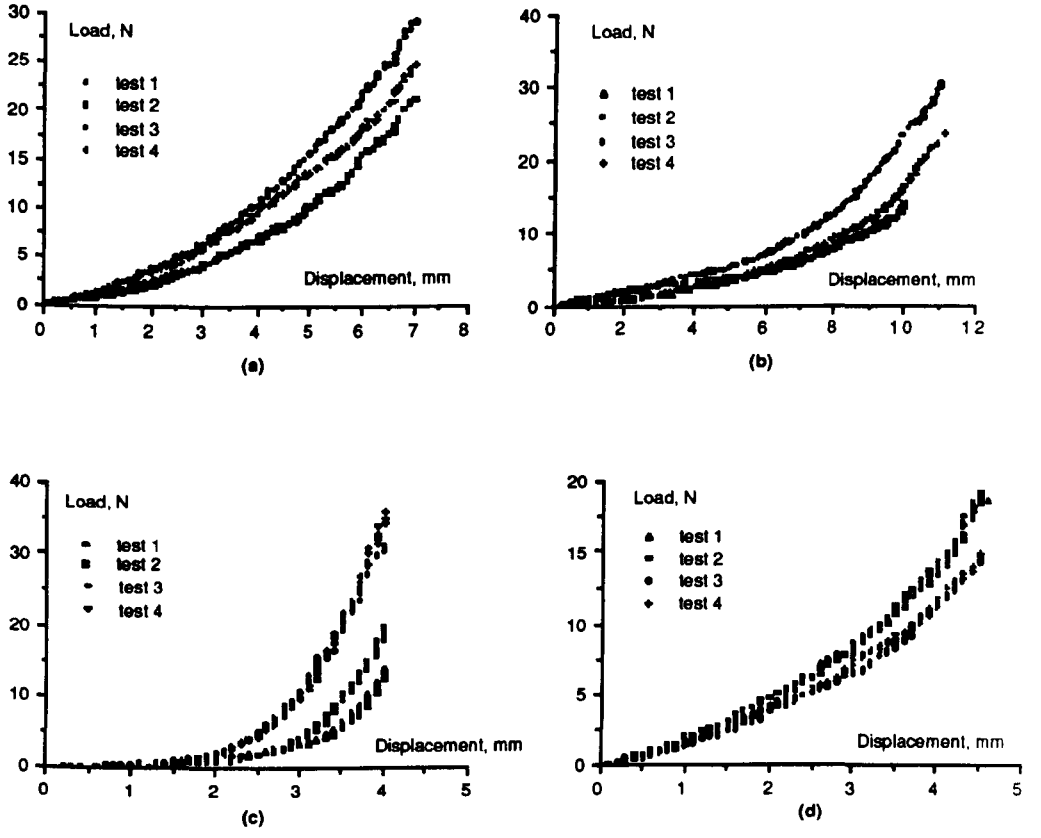

Figure 5.8 - Indenter load versus deflection at each site

(a) patellar tendon.

(b) popliteal.

(c) anteromedial.

(d) anterolateral

These generally show a similar degree of variability between runs as was experienced in the pilot tests. In the tests at the anteromedial site, however, it appears that some movement took place between tests 2 and 3 and that the tissues indented in the latter tests were of the order of 0.5 mm thinner than in the first two.

To deduce values of a tissue modulus, plots of nominal stress versus strain were prepared from test data of the most representative runs (figures 5.9 to 5.12). In these plots, strains were calculated using estimates of the initial thickness at each site from the X-rays and from the 'bottoming-out' observed in indentations. Thicknesses of 16, 30, 6, and 8 mm were used for the patellar tendon, popliteal, anteromedial and anterolateral sites respectively. These corresponded to values of d/h equal to 1.25, 0.67, 3.33 and 2.50 respectively.

Theoretical data for each aspect ratio were prepared using linear interpolation between the predicted stresses and strains presented in Chapter 3 for aspect ratios of 0.5, 1.0, 2.0 and 4.0. These curves, however, correspond to a unit modulus. To evaluate an appropriate modulus at each site, therefore, the interpolated curves were fitted to the plots of test data using a linear scaling of the predicted nominal stresses, as would be obtained by repeating the FE models with a different value of E. The fitted curves also appear in figures 5.9 to 5.12. For the patellar tendon, popliteal, anteromedial and anterolateral sites, curves were fitted using moduli of 145, 50, 50 and 120 kPa respectively. The relative magnitudes of these subjectively appear reasonable since the patellar tendon and anterolateral sites both felt 'firmer' than the other two.

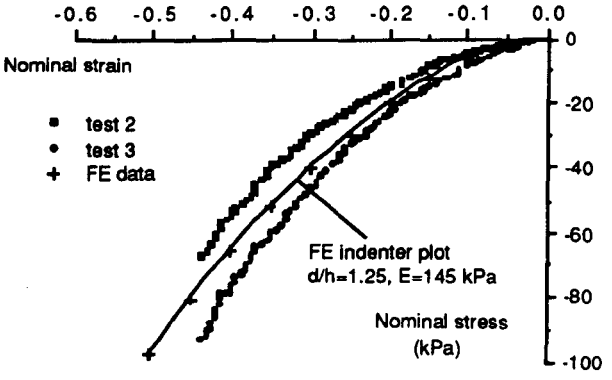

Figure 5.9 - Nominal stress versus strain for indentations at patellar tendon site.

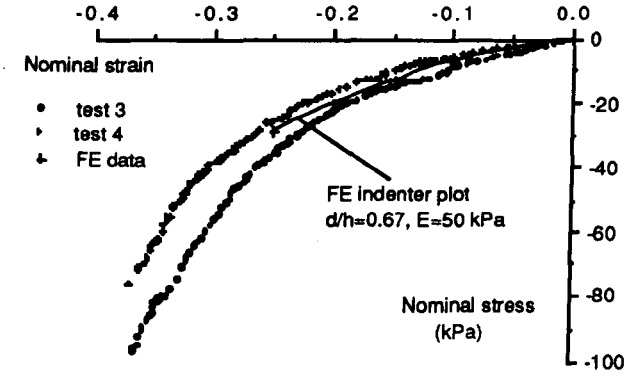

Figure 5.10 - Nominal stress versus strain for indentations at popliteal site.

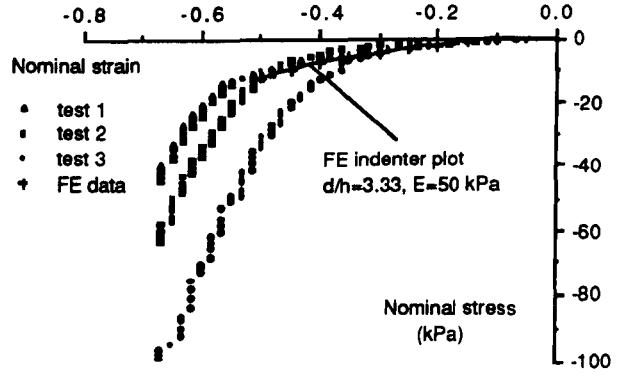

Figure 5.11 - Nominal stress versus strain for indentations at anteromedial site

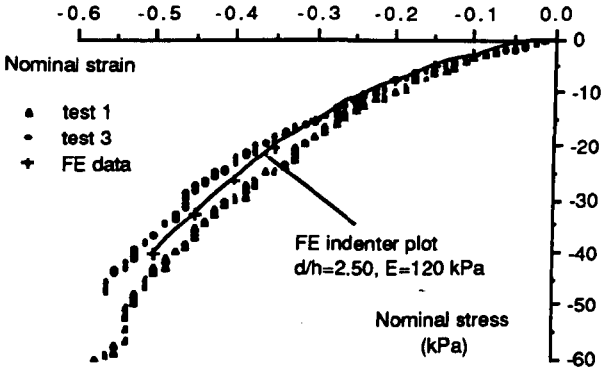

Figure 5.12 - Nominal stress versus strain for indentations at anterolateral site.

Discussion so far has been limited to the soft tissues. In view of the magnitudes of the moduli evaluated, however, it seems unlikely that strains in the bone structure will be significant. A Young's modulus for the tibia of 1.2 GPa has already been quoted. Under the same applied loads, therefore, soft tissue strains may be in the region of ten thousand times those of bones.

Displacements of the bones relative to one another are less easily estimated. For the tibia and fibula, the compressive loads experienced seem unlikely to produce significant relative displacements. When fully load bearing, the patellar may be retained by a tensed tendon. The tensile modulus for human tendon is approximately 250 MPa [YAMADA70]. A conservative estimate of patellar displacement might assume that 30% of a bodyweight of 700N is carried in a tendon with a cross-sectional area of 30 mm^{-2} (3 mm thick by 10 mm wide) and length 30 mm. Under these conditions a vertical displacement by approximately 0.8 mm of the patellar relative to the tibia may be assumed. Even this conservatively estimated displacement may not to disturb the pressure distribution greatly; however, sensitivity to the patellar displacement should be tested in future models.

For current purposes, a rigid structure comprising each bone is assumed.

5.3 Discussion of results.

The measurements of bones and external limb shape appear to have defined a realistic set of data which may be used in a limb model. The required accuracy with which data must be produced for an FE model will be more precisely known after some experience with these models.

Although this study has used a simple approach, further research may use a large database of bone measurements and from these improved algorithms may be developed to generate shape data more accurately from basic measurements. The positional relationship between the bones of below-knee amputees may be studied from CT or MRI scans of a number of subjects and this may help develop software capable of assembling individual bone data into a structure.

In a final system, anteroposterior and mediolateral X-rays may be used to obtain the basic bone measurements from which individual bone shapes may be generated. Computer graphics may be used thereafter to check the assembled limb model by comparison with the X-ray views.

The fit obtained between the predicted and measured data (figures 5.9 to 5.12) is surprisingly good since the predicted curves have been generated assuming a linear constitutive law and the experimental curves are from measurements on materials thought by many to be highly nonlinear. The shape of plots from the firmer patellar tendon and anterolateral sites is most similar to the theoretical plots. Most previous measurements of tissues in compression have been taken at sites where only a thin layer of skin and subcutaneous tissues covers bone. At the anteromedial site in the current test series, the tissue layer was the thinnest and the response was the most nonlinear.

A further assessment of linearity may be possible by comparing results from indentation tests on tissues with data from tests on an elastomer, which has been shown to approximate a linear constitutive law. Set of these data obtained in the current study, however, are for different aspect ratios and accurate comparisons are not possible.

The estimated values of appropriate tissue modulus are approximate since they incorporate a number of assumptions; however it is felt that better estimates have been achieved than was previously possible. The assumption that the limb tissues are elastic, homogeneous, isotropic and near-incompressible previously has been used

successfully as a first approximation in analyses of tissue deformations. The set-up during indentation, however, differs from that modelled in other ways.

Neither the tissue layer nor the underlying bone structure were flat and continuous as modelled. This deviation was probably most significant at the patellar tendon site, where a recess behind the tendon in the bones exists. Improved values may be obtained by repeating the indenter models, applying indentations to a mesh which represents the geometry of the actual test site. This would, however, require more accurate shape measurement than has been obtained. Alternatively, variations in the underlying bone geometry may be assumed and the sensitivity of the load versus deflection response to these variations may be studied.

In the frictionless FE indenter models, the upper surface of the near-incompressible elastic layer was free, not enclosed as in the experiments. The nodes on this surface, however, all moved downwards when indenting displacements were applied. Material under the indenter was therefore displaced sideways or was compressed. Because the residual limb is enclosed in a rigid shell during indentation, it might be assumed that there is great resistance to the reduction in volume introduced by the indenter. In practice, however, this volumetric reduction is small and contact of the limb and shell is not intimate over the full interface. The indentation, therefore, may have caused tissue near the testing site to move into an interface gap. Some compression, i.e. reduction in volume, of the limb may have occurred where blood inflow is restricted or where interstitial fluids move outside the shell.

Errors in the estimates of the initial thickness of the tissues might be expected to produce comparable errors in the resulting estimates of modulus. In fact this is not so, since, for example, an overestimated tissue thickness will result in underestimated strains and steeper stress-strain curves than in reality. An underestimate of the aspect ratio, d/h, will be made, however, and the theoretical stress-strain curves used for comparison with the experimental plots will also be steeper than in reality. For the results presented, each modulus was re-evaluated using a wide range of estimates for the tissue thickness (±20% of the values given). Deviations of the predicted modulus were all within ±12%.

In summary, sets of data describing the external shape and internal bone structure of a residual limb have been obtained and values of Young's modulus have been found to be:

145 kPa on the patellar tendon,

50 kPa in the popliteal region,

50 kPa on the anterior aspect, medial of the tibia,

120 kPa on the anterior aspect, lateral of the tibia.

These moduli have been evaluated from comparisons with the results of FE models and are assumed to be suitable for use in further models.

Chapter 6

FE models of idealised residual limbs.

6.0 Introduction.

By modelling idealised limbs with simplified geometry and mechanical behaviour, experience may be gained in techniques of FE analysis of a load-bearing residual limb and in the general patterns of interface loads that result. Axisymmetric models are both easier to define and cost less, in computer time, than full 3-dimensional models. In this chapter, four simple axisymmetric models are used first to demonstrate the influence of friction and distal-end bearing upon interface loads. Geometry is varied and rectification is included in subsequent models.

6.1 Frictional and end-bearing effects.

Using the mediolateral and anteroposterior X-ray views of the amputee subject (Chapter 5), an idealised axisymmetric structure consisting of a single rigid bone covered by an elastic soft tissue layer was constructed by taking average dimensions of the bones and soft tissues at a number of levels along the residual limb.

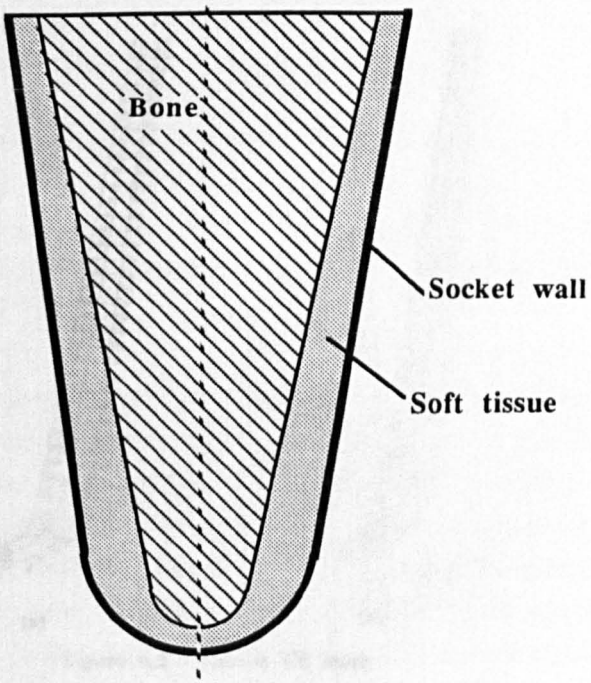

Figure 6.1 - Idealised limb geometry.
(scale 1:2 approx.)

A simple conical shape which blended into a segment of a sphere was used and this is shown in figure 6.1. Bisecting this figure along its axis yields a generator plane which was used to define the shape of the mesh of axisymmetric FE models. Both the bone structure and the socket were assumed rigid in these models and only the soft tissue layer was represented by finite elements. Each mesh was made up of elements of an elastic material which was homogeneous and isotropic, with a Young's modulus of 170 kPa and a Poisson ratio of 0.45.

In the first models, no rectification was applied and the internal surface of the modelled socket had the geometry of the external surface of the limb. The socket wall was modelled by applying restraints to nodes on the external surface of the soft tissue layer. Restraints were applied either to permit no movement of these nodes (figure 6.2(a)) or such that displacements occurred only along a local axis which coincided with the socket wall. The former case therefore models a 'totally rough' limb/socket interface (MODEL 'A') and the latter an interface which is 'frictionless' (MODEL 'B').

In the frictionless model, nodes at the conical sides of the socket moved along an inclined linear axis. Distally nodes were constrained radially about the centre of curvature of the distal end.

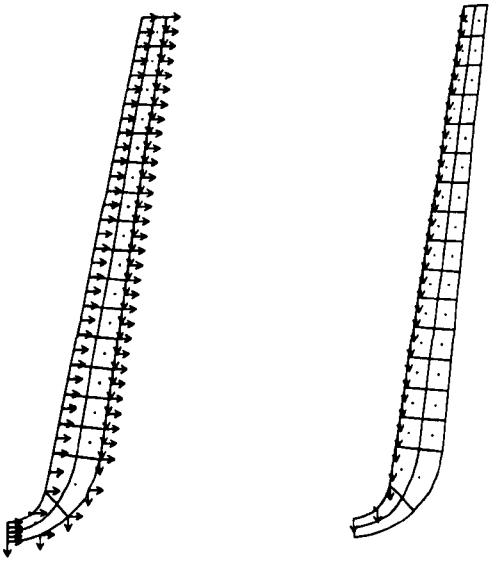

(a) (b)

Figure 6.2 - Coarse FE mesh

(a) Restraints to model socket wall.

(b) Displacements to bone structure.

Sockets designed by the UCL CASD system provide relief at the distal end. Models 'C' and 'D', therefore, were created with 'totally rough' and 'frictionless' conditions respectively but with no distal end contact. The algorithm used by the CASD program provides clearance between the limb and socket below a level approximately 1.5 inches from the distal end and for these models, therefore, no restraints were applied to surface nodes where clearance existed.

In these, and all limb models presented in the thesis, the socket wall is represented as a rigid boundary to the soft tissue mesh. Deformations, primarily in the soft liner, may alter the shape of the limb/socket interface and hence the load distribution here. For the present study, this additional variable was considered to be an unnecessary complexity to models and a rigid socket was felt more likely to develop contrasts in the pressure distributions.

Loading for all models took place via the rigid bone structure. This was achieved by prescribing vertical downward displacements to each node which lay along the internal surface of the soft tissue layer. This is shown on a coarse 34 element trial mesh in figure 6.2(b). In order to maintain the shape of the bone structure during loading, these nodes were restrained from moving horizontally. This technique therefore assumes no movement between the bone and soft tissue layer immediately adjacent.

The FE models were produced to predict interface loads and thus meshes were sought for each model which could yield accurate values of nodal reactions at the interface. Details of the mesh design process, for models 'A' to 'D', appear in Appendix D along with stress distributions in the most highly stressed region of each model.

Ten steps of bone displacement were used in iterative analyses of the final mesh to produce final values of interface reactions for each model. The benefit of the iterative solutions was to develop the load distributions of the various models better rather than to change the predicted vertical stiffness , i.e. the vertical bone displacement divided by the total vertical reaction at the interface. In model 'A' for example, the stiffnesses, calculated using either a linear or an iterative analysis in 10 steps, were only 1.3% different. The reaction at the interface node on the axis of symmetry, when calculated by an iterative solution, however, was 5.2% greater than in the linear analysis.

Pressure profiles

To obtain values of normal pressure along the limb/socket interface, a FORTRAN program was written which processed the calculated interface reactions. The components of the reactions, in a direction normal to element side, were found and summed for each element. Reactions at the corner nodes were shared between adjacent elements according to the ratio of their side lengths. The area of the element face was the area around the side of a frustrum for the conical part of the model and the surface area of a segment of 2 bases at the distal end. Interface pressure was calculated as the total normal load divided by the face area.

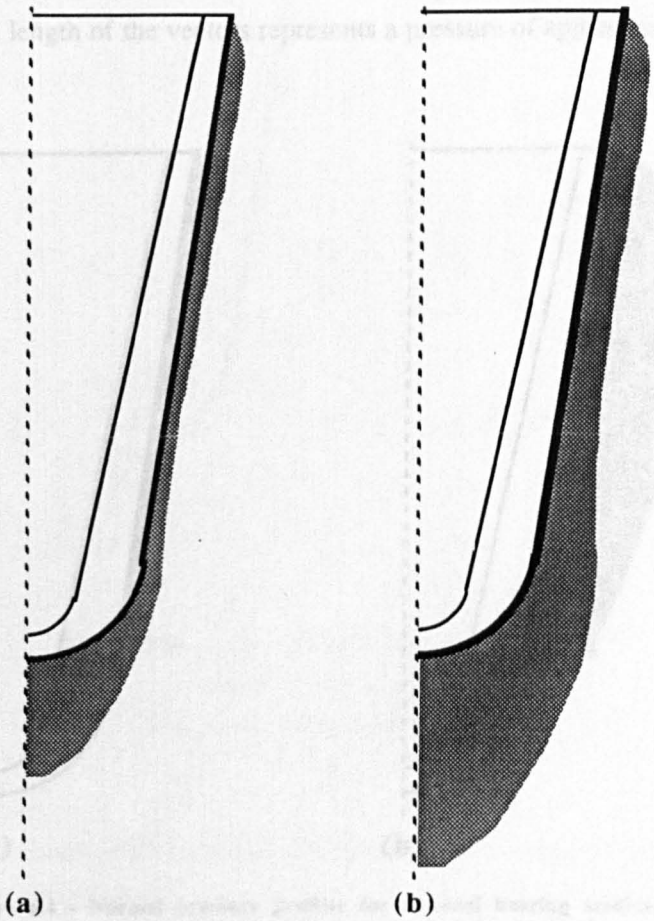

Figure 6.3 - Normal pressure profiles for end bearing models.

(a) model 'A'

(b) model 'B'

For a meaningful comparison between models, pressure distributions were prepared for the case where approximately half the body weight of the amputee subject is supported. An iterative process was used where the bone displacement was adjusted until a 350N vertical reaction (i.e. just over 5 stone, 70 lbs.) was produced.

Figures 6.3 and 6.4 represent normal pressure distributions under this applied load with and without end bearing respectively. Both interface conditions are shown. In these figures, the shaded region describes the profile of normal pressure calculated at the interface with the socket wall. The boundary of this region has been defined by a series of vectors normal to the surface of the elastic layer at the midside of each element. Each 1 mm length of the vectors represents a pressure of approximately 3.6 kPa.

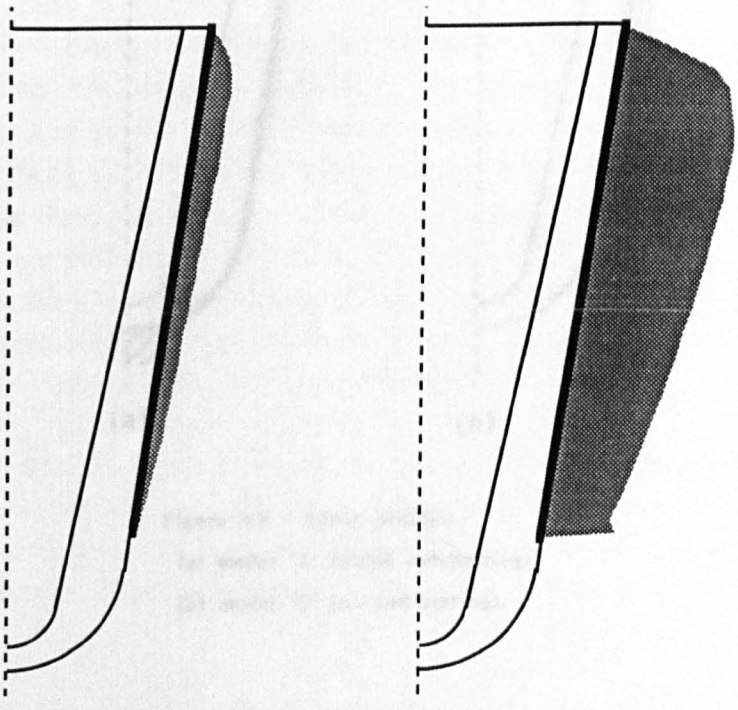

Figure 6.4 - Normal pressure profiles for non-end bearing models.
(a) model 'C' ('totally rough').
(b) model 'D' ('frictionless').

Shear profiles

Shear forces at the interface in the 'totally rough' models were calculated by another FORTRAN program which took the components of reactions parallel to the surface of

the socket wall. The distributions of shear force per unit area at the interface are shown in figure 6.5 for models 'A' and 'C'. Each 1 mm of normal displacement of the profile from the limb surface represents a magnitude of approximately 2.7 N mm^{-2} in these diagrams.

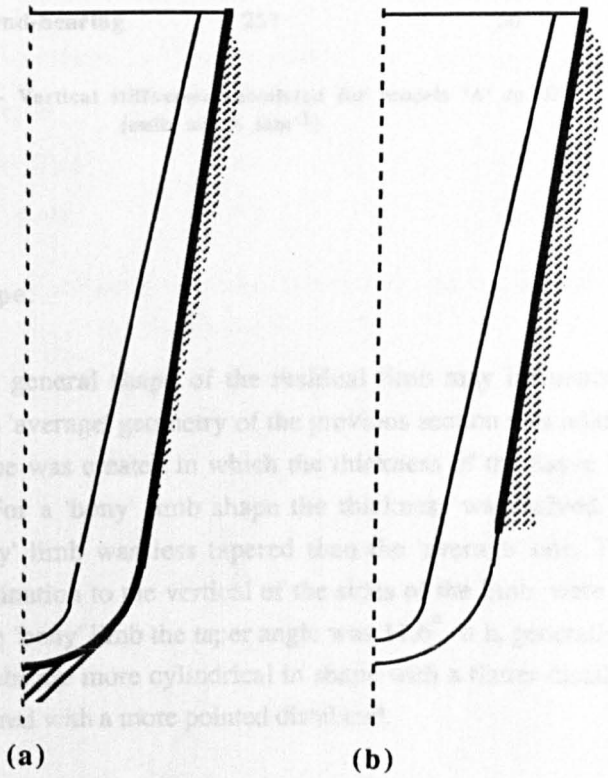

Figure 6.5 - Shear profiles.
(a) model 'A' (distal end-bearing).
(b) model 'C' (no end-bearing).

A difference in the direction of shearing action is shown by the change of hatching in the diagram for the end-bearing model.

A summary of the vertical stiffnesses the four linear models appears in figure 6.6

Interface conditions:	Totally rough	Frictionless
End-bearing	330	164
Non end-bearing	257	50

Figure 6.6 - Vertical stiffnesses calculated for models 'A' to 'D'. (units are N mm^{-1})

6.2 Effect of limb shape.

To demonstrate how the general shape of the residual limb may influence the interface loading pattern, the 'average' geometry of the previous section was adjusted. A 'fleshy' residual limb shape was created in which the thickness of the tissue layer was doubled everywhere. For a 'bony' limb shape the thickness was halved. The external shape of the 'fleshy' limb was less tapered than the 'average' one. Taper angles, i.e. the angles of inclination to the vertical of the sides of the limb, were 5.3° and 8.6° respectively. For the 'bony' limb the taper angle was 11.6°. It is generally the case that 'fleshy' residual limbs are more cylindrical in shape with a flatter distal end and bony limbs are more tapered with a more pointed distal end.

In each of the models, the bone structure was as shown previously barring the inclusion of a recess at the knee joint. This was a closer approximation to the X-ray views. Six models were used which calculated interface loads for the 'average', 'fleshy' and 'bony' limbs under both interface conditions. In all models, there was no distal end bearing.

The continuity of stresses around the point where the socket and limb came into contact was checked to evaluate trial meshes as well as the behaviour of individual reactions. Triangular isoparametric elements were incorporated to cope with the 'undesirable' geometry of the knee-joint recess. Final meshes for each limb geometry appear in the diagrams (a) of figures 6.7, 6.8 and 6.9.

Normal pressure profiles were produced for each geometry, under 'totally rough' and 'frictionless' conditions, from iterative runs using 10 increments of displacement.

These also appear in figures 6.7, 6.8 and 6.9, in which 1 mm of normal displacement of a profile represents a pressure of approximately 4.2 kPa.

The vertical stiffnesses, calculated by linear analyses of the 6 models, are summarised in figure 6.10.

Interface conditions:	Totally rough	Frictionless
'Bony' limb	461	112
'Average' limb	246	46
'Fleshy' limb	131	10

Figure 6.7 - Vertical stiffnesses of models with various tissue thickness. (units are N mm^{-1})

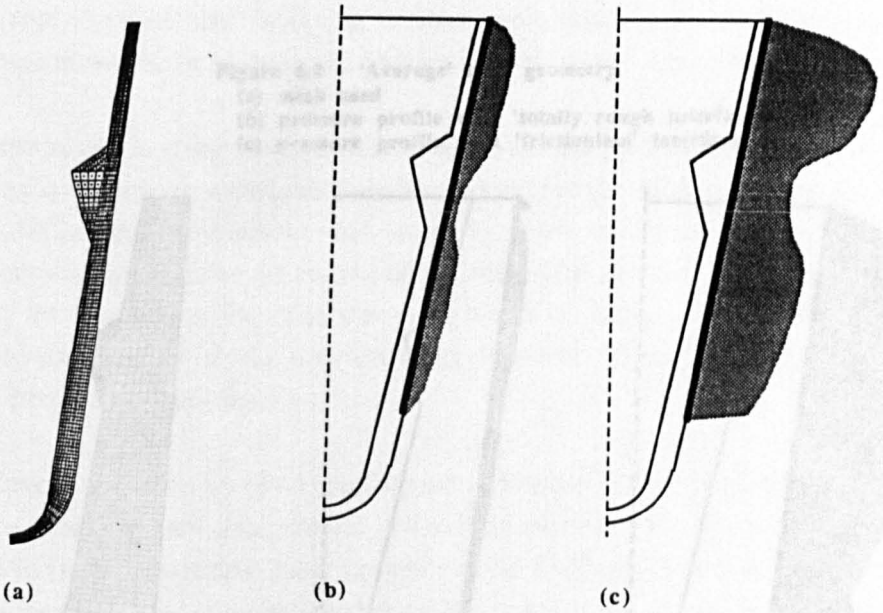

Figure 6.8 - 'Bony' limb geometry.

(a) FE mesh.

(b) pressure profile with 'totally rough interface.

(c) pressure profile with 'frictionless' interface.

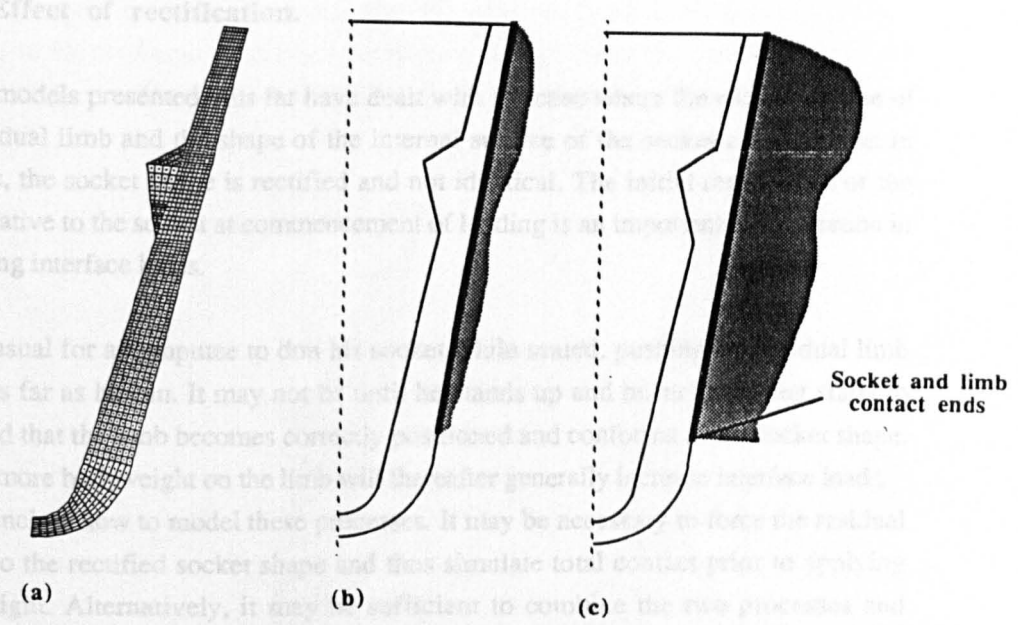

Figure 6.9 - 'Average' limb geometry.
(a) mesh used
(b) pressure profile with 'totally rough interface.
(c) pressure profile with 'frictionless' interface.

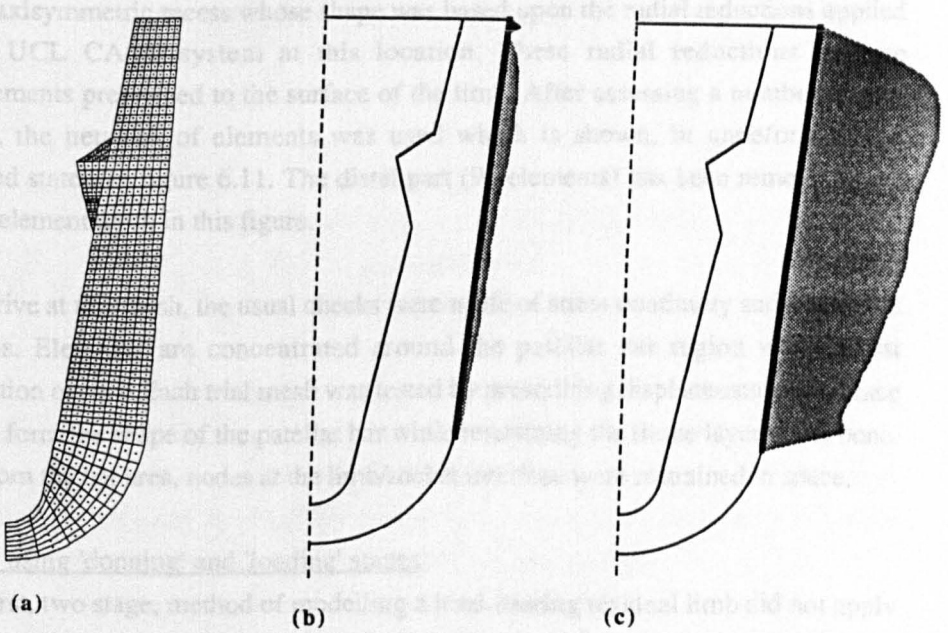

Figure 6.10 - 'Fleshy' limb geometry.
(a) mesh used
(b) pressure profile with 'totally rough interface.
(c) pressure profile with 'frictionless' interface.

6.3 Effect of rectification.

The models presented thus far have dealt with the case where the external shape of the residual limb and the shape of the internal surface of the socket are the same; in practice, the socket shape is rectified and not identical. The initial registration of the limb relative to the socket at commencement of loading is an important consideration in modelling interface loads.

It is usual for an amputee to don his socket while seated, pushing his residual limb into it as far as he can. It may not be until he stands up and his artificial leg starts to bear load that the limb becomes correctly positioned and conforms to the socket shape. Putting more bodyweight on the limb will thereafter generally increase interface loads.

It is unclear how to model these processes. It may be necessary to force the residual limb into the rectified socket shape and thus simulate total contact prior to applying bodyweight. Alternatively, it may be sufficient to combine the two processes and simply apply 'vertical' and 'rectifying' displacements simultaneously. To investigate differences in results due to these two methods, models were prepared via both routes.

The model of a rectified socket contained only a patellar bar type rectification which was an axisymmetric recess whose shape was based upon the radial reductions applied by the UCL CASD system at this location. These radial reductions became displacements prescribed to the surface of the limb. After assessing a number of trial meshes, the network of elements was used which is shown, in undeformed and deformed states, in figure 6.11. The distal part (96 elements) has been removed from the 864 element mesh in this figure.

To arrive at this mesh, the usual checks were made of stress continuity and calculated reactions. Elements are concentrated around the patellar bar region where most deformation occurs. Each trial mesh was tested by prescribing displacements to surface nodes to form the shape of the patellar bar while restraining the tissue layer at the bone. Away from the bar area, nodes at the limb/socket interface were restrained in space.

Model using 'donning' and 'loading' stages

The first, two stage, method of modelling a load-bearing residual limb did not apply any bodyweight to the residual limb until the socket was donned. The 'donning' stage was modelled by applying rectifications to nodes at the bar (figure 6.11) in the same manner used to test the trial meshes. In the final runs for the donning stage, however, a

10 step iterative analysis was used. Results were postprocessed by a FORTRAN program so the displaced mesh from the donning stage became the initial mesh for the 'loading' stage. A stiffening of the modelled tissue layer was therefore expected prior to load bearing.

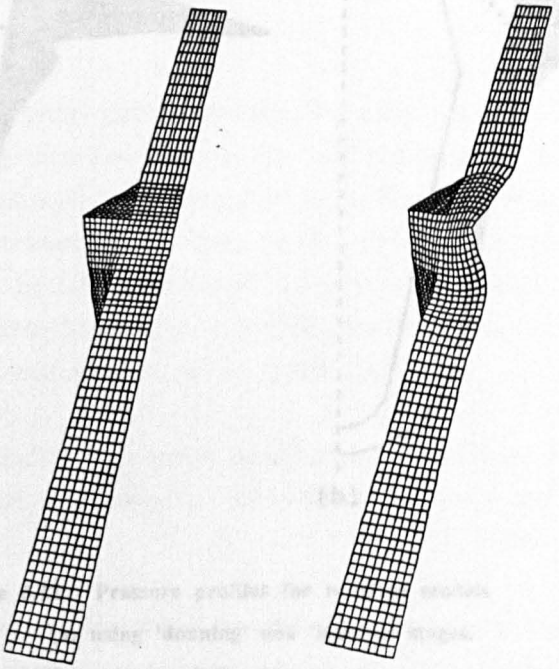

Figure 6.11 - Mesh for rectified limb model.
(a) original form.
(b) displaced form

Since the displacements applied in the donning stage were reacted by a vertical upward thrust of 391N, a load in excess of half-bodyweight must be applied to maintain equilibrium. A further 309N was therefore applied in the loading stage to give a model under full bodyweight. This was, in fact, achieved by displacing the bone down by 0.95 mm. Again a 10 step iterative analysis was used.

By summing the calculated reactions of the two stages, a profile of the total normal interface pressure was produced and this appears in figure 6.12 (a).

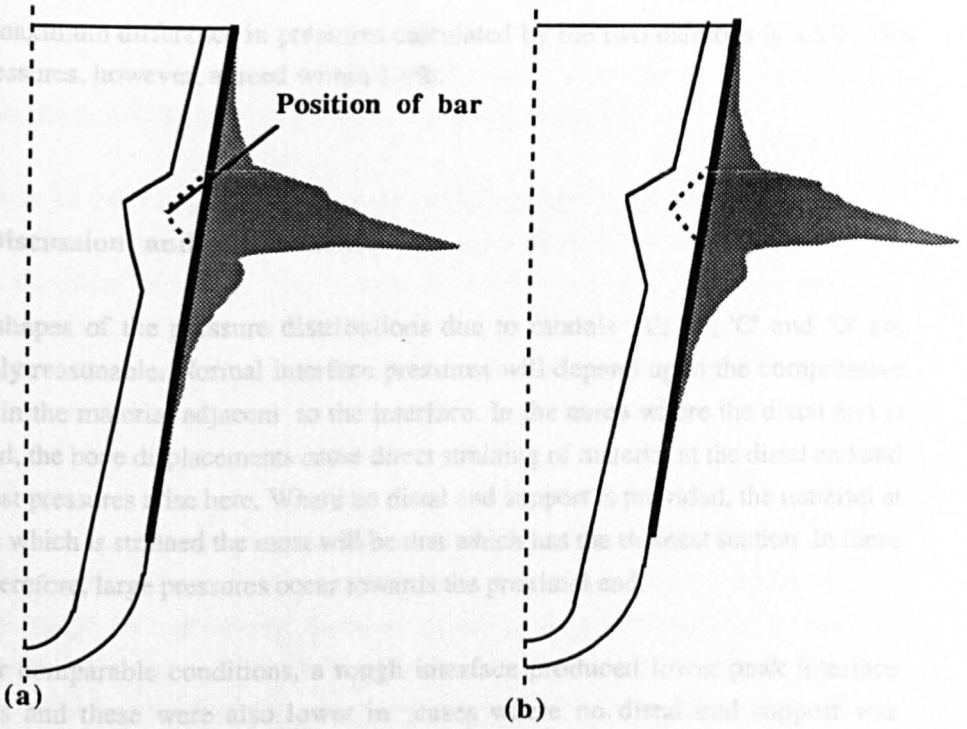

Figure 6.12 - Pressure profiles for rectified models
(a) using 'donning' and 'loading' stages.
(b) using a single stage.
(scale 1 mm : 10 kPa approx.)

Single stage model

An alternative, simpler method ignores the existence of separate 'donning' and 'loading' stages and prescribes displacements to surface nodes to simultaneously push the socket up onto the limb and apply rectifications which force the limb into the socket shape. While these displacements are applied, nodes at the bone are restrained. In the early stages of loading, therefore, the limb is supported by a very lightly rectified socket. It is only when fully load-bearing that the limb conforms to the shape of the rectified socket. An iterative solution applied 10% of both vertical displacements and rectifications with each increment and the model was repeated until the total vertical load reacted by the socket was 700N. A vertical displacement of the socket relative to the bone of 1.09 mm was used. A profile of the normal interface pressure from this model is shown in figure 6.12 (b).

The maximum difference in pressures calculated by the two methods is 4.5%. The peak pressures, however, agreed within 1.0%.

6.4 Discussion and conclusions.

The shapes of the pressure distributions due to models 'A', 'B', 'C' and 'D' are intuitively reasonable. Normal interface pressures will depend upon the compressive stresses in the material adjacent to the interface. In the cases where the distal end is supported, the bone displacements cause direct straining of material at the distal end and the largest pressures arise here. Where no distal end support is provided, the material at the sides which is strained the most will be that which has the thinnest section. In these cases, therefore, large pressures occur towards the proximal end.

Under comparable conditions, a rough interface produced lower peak interface pressures and these were also lower in cases where no distal end support was provided.

With distal end-bearing, the structure which includes a 'totally rough' interface showed the action of the shear forces to be effective at providing vertical support, as is expected. This structure was roughly twice as stiff and peak Von Mises and compressive stresses for a given load were roughly half the magnitude, as in the case where the interface was 'frictionless'.

Without distal end-bearing, a 'totally rough' interface produced a structure which was over 5 times stiffer than where shear forces were absent. Compressive stresses were lowered where interface shear forces were present; however, a larger deviatoric (Von Mises) stress existed where material at the bottom of the rough interface was adjacent to material which was free to displace downwards.

When the limb geometry was varied, large differences in normal pressures also existed between models under the different interface conditions. The changes in limb geometry, themselves, had far less effect under the same interface conditions.

With a 'totally rough' interface, an increase in the thickness of the tissue layer produced a more compliant structure and lower pressures. The increase in compliance

may be largely as a direct result of the change in thickness since a given displacement will cause the smallest strains in the most 'fleshy' limb model; the relative compliance of each model was roughly in proportion to the tissue thickness.

The cause of the changes to the pressure distribution may be due to variations of the geometry of the interface. Since the length and taper of the modelled limbs differs, so does the interface geometry. The 'fleshy' limb has the largest interface area and therefore interface loads per unit area will be the least. In addition, since much of the applied load will be reacted by interface shear forces and the taper angle of the 'fleshy' limb is the least, the components in the vertical direction of a given shear force will be largest for this geometry.

For the case where the interface was 'frictionless', the stiffness again was reduced as the tissue thickness increased. The normal pressure, however, was a minimum in the case of 'average' limb geometry. Since all of the applied load must be reacted by normal pressures in these cases, the magnitude of the pressures may be assumed to depend upon the area produced by a projection of the interface onto a horizontal plane. This area is largest for the 'average' model and pressures, therefore, are the smallest.

The frictionless models accentuated the influence of the knee recess. As expected, the additional material due to the recess causes the most dramatic disturbance to the pressure distribution in the case where the tissue layer is thinnest.

For the model which included rectification at the bar, peak calculated pressures were far higher than in previous models. The pressure on the element immediately above the deepest part of the bar was approximately 379 kPa.

Only small differences existed between results due to the 2 modelling methods. In these models, a 'totally rough' interface existed and effective bone displacements were small and differed, in absolute terms, by a very small amount. At equivalent stages of the rectification process, therefore, the thickness of the tissue at a given location was similar in either model. The forces required to produce a further given rectification, therefore, will also be similar. Differences may have been greater in a more compliant structure and the use of the single stage modelling method may not be justified for 'frictionless' models.

The main conclusions of this study are that the presence of friction may greatly influence normal pressures at the interface and that, as expected, the distal end may bear a large proportion of applied loads if end-bearing is permitted.

Chapter 7

Experimental measurements on a limb model.

7.0 Introduction

The axisymmetric FE models discussed in the previous chapter have supplied theoretical values of normal interface pressures under various conditions for idealised limbs with simplified geometry and mechanical properties. These pressures may be compared with measurements taken under conditions which are controlled to give a close physical representation of the theoretical models. Measurements of the load versus deflection response of the physical models may also be compared with theoretical predictions.

7.1 Apparatus

Limb/socket model

A physical model representing a bone structure, tissue layer and socket was made in the Bioengineering Centre's workshop; each component was manufactured with the geometry shown in figure 7.1.

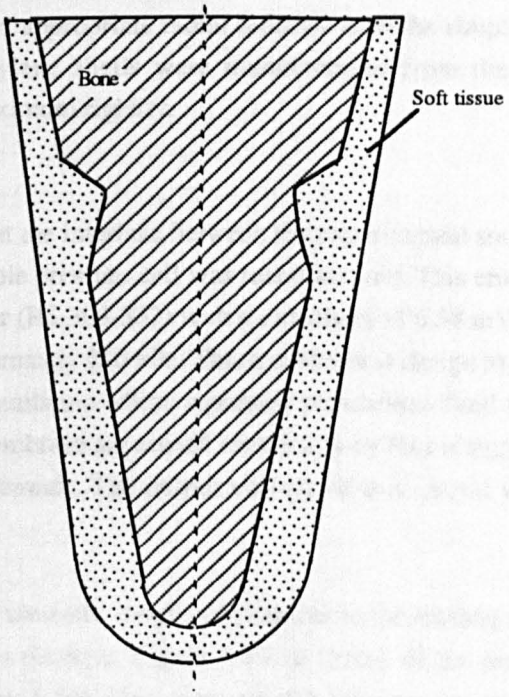

Figure 7.1 - Geometry of physical limb model.

This geometry corresponds with the boundary of the 'average' limb mesh (section 6.2) everywhere bar the filleted radii.

The bone structure, assumed rigid in the finite element models, was constructed out of dural using an hydraulic template follower on a lathe. The sharp edges at the knee joint were filleted with a small radius. The tissue layer covering the bone model was moulded from Q3-3320 elastomer. The external geometry of the tissue mould was generated in the form of a CASD shape data file by a simple PASCAL program and this shape was carved as a plaster positive using a 1/8" axial carving pitch. The mould was then formed over the positive shape from a polypropylene preform in a RAPIDFORM machine. The dural bone was mounted in the chuck of a pillar drill to position it centrally and at the correct vertical displacement from the bottom of the mould before a batch of elastomer mix was poured in to form the tissue layer. After all testing was complete, the elastic layer was sliced in half and measured at a number of locations. The thickness was within 1 mm of the geometry of figure 7.1 at all locations along the sides and was immeasurably different at the bottom.

The polypropylene mould was used as an unrectified experimental socket. The shape of a second socket, rectified at the patellar tendon level, was created by another PASCAL program which applied appropriate radial reductions to the simple conical shape. Both of these polypropylene shells were manufactured from the thickest 'preforms' available to ensure maximum rigidity.

Pressure cell

To measure normal pressures at the interface between the experimental sockets and the limb model, a cheap and simple pressure cell was manufactured. This employed a piezo-resistive pressure transducer (RS 303-337) with a sensitivity of 0.38 mV per kPa and a full scale loading of approximately 210 kPa. This transducer is design to measure fluid pressures and contains a membrane which separates pressurised fluid from the atmosphere. Deflections of the membrane are sensed electrically by four integral piezo-resisitors connected as a bridge circuit. The output voltage of this circuit was read directly from a digital voltmeter.

A fluid medium was needed to transmit interface pressures to the transducer and a cell was filled with water for this purpose. Figure 7.2 is a sketch of the assembled pressure cell with the transducer push-fitted into one end and a pressure measurement area, covered with a PVC membrane, at the other. Heavy duty PVC tape was found

suitable for this. The cell itself was manufactured from dural and screwed directly into tapped ports at all pressure measurement sites.

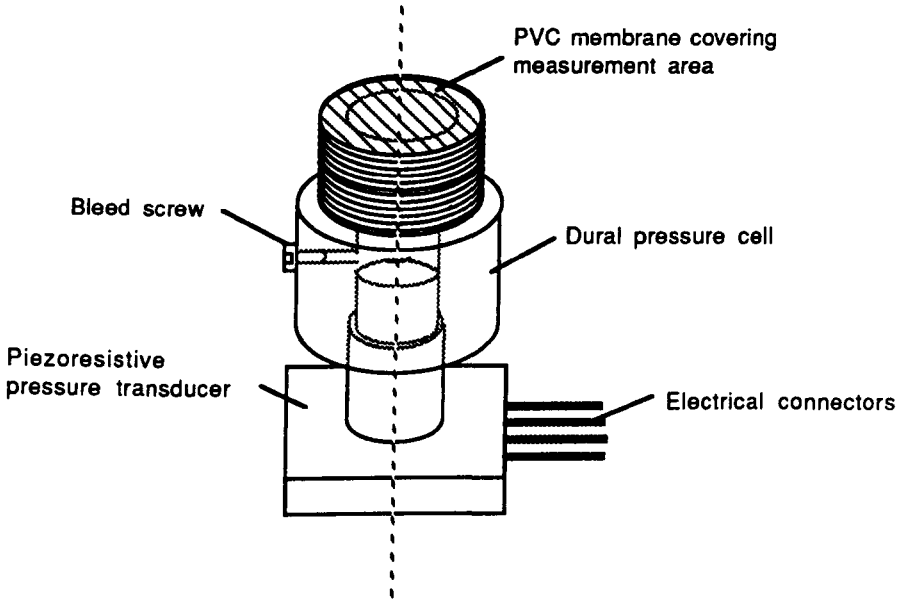

Figure 7.2 - Pressure measurement cell.

(scale 2:1 approx.)

To assemble the cell, the membrane was first stuck in place and the cell was filled with water, scraping the inside surfaces to free trapped air bubbles. The transducer was also completely filled with water using a syringe and was carefully pushed home into the cell having removed the small bleed screw. With the bleed screw replaced, the cell was ready for use.

Design criteria for transducers to measure pressures at body/support interfaces have been evaluated previously [FERGUSON80]. The need was emphasised for a calibration technique compatible with the mechanical conditions under which measurements are taken. Controlled calibration of the pressure cell used in the current study again employed the Zwick 1474 testing machine. An apparatus was manufactured to mount the pressure cell rigidly within a flat plate (figure 7.2). A cylindrical specimen of Q3-3320 was placed upon the plate and a uniaxial load was applied by another plate attached to the crosshead of the Zwick machine. A lubricating oil was used on all touching surfaces and hence a uniform pressure over the specimen was expected. This was confirmed by positioning the centre of the elastomer specimen at various locations relative to the pressure cell.

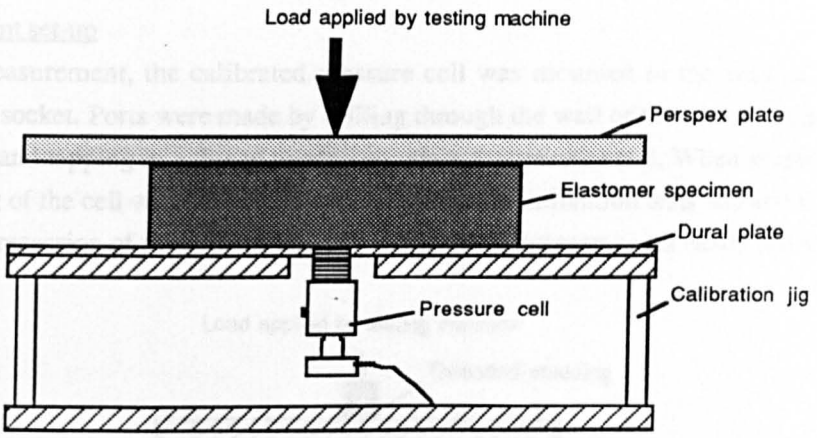

Figure 7.3 - Cell calibration set-up.

By taking readings of the output voltage of the transducer, the applied load and the specimen diameter calibration plots were obtained which were used to establish the relationship between output voltage and interface pressure for the cell. Figure 7.4 is an example plot.

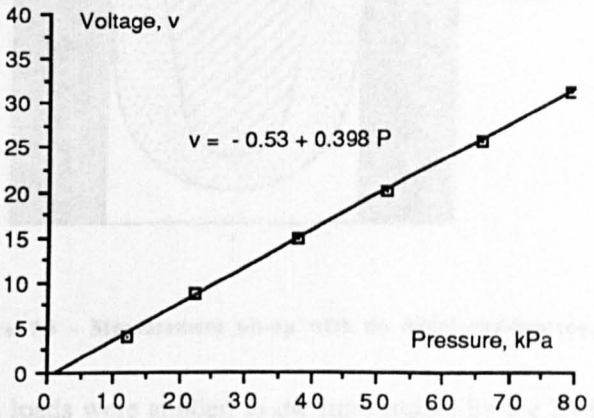

Figure 7.4 - Calibration plot

Calibration was repeated several times throughout the series of tests and the response was each time near-linear with a sensitivity of 0.385 mV per kPa ± 8%.

Measurement set-up

During measurement, the calibrated pressure cell was mounted in the wall of an experimental socket. Ports were made by drilling through the wall of the socket normal to its surface and tapping in a thread to accommodate the pressure cell. When screwed in, the seating of the cell was checked 'by feel'. A few trial calibration tests showed that protrusion or recession of the cell sufficient to disturb measurements was easily sensed.

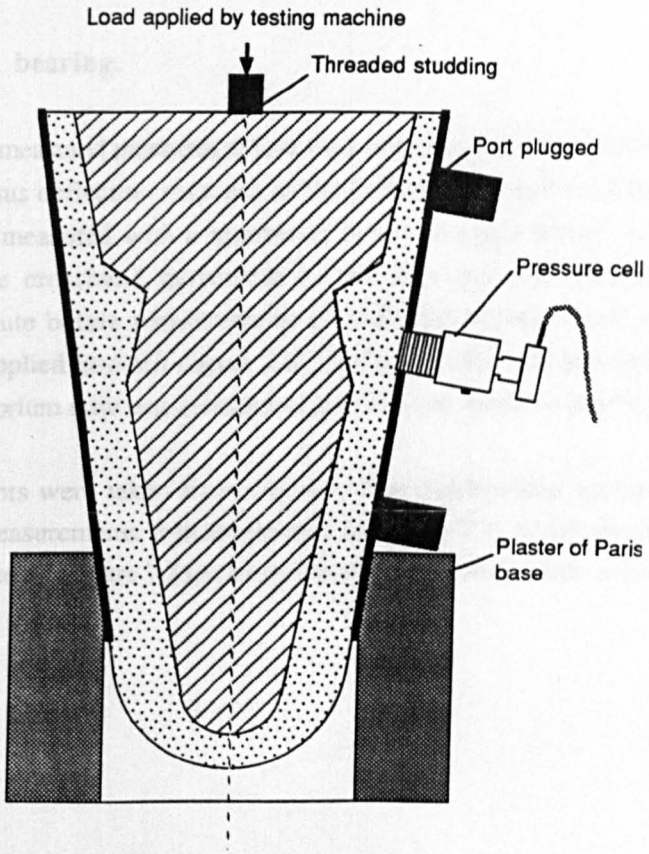

Figure 7.5 - Measurement set-up with no distal end-bearing.

Measured, controlled loads were applied to the limb model by the Zwick testing machine; the dural bone model threaded directly into the fitting on the machine's load transducer. Bone displacements were measured by the extensometer module. A plaster of paris base cast around the experimental sockets rested on the base of the testing machine to provide a firm support. This base had a hollow core to enable pressures at the base of the socket to be measured.

For the case where no distal end bearing existed, the most distal 1.5" of the socket was cut off and the plaster base was recast, ensuring clearance for the pressure cell (figure 7.5).

To approximate frictionless conditions, light lubricating oil was spread over the limb model and the socket surface. No 'totally rough' models were produced.

7.2 Tests with end bearing.

The first experiments measured pressures at four sites on the unrectified experimental socket and the load versus deflection response as the limb model was forced into the socket. Pressures were measured with a number of levels of applied load. At each measurement point the crosshead movement of the machine was stopped for approximately one minute before measurements of load and pressure were noted. During this period the applied load fell (figure 7.6), as did the measured pressure, to a steady value. This equilibrium state was assumed to give the best available reading.

Pressure measurements were taken from typically four load/unload cycles. The repeatability of these measurements is demonstrated by figure 7.7, which shows the pressures measured at site 'C' (figure 7.8) at a number of loads through four cycles.

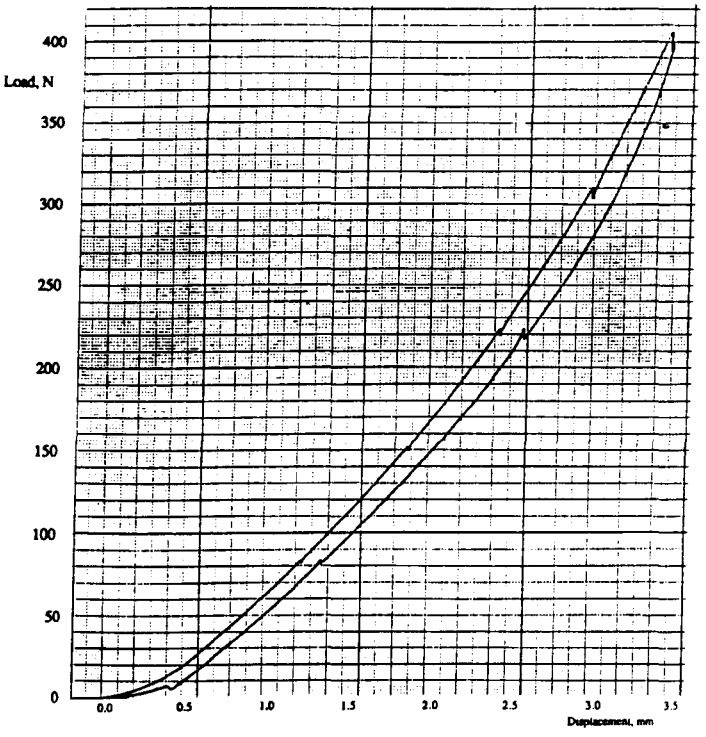

Figure 7.6 - Load relaxation during testing.

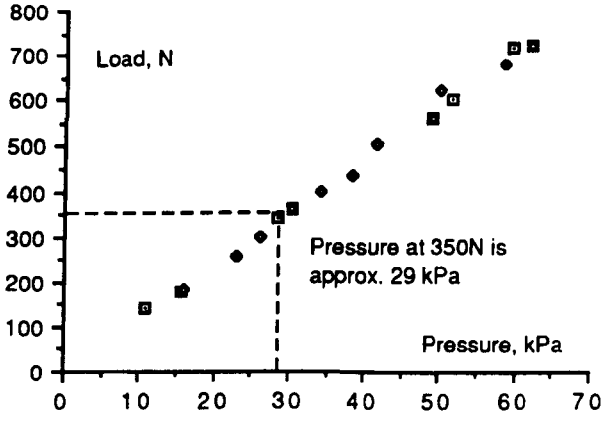

Figure 7.7 - Load versus pressure for site 'C'.

From similar load versus deflection data, the figures on the left hand side in figure 7.8 were produced which are the pressures measured at each site with an applied load of 350N. Corresponding theoretical values, from a model not presented in Chapter 6, appear on the right hand side. Theoretical pressures for 'totally rough' conditions are included in italics below the 'frictionless' values.

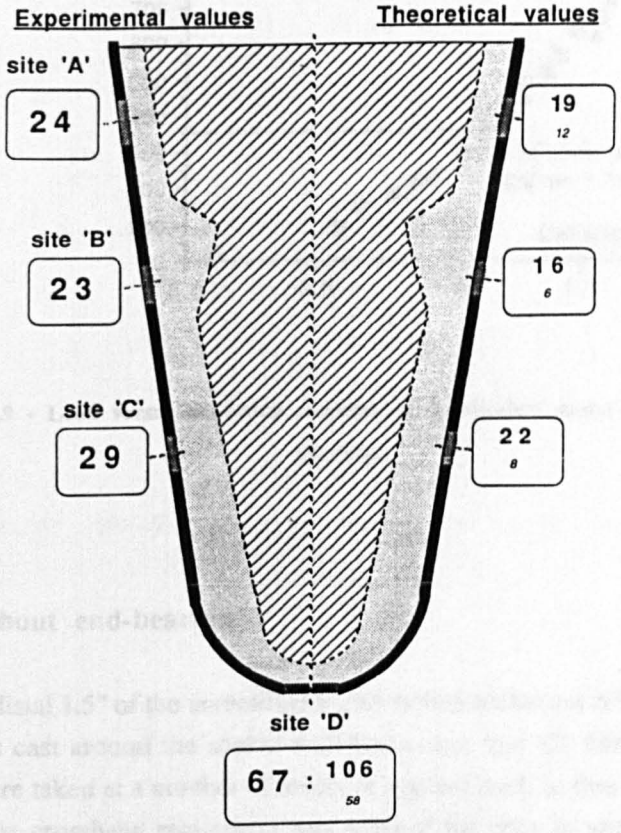

Figure 7.8 - Measured versus predicted pressures with distal end-bearing.

(at an applied load of 350N)

The load versus deflection response of the limb/socket model, using data from 7 tests is shown in figure 7.9.

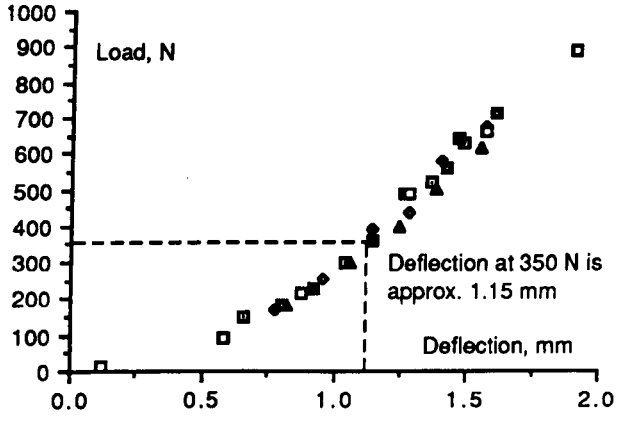

Figure 7.9 - Load versus deflection response of limb/socket model with distal end-bearing.

7.3 Tests without end-bearing.

With the most distal 1.5" of the unrectified experimental socket cut off, a new plaster of paris base was cast around the socket wall below test site 'C'. Measurements of pressure again were taken at a number of levels of applied load. In these experiments, however, when the crosshead movement was stopped the drop in applied load to a steady state was more significant and the measured pressure *rose* to a steady value.

The left hand side of figure 7.10 shows the measured pressures at the three remaining sites which correspond to an applied load of 350N. Again theoretical values under 'frictionless' conditions appear in bold on the right hand side with pressures under 'totally rough' conditions shown in italics.

The load versus deflection response of the system, measured in 6 tests, is shown in figure 7.11.

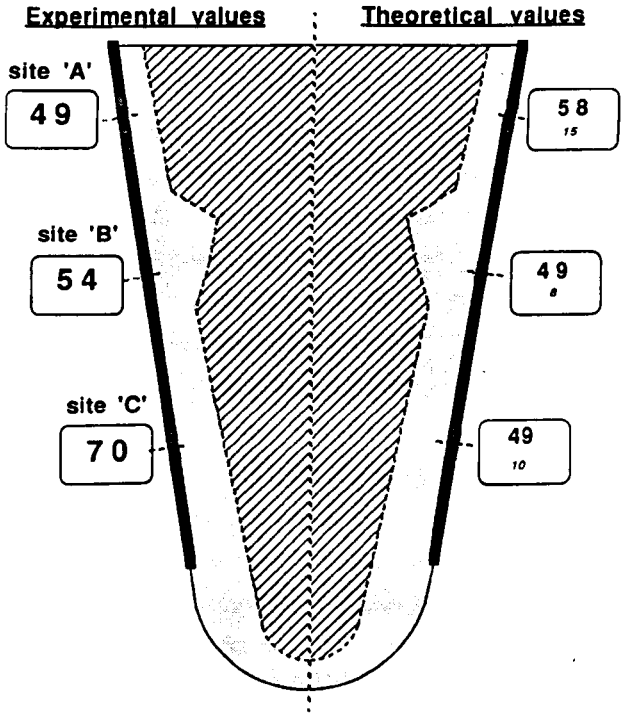

Figure 7.10 - Measured versus predicted pressures without distal end-bearing. (at an applied load of 350N)

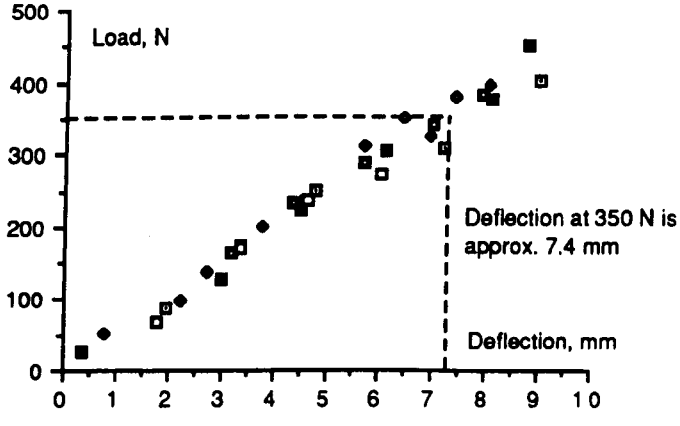

Figure 7.11 - Load versus deflection response of limb/socket model without distal end-bearing.

7.4 Tests with rectified socket.

Attempts to measure pressures at the interface between the rectified socket and the limb model were unsuccessful. As the limb model was forced into the rectified socket, the bond between the elastomer layer and the bone model was broken and the axisymmetric bar caused the elastic layer to 'ride up' over the bone. Testing was abandoned at a maximum load of approximately 500N since boundary conditions were felt to be totally unrepresentative of the conditions of the FE model. At this load, there was still no contact between the limb model and socket wall below the bar.

No meaningful pressure measurements were obtained.

7.5 Discussion of results.

With distal end-bearing, measured pressures generally were closer to those predicted by the 'frictionless' rather than 'totally rough' FE model. At the 3 sites on the side wall of the socket, however, measured pressures were 30-40% greater, and the measured pressure at the base was nearly 40% lower, than that predicted under frictionless conditions. Small differences in geometry or variations in the mechanical properties of the elastomer are considered unlikely to cause such a significant bias in loading towards the side walls relative to the FE model. A more probable explanation is that the lubricating oil transmits the higher pressures along the interface from the distal end and 'evens out' the distribution. It was found that with the crosshead movement stopped measured pressures fell and this may have been due to a slow outflow of excess compressed oil. Future tests should investigate pressure transmission within lubricating oil; the inclusion of a few small holes in the socket wall may prevent it.

The measured load versus deflection response with distal end-bearing (figure 7.9) was nonlinear; at an applied load of 350N the bone deflection was approximately 1.15 mm. The corresponding deflections in the 'frictionless' and 'totally rough' models were 2.2 and 1.1 mm respectively. An excess of lubricating oil may have transmitted pressures across the interface at an earlier stage of bone displacement than was predicted. The slow fall in applied load when the crosshead movement was stopped was probably due to a relaxation of a temporary shearing action at the interface which occurred because of a delayed sliding of the elastomer's surface along the socket wall.

With the distal end removed, pressures were also closer to those predicted by the 'frictionless' FE model. Relative to this model, the pressure measured at site 'A' was low whereas the pressure at site 'C' was more than 40% greater. This bias in loading towards the distal part of the interface may have been largely due to increased in friction at the cut distal edge of the socket wall which may have restricted sliding of the elastomer here. Although this frictional force contributes to the vertical support of the limb it probably causes a 'build-up' of material above the cut edge which increases strains and interface pressures. With increased support at the distal end lower interface pressures are expected proximally.

In addition, differences existed between the modelled boundary conditions and those in practice since restraints in the FE models are applied to nodes which are displaced. In effect, therefore, the modelled socket wall moves down with the displaced nodes and, since these nodes 'spread out', the wall increases in length.

There are two main consequences of this. Firstly, since the simple FE model did not 'free' nodes which slid over the location of the cut distal edge, a larger area of contact, by 7 % at an applied load of 350N, was modelled than existed in experiments. Predicted pressures may therefore be expected to be correspondingly lower. Secondly, to provide a comparison with the experimental measurement sites, pressures on the FE models had to be located on the mesh in its displaced form.

A fall in load again occurred when the crosshead was stopped; however, since this was probably due to a delayed downward movement of elastomer, the through-thickness strain increased and the normal pressure rose. With both the top and bottom of the socket open to atmosphere, the lubricating oil has far less influence.

The measured load versus deflection response was close to that for the 'frictionless' model and was more linear (figure 7.11) than for the distal end-bearing conditions. Experimental and theoretical bone displacements under an applied load of 350N were approximately 7.4 and 7.6 mm respectively.

7.6 Conclusions

Measurements of interface pressures have been taken on a limb/socket model. The differences found between these measurement may be partly due to experimental conditions.

With no distal end-bearing, the correlation between experiment and theory, in terms of normal pressures and vertical stiffness, was generally superior where no distal-end support was present.

The inclusion of an axisymmetric bar around the socket wall greatly increased the vertical reaction on the limb model; however, this introduced practical difficulties.

Chapter 8

FE models using measured amputee data.

8.0 Introduction.

In Chapter 6, FE models of socket loading have been presented which were based upon idealised geometry and assumed mechanical properties. In this chapter, the geometry and mechanical properties measured from an amputee are used. Models have been prepared to assess the effects of rectifications, the mechanical properties used in the models and the line of action of bodyweight loads.

8.1 Preparation of models.

Use of 3-dimensional elements

All 3-dimensional models discussed previously have contained idealised geometry and loading so that an economical FE solution could be obtained using an axisymmetric analysis. To model 3-dimensional structures in which geometry and loading are asymmetric, an FE mesh must be defined in 3-dimensional space. The latter type of model generally will contain more degrees of freedom than axisymmetric models and their solutions will have a greater front size (see Appendix A).

The consequences of this upon solution time may be observed by comparing two analyses of an idealised axisymmetric limb structure, one of which uses 2-dimensional elements and an axisymmetric solution and the other a mesh of 3-dimensional elements. The geometry of model 'A' of Chapter 6 (section 6.1) was the basis of these models and displacements were applied to nodes in contact with the rigid bone structure while restraints to the outer surface modelled a 'totally rough' interface. The coarse axisymmetric mesh contained 20 isoparametric elements with 8 nodes. The 3-dimensional mesh was made up of 360 elements in all; 16-noded isoparametric brick elements were used at the side and 12-noded wedge elements at the distal end.

Reactions per unit area along the interface, calculated using these coarse meshes, agreed within 1%. The axisymmetric mesh yielded 105 degrees of freedom and a front size of 15 and was assembled and analysed in less than 3 minutes of central processor time on the MicroVAX II computer. The 3-dimensional mesh contained 3252 degrees of freedom; the solution had a front size of 427 and analysis took 108 minutes, i.e. nearly forty times that of the simpler model.

In addition to the increased run-time over axisymmetric models, 3-dimensional meshes take longer to generate. The FE mesh was created automatically using the mesh generation facility 'PAFBLOCKS'. Identification of the nodes to displace and restrain, however, required use of the PIGS graphical package. This process was complicated for 3-dimensional meshes and prone to errors. Interpretation of results was also difficult since PIGS was unable to postprocess reaction data to provide a picture of the interface pressure distribution.

From the simple 3-dimensional models it became evident that some purpose-written pre- and postprocessing software was needed. For preprocessing, this is required to accept existing limb data and generate a mesh in which the nodes to displace or restrain can easily be determined. Some optimisation of element numbering is also desirable in order to reduce front size. To postprocess results, reactions at restrained nodes are extracted from output files and these may be used to compute the interface pressure distributions.

Creation of the FE mesh

The geometry of an amputee's residual limb has been measured together with a bone structure which radiographic evidence has shown to be similar to that of the amputee subject. These data are stored in files of radial measurements taken at regular axial and angular intervals and the two sets of measurements are about a common set of axes. To create a FE mesh, some of the points which describe these surfaces became nodes within the mesh. Nodes which have the same axial and angular coordinates were connected to form the edges of 3-dimensional elements. To refine this mesh more nodes and edges were used and new nodes were located along the edges to create a number of layers of elements through the thickness of the tissue layer.

A PASCAL program was written to generate models from the measured data. This selected radial measurements and generated all nodal data in Cartesian coordinates. These data were supplied with appropriate node numbers and were written to form a PAFEC 'NODES' module in a text file. An 'ELEMENTS' module was also written by this program to complete the definition of the mesh geometry. In this module, the topology of each element is described in terms of the corner nodes. The system used to number elements affects the dimension of the system stiffness matrix and therefore the time taken to produce a frontal solution. Elements were numbered so as to minimise solution time by ordering them around each slice, one layer after another, working up through the slices of layered elements (figure 8.1). 8-noded brick elements were used

throughout the mesh. 20-noded isoparametric elements with midside nodes could not be generated from the limb and bone data since it is a requirement that midside nodes be equidistant from corner nodes and this was not the case in the measured data.

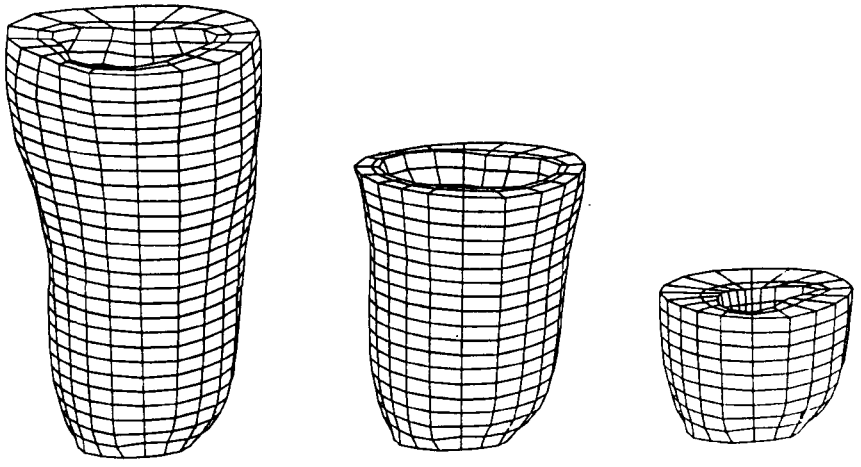

Figure 8.1 - The limb mesh.

The FE mesh for this 'first generation' limb model was designed by selecting an appropriate density of elements through the thickness of the tissue layer and over its surface. Axisymmetric models of idealised limbs have shown that a number of layers of elements may be required through the thickness of the soft tissue layer to give accurate values of interface loads. For an irregularly shaped tissue layer, many elements may be needed to define closely the internal and external surfaces. Large numbers of elements may therefore result in the 3-dimensional models and in order to keep within practical size limits a compromise had to be reached between the number of layers of elements and the accuracy with which the limb geometry was represented. In future models, refinement should be undertaken in the highly stressed parts of the mesh.

A number of meshes were generated and discrepancies were observed between the surface geometries of these and the data as measured. The meshes used in this series of limb models contained 2 layers of elements with nodal data axially spaced $^1/_4$" apart and at 20° angular intervals. This is shown in figure 8.1, where a view of the full mesh appears with views in which the proximal one or two thirds of the mesh have been removed.

Compared with the 'near-convergent' axisymmetric models this is a coarse mesh. Analyses, however, contained in the region of 3500 degrees of freedom with a front size of around 200.

As with CASD sockets, no support was provided at the distal end of the limb mesh. In the axisymmetric models, the rounded distal end was found to be made up of largely redundant elements under these conditions. For the more expensive 3-dimensional models, therefore, no mesh was used to cover the distal end of the bone structure. Instead, the bone data used to generate the mesh was one slice short of the measured limb data. Nodes, whose coordinates were based upon the shape of the most distal slice of bone data, were located on the inner surface of the tissue layer. Thus, the modelled tissue layer continued beyond the end of the modelled bone (figure 8.2). The 'missing' tissue at the distal end was then replaced by restraints which allowed these nodes to move only vertically.

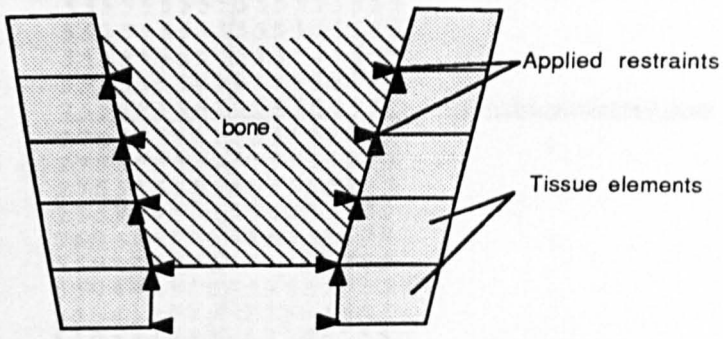

Figure 8.2 - Distal part of the FE mesh

To test this method two axisymmetric, idealised limb models were created; in one the distal end was covered with tissue, in the other the tissue was replaced by restraints as described. The reactions at the interface calculated by these analyses agreed within 1.3% at the most distal part of the interface and within 0.5% elsewhere. This method was therefore considered acceptable for the 3-dimensional models.

Mechanical properties

The four values of tissue modulus evaluated on the amputee subject and presented earlier in Chapter 5 were also included in the PAFEC data file by the model generation program. The locations of the four experimental sites were assumed to coincide with the corresponding 'modifiable' CASD rectification regions at the patellar bar, popliteal depression, and anterolateral and anteromedial tibial sites. Experimental moduli were used for elements within these regions; a mean modulus was calculated for use elsewhere. The modulus of the patellar tendon was omitted from this mean since the tendon was felt to be atypical of the soft limb tissues. One third of the sum of the moduli of the other regions was therefore used. To avoid sharp transitions in mechanical properties, intermediate values of modulus were used for elements at the boundaries of each experimental region. The intermediate values were a straight average of the experimental modulus and the mean modulus. At each location, the same modulus was assigned to all elements through the thickness of the tissue layer.

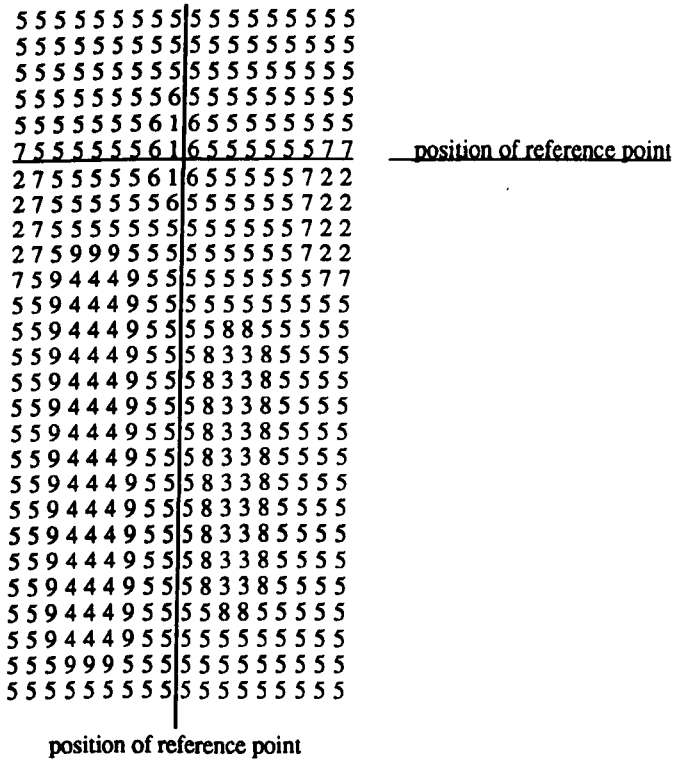

Figure 8.3 - Assignment of material property numbers to elements

Values of Young's modulus were defined by property numbers within a 'MATERIALS' module. The 'ELEMENTS' module, written by the model generation program, assigned these property numbers to individual elements and together these modules described the assumed distribution of mechanical properties in PAFEC data files. A PASCAL program which checked these files was used to produce figure 8.3. This shows the distribution of Young's modulus used in the models using the usual slice- and strip-wise format.

In this figure property numbers 1 to 4 assign to elements the measured moduli at the patellar bar (145 kPa), popliteal depression (50 kPa) and anterolateral (120 kPa) and anteromedial (50 kPa) tibial sites respectively. The intermediate values are assigned to the surrounding elements by property numbers 6 to 9 and the mean modulus (73 kPa) exists elsewhere using property number 5.

Loading, restraint and rectification

Interface loads were to be evaluated which arise when an amputee subject stands. These are due to bodyweight and compressive strains which occur where socket rectifications alter the unloaded limb shape.

Under the action of gravitational forces, the body tends to move vertically downwards and this motion is resisted by ground reaction forces applied to the feet. If all forces are assumed to be transmitted through the bones, then the bone structure below the knee will apply to a residual limb a vertical force and a moment, the magnitude of which is determined by the magnitude of the ground reaction forces and their position relative to the axis of the knee. In amputee stance, the knee moments probably tend to flex and adduct the limb.

A standing position with roughly equal weight bearing on either foot and neither foot in advance of the other would seem a reasonable aim for an amputee; although there is evidence that less weight is generally borne on the prosthetic side [SMITH85]. For the FE models, a vertical force equal to half the subject's bodyweight was assumed. Estimation of the knee moment was more of a problem; however, it might be assumed that the orientation of the knee joint is maintained as load is borne and the increasing moment is resisted at the knee.

Based upon these assumptions, the external loading in amputee stance may be modelled by displacing the bone structure vertically downwards relative to a static

socket or by displacing the socket vertically upwards relative to a static bone. The orientation of the residual limb and socket in space, however, must be taken into account and this will be determined by the alignment of the socket relative to the shank of the artificial limb.

For flat-footed stance it was assumed that the prosthetic shank is vertical and in the FE models the bench alignment recommended by Radcliffe and Foort was used. Figure 8.4 shows this recommended set-up, where the right-handed Cartesian axes used to locate the nodal coordinates of the limb mesh are tilted in space. This results in the long axis of the limb being tilted to the vertical in both the frontal and sagittal planes by angles ϕ and ψ respectively.

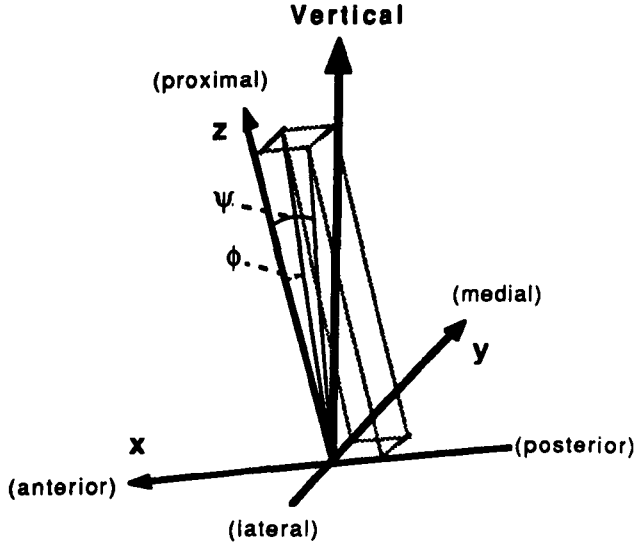

Figure 8.4 - Inclination of limb axes to the vertical

A unit vertical displacement, in an upward direction as shown, is therefore effected by orthogonal displacements of

$$\frac{\tan\psi}{(1+\tan^2\phi+\tan^2\psi)^{\frac{1}{2}}}, \quad \frac{\tan\phi}{(1+\tan^2\phi+\tan^2\psi)^{\frac{1}{2}}}, \quad \frac{1}{(1+\tan^2\phi+\tan^2\psi)^{\frac{1}{2}}}$$

in the x-, y- and z-directions respectively. In the recommended set-up both angles are 5°.

In the axisymmetric analyses, restraints were used to model a frictionless interface by defining a convenient set of local axes and restraining a degree of freedom relative to these axes at each interface node. In this way interface nodes remained on a line or circular arc when displaced, as they might when in contact with a regular rigid socket surface. With an irregularly shaped socket, interface nodes are not usually displaced along straight lines or circular arcs but follow the local contours of the socket and therefore their direction of motion may vary with displacement. Models which can cater for these varying degrees of freedom will be complex and for this study only 'totally rough' models were produced.

Since a frictionless interface was not to be used, it was most economical to apply restraints only at the bone while displacing the nodes assumed in contact with the socket. A smaller number of degrees of freedom and prescribed displacements resulted in this than in alternative methods and solution time was reduced. To produce this restraint, the model generation program identified all nodes assumed in contact with the bone and wrote a PAFEC 'RESTRAINTS' module to fix these in space.

Adjustments, made to the unloaded limb when a socket is donned but unloaded, were modelled by prescribing displacements to nodes on the external surface of the limb mesh. The radial increments by which the limb shape is adjusted were obtained from an altered version of the CASD program which wrote these rectification data to a file. The model generation program read this file and converted the radial increments into components of nodal displacements in global Cartesian coordinates. Only displacements which tend to increase interface pressures, i.e. those which remove material from a positive model, were processed into global components. Locations where rectifications aim to relieve interface pressures are generally where there is a thin layer of soft tissue covering a bony prominence and little expansion of tissues into interface gaps is expected. For this reason it was considered appropriate to leave these nodes free rather than force them to comply to the surface of the rectified shape. To model sockets which provide no distal end-bearing, nodes within the most distal 1.5" of the limb mesh were also left without restraint or prescribed displacements.

Axisymmetric models have previously been discussed in which displacements which produce a vertical load and those which adjust external shape were applied

independently or simultaneously. Similar results were obtained using the two methods and, for the 3-dimensional models, the latter method was used to give more economical solutions. Vertical socket displacement relative to a fixed bone structure modelled bodyweight loading and, where a rectification existed, the components which produce this vertical displacement were added to those which provide radial adjustment. The components of displacement for each interface node was associated with its node number and was written to form a 'DISPLACEMENTS.PRESCRIBED' module for inclusion in a PAFEC data file.

Analyses and postprocessing

For each analysis, an iterative solution was used in 10 equal steps of deformation. Components of socket displacement were calculated and the total reactions resulting at the bone structure were used to obtain the net vertical force on the amputee. Using this result, the components which provide vertical socket displacement were adjusted and the solution re-run until until the net vertical force on the bone structure was 350N.

To postprocess results into a meaningful form, the reactions at the interface were used to produce normal pressure distributions. A PASCAL program was written for this purpose which calculated the total normal load applied to the face of each element at the interface and divided this load by the face area.

Figure 8.5 shows the face of an element with corner nodes A,B,C and D which are

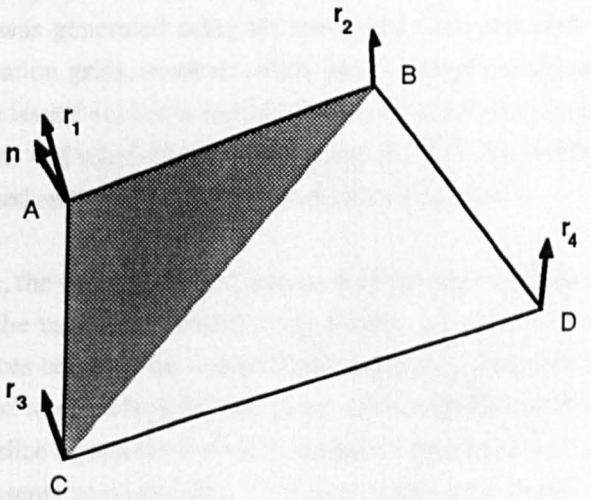

Figure 8.5 Reactions on an element face

part of the displaced mesh and therefore represent one facet of the socket surface. The nodal reactions, $\mathbf{r}_1$, $\mathbf{r}_2$, $\mathbf{r}_3$ and $\mathbf{r}_4$, on the element are calculated by a PAFEC analysis which gives the components of these in global Cartesian coordinates.

The contribution of each nodal reaction to the total normal load on the face is calculated by dividing ABCD into triangles to define flat planes adjacent to each node. The shaded triangle ACB shown in figure 8.5 is used to calculate the normal load at node A. The line vectors **AB** and **AC** are determined and the cross product of these provides the vector, **n**, normal to ACB and the area of a parallelogram between **AB** and **AC**. The unit vector normal to ACB is obtained by normalising **n** by this area, which is twice that of ACB. The dot product of the nodal reaction $\mathbf{r}_1$ with the unit normal vector gives the normal component of the nodal load at A. Reactions are assumed to be shared equally between adjacent elements and therefore one quarter of this normal load is attributed to the face ABCD. Similar calculations are repeated for areas BAD, DBC and CDA to find the total normal load on ABCD and its area and these figure are used to calculate the required normal pressure. The process is repeated by the program for all elements at the interface to provide the full pressure distribution.

8.2 Effect of rectification.

Three FE models were prepared to investigate the effect of rectification. For each of these, the same mesh was generated using the measured bone and limb shape data. Three different rectification grids, however, were used to generate displacements for models of the subject's issued socket, a heavily rectified socket and a socket with no rectification except distal end relief. Figures 8.6 (a) and (b) show the rectification grids used to produce the issued and heavily rectified sockets respectively.

For the latter of these, the CASD program was used to increase rectifications in each 'modifiable' region to the maximum used for any subject on the CASD trial. These grids show the differences between the socket shape and the aligned unrectified shape which has been stretched to provide distal end relief. Displacements in the y-direction from the datum of each slice represents the radial increment applied at each point, where 1 mm on the plots represents approximately 2.5 mm of radial adjustment. Data on the right hand side of these, and all grids shown in this chapter, relate to the lateral side of the limb.

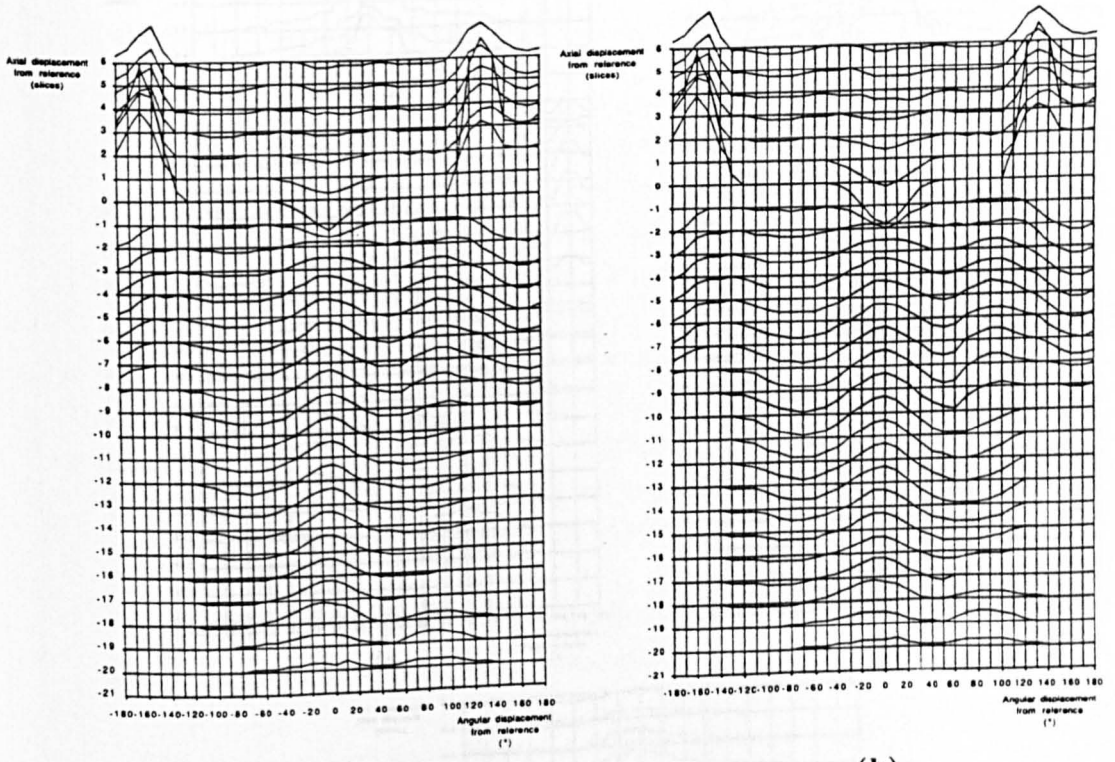

Figure 8.6 - Rectifications applied to give socket shapes.

(a) issued

(b) heavily rectified

The pressure distributions resulting from the FE analyses of the 3 models are shown in figures 8.7 (a) to (c). In these figures, a horizontal bar is plotted to represent the mean pressure on each interface element. On the grids, values of pressure are located at the centre of each element with respect to the mid patellar tendon reference point. A displacement of 1 mm from the datum of each slice represents a pressure of approximately 12 kPa.

The vertical stiffnesses of the issued, heavily rectified and unrectified sockets were 106 ,187, 86 Nmm^{-1} respectively.

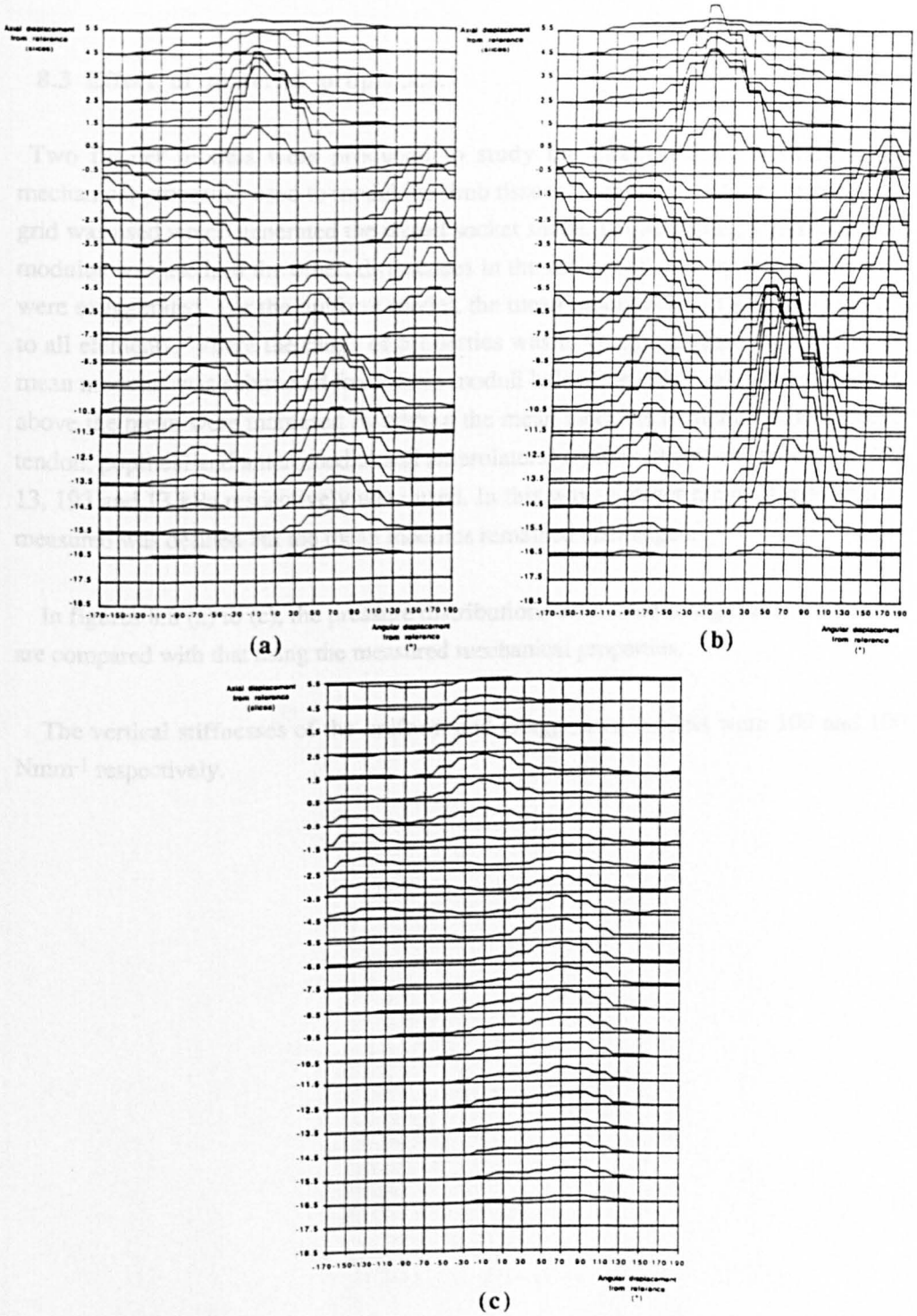

Figure 8.7 - Effect of rectification upon interface pressure distribution.
(a) issued socket.
(b) heavily rectified socket.
(c) unrectified socket.

8.3 Effect of material properties.

Two further models were produced to study the effects of the distribution of mechanical properties used to model the limb tissues. In these models, the rectification grid was used which generated the issued socket shape. In one model, a uniform tissue modulus was used; in the other, differences in the measured distribution of properties were exaggerated. For the uniform model, the mean modulus of 73 kPa was assigned to all elements. Where the range of properties was to be exaggerated, one half of the mean modulus was subtracted from those moduli below the mean value, whereas those above the mean were increased by adding the mean modulus to them. For the patellar tendon, popliteal and anteromedial and anterolateral regions, therefore, moduli of 218, 13, 193 and 13 kPa respectively were used. In this way, a larger range of moduli than measured was defined but the mean modulus remained unchanged.

In figures 8.8 (a) to (c), the pressure distributions calculated using these two models are compared with that using the measured mechanical properties.

The vertical stiffnesses of the uniform and exaggerated models were 109 and 100 Nmm^{-1} respectively.

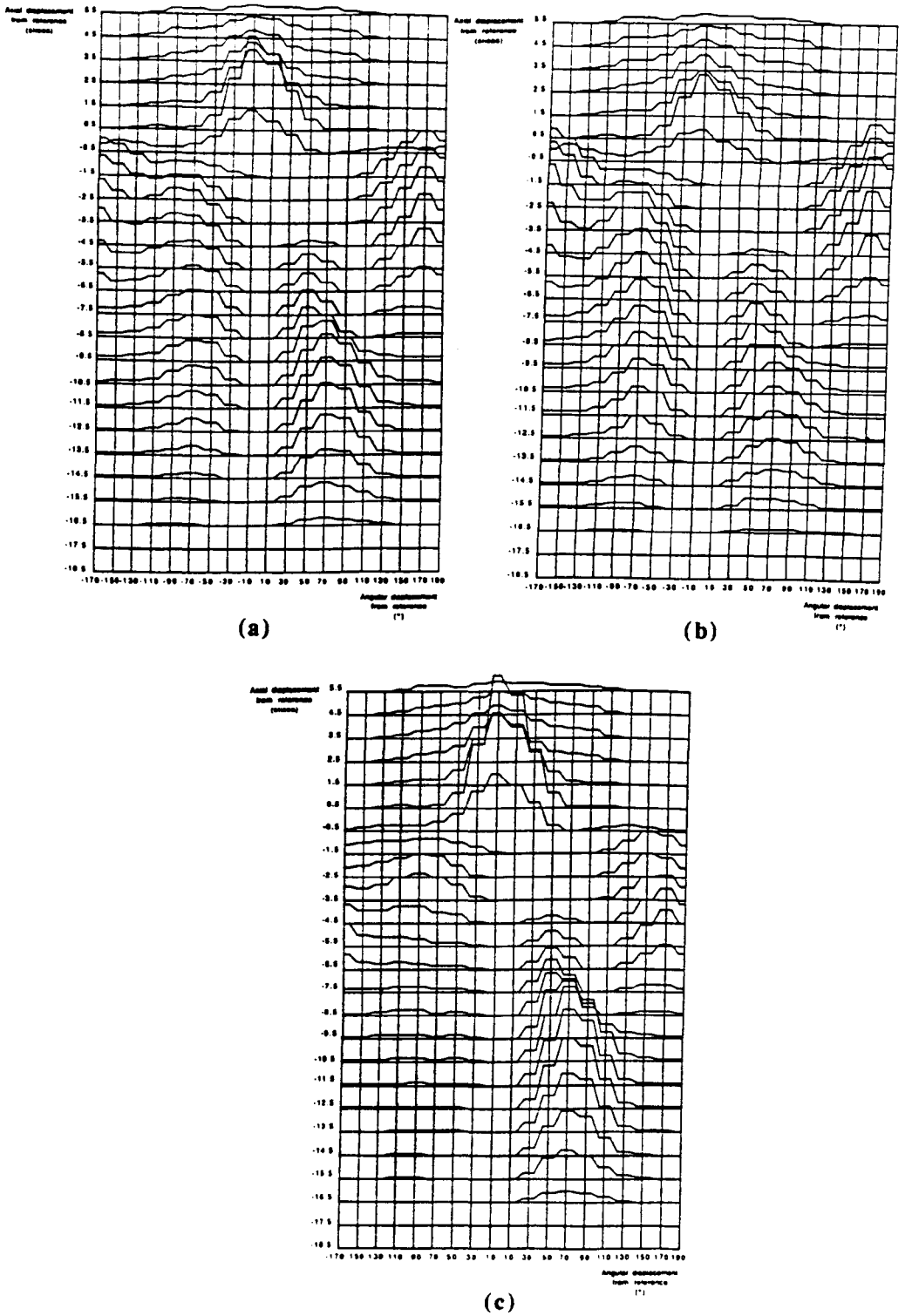

Figure 8.8 - Effect of material properties upon interface pressure distribution.
(a) measured properties.
(b) uniform modulus.
(c) exaggerated range.

8.4 Effect of alignment.

The effect of socket alignment upon the calculated interface pressure distribution was investigated by repeating the model of the subject's issued limb, again using the measured mechanical properties, but assuming that the neutral axis of the limb was vertical during loading. Only a z-wise component of displacement to the socket was used, therefore, to model the half-bodyweight loading.

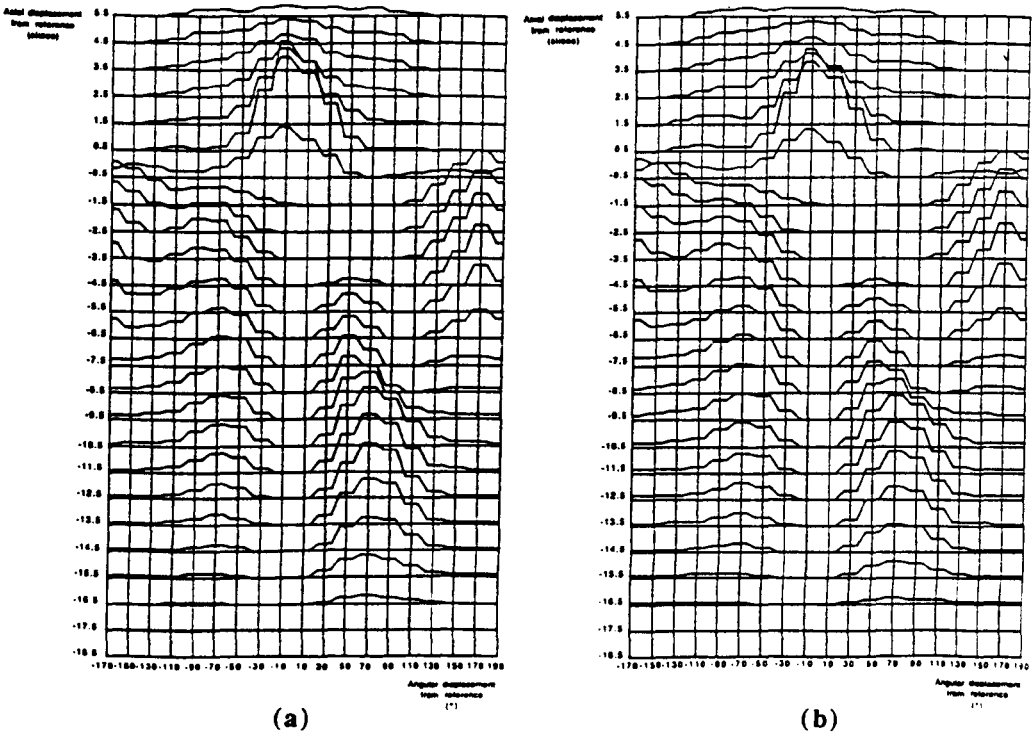

(a) (b)

Figure 8.9 - Effect of alignment upon interface pressure distribution.

(a) with bench alignment.

(b) with neutral alignment.

In figures 8.9 (a) and (b) the pressure distribution under these conditions is compared with that which incorporated the bench alignment.

The vertical stiffness of the neutrally aligned model was 108 Nmm^{-1}.

8.5 Discussion of results.

Effect of rectification

The correlation between the rectification grids and pressure grids of figures 8.6 and 8.7 is intuitively reasonable. Areas which are heavily rectified have high normal interface pressures. In addition, the influence of the distribution of mechanical properties is seen with higher pressures in the stiffer regions.

The peak pressure encountered in the model of the issued socket was 196 kPa in magnitude and was located at the patellar bar. In this model, other peaks were identified in the popliteal depression and in the anteromedial and anterolateral tibial regions. The maximum pressures at these locations were 115, 71 and 105 kPa respectively.

When heavy rectification was applied to the limb shape, the peak pressure at the patellar tendon rose to 291 kPa; the rectification here had been increased by approximately 50%. In the popliteal, anteromedial and anterolateral regions peak pressures increased to 152, 105 and 287 kPa respectively. At each of these locations pressures could be predicted, within 20%, by linearly scaling those values found in the previous model by the proportional increase in rectification. The results from this model might be expected to show a redistribution of pressure with higher localised pressures in those areas where rectification has been increased and reduced pressures elsewhere. Nevertheless, the analysis does not show this, and normal pressures all over the interface have been increased. The influence of shear forces at the interface in these 'totally rough' models must not be forgotten, however, and it may be that in the heavily rectified socket shear forces contribute less to the support of the limb.

With no rectification, a maximum pressure of 44 kPa was found at the base of the patella and a large region of normal pressure existed to the lateral side of the tibia, although pressures here were all below 42 kPa. The wall of this 'socket' will have only small inclination to the vertical over most of its surface and the action of shear forces may contribute efficiently to the support of the limb. This may account for the low pressures calculated.

Shear force distributions have not been produced since no measured experimental values have been found with which comparisons may be made and because it is not possible to define a consistent set of axes on the irregular socket surface from which components of these forces may be calculated. With no knowledge of the directions in which shear forces are acting it is difficult to determine what contribution they make to the support of the limb. It might, however, be assumed that an increase in the relative movement between the bone and socket will increase the shearing action at the interface. Relative displacements in the heavily rectified socket, issued socket and unrectified socket were 1.9, 3.3 and 4.1 mm respectively and therefore the influence of shear forces may be expected to increase where less rectification is used. An overall reduction in normal pressures would be expected to accompany increased shear and this is consistent with the results of the models.

Effect of material properties

Where a uniform modulus was used, a redistribution of pressure is observed. In this model, lower pressures were found in the patellar tendon and anterolateral regions, which were made more compliant with respect to the measured moduli. In the popliteal and anteromedial regions, which had been stiffened, pressures rose, although less significantly. This is to be expected since the deviations from the measured moduli here are smaller than those in the stiffer regions. The maximum pressure in this model was located at the patellar bar and was 138 kPa.

With the range of moduli exaggerated, the reverse trend was observed, as expected. Pressures in the stiffer regions rose with respect to those modelled using the measured properties, while pressures fell in the more compliant regions. Again, the changes in calculated pressures were more significant in the stiffer regions. The maximum pressure in this model was 272 kPa. This pressure is at the high end of the range of published pressured measured during walking and it would seems unlikely that such high pressure will exist in a comfortable socket in standing. This might indicate that the exaggerated range of moduli is unlikely to exist in a real limb.

Variations in the effects of shear in these models are expected to be small. Relative movements in models using the uniform or the wide range of moduli were 3.2 and 3.5 mm respectively.

Effect of alignment

With bench alignment, flexion and adduction of the knee are encouraged and pressures on the anterior and lateral aspects of the limb are expected to be higher than with the socket in neutral alignment. This is found in the FE models. The model using neutral alignment shows increased pressures on the posterior and medial aspect of the limb with respect to those found using the bench alignment; reduced pressures are calculated on the anterior and lateral aspects. Alterations to the pressure distribution are not great; a maximum difference in local peak pressures of 13% is found in the anterolateral region.

The vertical displacement with neutral alignment was 3.2 mm and therefore a similar shearing action at the interface may be expected to that encountered with the bench alignment.

8.6 Conclusions.

A FE model has been produced of an amputee subject's residual limb which has predicted a pressure pattern which is intuitively reasonable. The normal interface pressures calculated are above the few published values of pressures measured in standing but are below values from walking subjects.

When heavy rectification or an exaggerated range of material properties was modelled, peak calculated pressures generally were higher than published measurements from walking amputees.

Changes in material properties and alignment affected calculated pressure distributions logically. Where changes were made to the applied rectifications, the stiffness of the models was greatly affected. This is presumed to have had a significant effect upon the magnitude of interface shear forces and this may explain unexpected effects of rectification upon the normal pressure distributions.

From the fact that the FE models have shown a sensitivity to changes socket shape and tissue properties, further use of the FE method for researching the fundamentals of socket loading appears justified and the potential of FE models in assessment of socket designs may be of use in a clinical environment.

Chapter 9

Summary and strategy for future work.

9.0 Summary of the main findings of the current project.

In Chapter 1, the concept was introduced of an automated system capable of replacing the conventional socket design and production procedure. The lack of fundamental knowledge, which may permit design based upon a fuller description of the residual limb, was noted and a CAE study was proposed with the aim of identifying key design parameters. In a review of the literature, only very specific stress-strain relationships for soft tissues were found and a paucity of information was revealed of tissues under compressive loads.

In Chapter 2, the UCL CASD system was described which has undergone patient trials during the course of the thesis project. The system has been shown to be as successful as conventional practice as far as can be evaluated subjectively.

In Chapters 3,4 and 5, FE models were developed and evaluated and theoretical results from the models were fitted to experimental data to evaluate a soft tissue modulus for use in a static FE limb model. Work presented in Chapter 5 additionally obtained data which describes the geometry of the external surface of a residual limb and the bone structure within.

The axisymmetric limb models of Chapter 6 have shown that normal interface pressures may be greatly reduced by the action of interface friction and support at the distal end; the vertical compliance of the limb/socket structure was also reduced. Simple variations in the idealised limb geometry affected the compliance of the modelled structure but had far less influence upon interface pressures. In Chapter 7, attempts to measure these pressures showed that, although measured pressures were of similar magnitude to those predicted, experimentation is not straightforward, even on idealised limb models.

The FE limb models of Chapter 8 showed that increased rectification produced a structure with a greater vertical stiffness; normal interface pressures were also increased. The distribution of material properties used in these models affected interface pressure distribution greatly but had only a small influence upon the vertical stiffness of the modelled structure. A change in alignment, that would in practice be expected to affect gait significantly, had a small effect upon the interface pressure distribution and the vertical stiffness of the static models.

9.1 An improved CASD system.

In this section, an improved system is outlined which makes use of static FE modelling to base socket design upon a fuller description of residual limbs. Figure 9.1 is a flow-diagram for the processes used by the improved system.

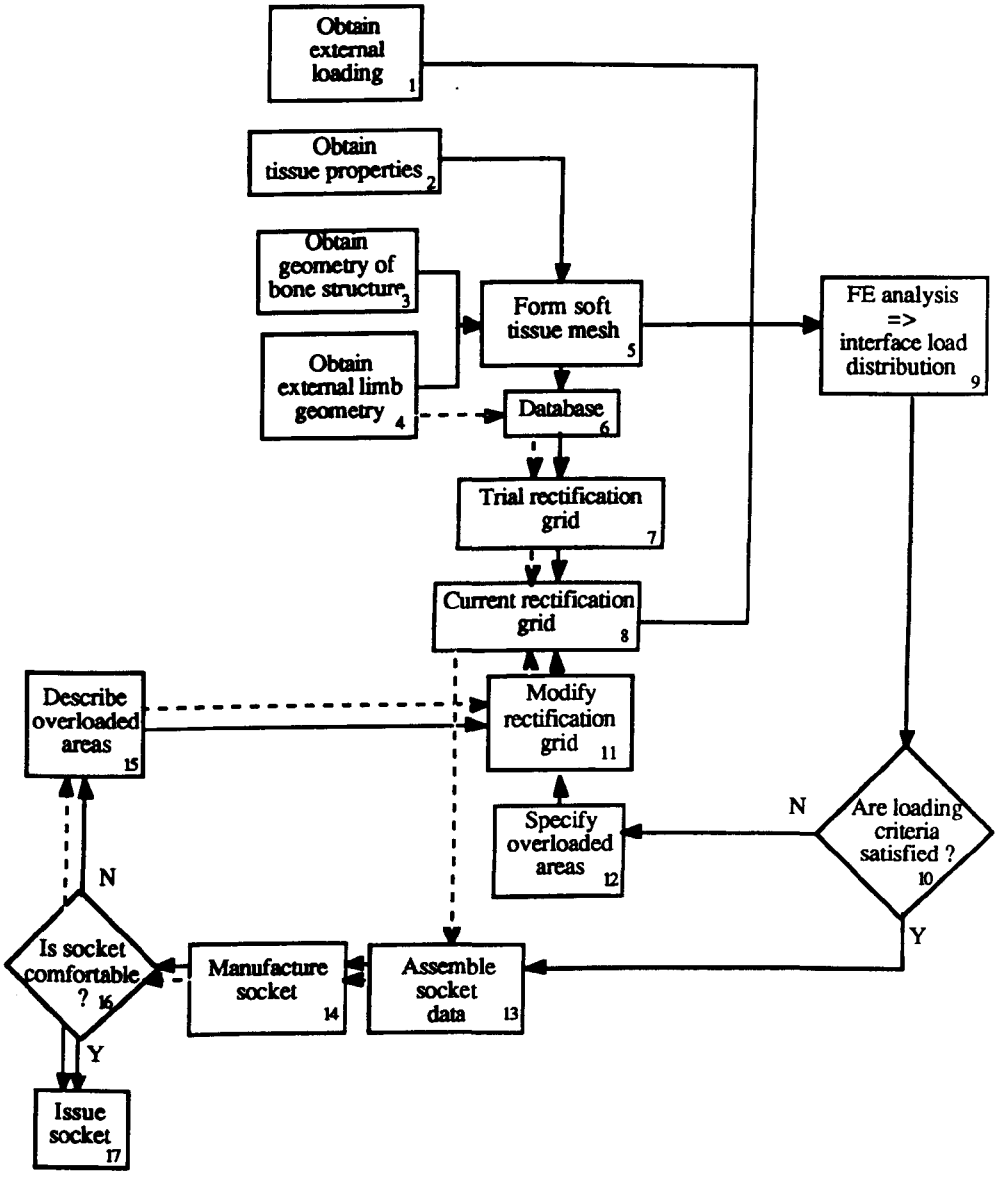

Figure 9.1 - Flow diagram for an improved CASD system.

In figure 9.1, the logic of the processes of the existing system is shown by dashed lines. The measured external geometry (box 4) is combined with a rectification grid (boxes 7 & 8) to design a socket (box 13) and this is manufactured and assessed (boxes 14 & 16). The socket is then issued (box 17) or the rectification grid is modified (box 11) and a new design evaluated.

The data used for design by the improved system is shown in boxes 1 to 4 of figure 9.1. The loads applied by the socket or bone structure to the limb (box 1) may be idealised, as in the current models, using half-bodyweight loading. The tissue property data (box 2) may take the form of a large number of measurements or, more probably, a standardised grid customised according to a few measurements of tissue compliance. The geometric data of boxes 3 and 4 may be obtained by a variety of methods discussed previously. In the improved system, these are used to create a soft tissue mesh. From a database of soft tissue meshes and successful rectification grids, a trial rectification grid is proposed.

These five sets of data are used to form a FE model (box 9). Analysis of the model predicts an interface load distribution which is compared with pre-determined criteria to judge whether the rectification guess is likely to produce a comfortable socket (box 10). If this test is failed, the rectifications are modified according to the overloaded areas predicted and the analysis is repeated until the load criteria are satisfied. The rectification grid and the measured external geometry are then assembled as socket data and these data are used for automated manufacture (boxes 13 & 14). The socket is then assessed and will be issued if comfortable.

If a comfortable fit does not result, a description of the overloaded areas is entered by the prosthetist which will be used to adjust the rectification grid. In this case the system has failed to design a comfortable socket using its own expertise. The role of the database in this system is limited to providing an initial guess for the rectification grid. In a fully-blown expert system, a broader base of information may be used from which the interface loading criteria may be revised or may be specific to the amputee.

Towards this improved system, the current project has studied methods by which to obtain the geometric and mechanical properties of the limb tissues (boxes 2 to 4). Algorithms have been developed which can form a soft tissue mesh (box 5). Standardised rectification grids have been prepared which are a starting pont for socket design (box 7) and a means of modifying these grids has been provided (box 11). FE models have been produced which have predicted interface load distributions (box 9).

Software has been written to define a socket shape from a rectification grid and measurement grid (box 13) and this shape may be automatically carved (box 14).

9.2 Suggestions for future fundamental research.

A great deal of ground remains uncovered. More sophisticated models based upon available data will improve the understanding of socket loading. Parameters which influence socket comfort include the geometric and mechanical properties of the socket, the geometric and mechanical properties of the residual limb and the configuration of loads applied to the prosthesis. These all affect the load distribution at the interface and the stresses that will be produced in the limb tissues. Further fundamental research in these areas will provide data which will permit a more scientific design philosophy.

Improved models

During the development of the 'first generation' limb models presented, a number of areas have been identified in which improvements may be made using existing limb data.

An iterative process can yield a limb model containing a 'frictionless' interface. This is considered valuable for two main reasons. Firstly, the use of limb socks and talcum powder to reduce interface friction, especially during gait, is commonplace. Secondly, the skin appears to be relatively free to slide over the underlying tissues and a 'low friction' interface can therefore exist within the soft tissues a small distance from the socket wall. A FE model with a 'frictionless' limb/socket interface will probably approximate these two conditions more closely than a 'totally rough' model. The 'frictionless' model will be complex, requiring software to check frequently the movement over the socket wall of nodes on the limb surface and to change the direction of applied restraints so that the socket contours are followed.

In the current models, the bone structure was displaced vertically down relative to the socket and it was assumed that an extension moment at the knee from the quadriceps would maintain the orientation of the bone structure during loading. In future models, this moment should be evaluated from the nodal reactions at the bone. Other knee moments can be modelled by applying a rotation to the bone structure or socket as well as a vertical displacement.

Using a model in which the bone structure is represented, the sensitivity of interface loads to displacements of the patella can be studied. Patellar elements may be attached to elements of the main bone structure by spring elements of various stiffness to model extensions of the patellar tendon.

By representing the socket by finite elements as part of a limb model, the effects of distortions in the socket wall and deformations of soft liners can be studied. The main benefit of this is thought to be in the selection of improved liner materials. Static analyses of distortions of the socket wall, especially for flexible sockets, are thought to be of limited use; the main benefit of flexible sockets is probably that the socket wall is able to distort under the action of local interface pressures during gait and this probably reduces strains which occur in tissues covering a bony prominence.

In a conventional 'hard shell' socket, discomfort and damage usually occurs during gait where the socket is ill-fitting over a bony prominence. FE models of areas where a socket is relieved locally over a prominence will permit study of the sensitivity of interface loads and tissue stresses to misshapen or mislocated 'rectification patches' of the socket wall. Various displacements may be applied to the modelled socket wall to represent relative displacements between the socket and bone structure during gait. This may yield a better fundamental understanding of how to accommodate the bone structure within a socket.

Quasi-dynamic models may apply a loading configuration to the limb which is assumed to exist at an instant in the gait cycle. These models, however, will require further investigation of the time-dependence of tissue behaviour before trustworthy results may be obtained.

In the FE analysis which derives strain-displacement matrices as a function of the nodal displacements it is not possible, with available software, to adjust boundary conditions during deformation. With new software, it may be possible to change the strain-displacement matrix during an iterative modelling process in which boundary conditions vary and refer displacements to the undeformed state of the FE mesh at any stage of deformation.

Geometric and mechanical properties of sockets

The design algorithms used by the UCL CASD system are based upon a small sample of data describing the location and magnitude of rectifications. In future, algorithms may be derived for a larger statistical sample of limb and socket shapes. The main difficulty in quantifying rectification changes is that measurements of unrectified and rectified prosthetic shapes are required about a common axis. This is generally not available. For the development of the UCL CASD system, measurements were taken of a plaster positive both before and after rectification and the two sets of data collected, therefore, were about the same axis. Software which can take unrectified and rectified data, aligned arbitrarily, and bring the two shapes into registration must be provided with the locations of points on each shape which are not changed by rectification. The two shapes may then be re-aligned to make these common points coincident in space. Thereafter, differences between the shapes may be examined.

An alternative to this process exists in facilities provided in the latest version of the UCL CASD software. With this program, the user is able to make changes to measured limb data by modifying the numerical surface data with the aid of a graphical display. Sockets may be designed using the CASD software as a sculpting tool. This is not recommended as a routine practice; however, since changes made in this way are stored as alterations to the measured limb data, they are in a form which can readily be used to define new rectification grids.

In the current project, sockets were assumed rigid. Measurements or models of distortions in sockets during standing or gait will provide a better indication of how the socket wall should be modelled in the future. These data will be especially important for analyses of flexible sockets.

Geometric and mechanical properties of limb tissues.

Further measurements of tissue geometry have been discussed in Chapter 5 which may lead to improved bone scaling and orienting algorithms. Assessment of the variability in tissue geometry between amputees and analysis of the sensitivity of limb models to changes in tissue geometry will indicate the accuracy to which such data must be obtained for socket design and whether standardisation of geometric data is possible.

Similarly, the evaluation of tissue modulus on a large sample of amputee subjects will indicate the variability of this parameter between subjects and therefore whether individual measurements are necessary to enable consistent socket design. A degree of standardisation in the distribution of tissue properties is thought likely.

For the purposes of the current study, a linear, time-independent stress-strain relationship has been assumed for the soft tissues. It is felt that the results obtained are, at least, 'semi-quantitative' and that they will be of value in assessing trial socket designs. Comparisons between mathematical or physical models and experimental measurements may examine tissue behaviour further and establish more accurate stress-strain relationships. Nevertheless, for results to be of direct use to a particular application, tests should reflect appropriate modes of deformation. For example, interface pressure and shear measurements taken over a period of time will reveal more clearly how these loads change during standing.

Measurements of tissue properties using a scanning technique such as ultrasound may indicate the magnitude of differences between the properties of individual soft tissues. The effect that these variations have upon interface loads and tissue stresses can then be investigated in FE models.

Configuration of external loads.

Measurements of the spatial location of markers on a socket, combined with forceplate data are able to determine the location of the ground reaction force relative to the socket. These data can be used to establish prosthetic loading more accurately than in the current study. The FE models, however, have shown alignment changes to have little effect upon interface pressures. The benefits of these measurements may be greater in quasi-dynamic models.

Appendices.

Appendix A

Outline of the FE Theory Used

Many real structures have geometry, loading configurations and constraints which are complex and analysis of these frequently yields differential equations which are difficult or impossible to solve. The FE method is an approximate technique for solving such differential equations by discretising them in their space dimensions.

By choosing subdomains, or elements, of simple shape a number of readily solved differential equations may be formulated that govern behaviour. A variational principle, valid in the full domain of the problem, is then postulated and the required solution is that which minimises some functional. In the case of stress analysis we shall, in general, be minimising the total potential energy, defined as a functional of the displacements.

Let us first consider a simple rectangular element which lies in a plane within a linear elastic structure. Deformations of this element shall be assumed to occur within this plane. The thickness, t, of the element shall be assumed constant and its sides shall remain straight. Forces acting on the element shall be assumed to be concentrated at the nodes.

The deformation of the element at any point can be described by two independent displacements u_x and u_y. We shall assume that these are described anywhere within the element by

$$u_x = \alpha_1 + \alpha_2 x + \alpha_3 y + \alpha_4 xy \qquad \text{- A.1}$$

$$u_y = \alpha_5 + \alpha_6 x + \alpha_7 y + \alpha_8 xy$$

where x and y are Cartesian coordinates. Separating the polynomial from the constants, α, the displacement in the x-direction, written in matrix, form is

$$\left[u_x \right] = \left[P \right] \left[\alpha_{1,4} \right] \qquad \text{- A.2}$$

We know the (x,y) coordinates of the element at its nodes and can therefore write

$$\begin{bmatrix} u_{x1} \\ u_{x2} \\ u_{x3} \\ u_{x4} \end{bmatrix} = \begin{bmatrix} 1\ x_1\ y_1\ x_1y_1 \\ 1\ x_2\ y_2\ x_2y_2 \\ 1\ x_3\ y_3\ x_3y_3 \\ 1\ x_4\ y_4\ x_4y_4 \end{bmatrix} \begin{bmatrix} \alpha_1 \\ \alpha_2 \\ \alpha_3 \\ \alpha_4 \end{bmatrix} \qquad \text{- A.3}$$

or

$$\left[u_{xn} \right] = \left[a \right] \left[\alpha_{1,4} \right] \qquad \text{- A.4}$$

and from this we have

$$\left[\alpha_{1,4} \right] = \left[a^{-1} \right] \left[u_{xn} \right] \qquad \text{- A.5}$$

Equation A.5 can be substituted into equation A.2 and its counterpart for y displacements, to give

$$\begin{bmatrix} u_x \\ u_y \end{bmatrix} = \begin{bmatrix} [P]\ 0 \\ 0\ [P] \end{bmatrix} \begin{bmatrix} [a^{-1}]\ 0 \\ 0\ [a^{-1}] \end{bmatrix} \begin{bmatrix} u_{xn} \\ u_{yn} \end{bmatrix} \qquad \text{- A.6}$$

The product of the [P] and [a] matrices is sometimes written as one matrix [N] and termed the matrix of shape functions.

The relationship between the displacements and the direct strains ε_{xx}, ε_{yy} and shear strain τ_{xy} may be written, in matrix form as

$$\begin{bmatrix} \varepsilon_{xx} \\ \varepsilon_{yy} \\ \tau_{xy} \end{bmatrix} = \begin{bmatrix} \frac{\partial}{\partial x} & 0 \\ 0 & \frac{\partial}{\partial y} \\ \frac{\partial}{\partial y} & \frac{\partial}{\partial x} \end{bmatrix} \begin{bmatrix} u_x \\ u_y \end{bmatrix} \qquad \text{- A.7}$$

Substituting equation A.6 into this gives

$$[\varepsilon] = [B][A][u_n] \qquad \text{- A.8}$$

where

$$[B] = \begin{bmatrix} \frac{\partial P}{\partial x} & 0 \\ 0 & \frac{\partial P}{\partial y} \\ \frac{\partial P}{\partial y} & \frac{\partial P}{\partial x} \end{bmatrix} \qquad \text{- A.9}$$

since only [P] is dependent upon x and y and the matrix containing the submatrices [a] has become [A]. The stress-strain relationship for plane stress may be written, in matrix form, as

$$\sigma = \begin{bmatrix} \sigma_x \\ \sigma_y \\ \tau_{xy} \end{bmatrix} = \frac{E}{1-\nu^2} \begin{bmatrix} 1 & \nu & 0 \\ \nu & 1 & 0 \\ 0 & 0 & \frac{(1-\nu)}{2} \end{bmatrix} \begin{bmatrix} \varepsilon_x \\ \varepsilon_y \\ \gamma_{xy} \end{bmatrix} = D \quad \varepsilon$$

- A.10

To obtain solutions for this system of equations the concept of strain energy, S, is used. This is an integral over the element volume

$$S = \frac{1}{2}\int [\varepsilon]^T [\sigma]\, dV \qquad \text{- A.11}$$

With substitutions from equations A.8 and A.10, the strain energy is integrated over the area, A, of the element which has thickness t. The integral used is

$$S = \frac{t}{2}[u_n]^T [A^{-1}]^T \int [B]^T [D][B]\, dA\, [A^{-1}][u_n] \qquad \text{- A.12}$$

which may be written

$$S = \frac{1}{2}[u_n]^T [K_e][u_n] \qquad \text{- A.13}$$

where $[K_e]$ is known as the element stiffness matrix.

Castigliano's theorem states that the derivative of strain energy with respect to a displacement gives the force in the direction of that displacement. Equation A.13 may be differentiated to give the nodal forces, F_n, which have produced the nodal displacements, u_n, i.e.

$$[F_n] = \frac{\partial S}{\partial [u_n]} \qquad \text{- A.14}$$

Performing this differentiation yields

$$[F_n] = [K_e][u_n] \qquad \text{- A.15}$$

and the task is reduced to evaluating the simple integral for $[K_e]$.

So far we have only considered a single element which might lie in a mesh representing a structure. The variational principle, valid in the full structure, must now be applied and the principle of minimum potential energy is used. This states that 'among all the admissible displacement functions, the actual displacements make the total potential energy an absolute minimum.' [WASHIZU75] and is satisfied by the condition of equilibrium. On the elements chosen, forces are transmitted only at the nodes. Thus, for equilibrium of a structure made up of these elements, the sum of the forces at the nodes must be zero. Force-displacement equations of each element, if referred to a global frame of reference, may be used to calculate the nodal forces due to that element. This summation process is, in practice, performed during assembly of the structural stiffness matrix, $[K_S]$. A simple example of this is given in [PAFEC84]. Assembly of the structural stiffness matrix is equivalent to evaluating the integral of the strain energy equation for the full structure of discrete elements.

The rectangular element discussed above was a conveniently regular shape and formulation of shape functions for this element was a relatively simple matter. Shape functions for a general element, which may have curved sides, are obtained by first mapping the distorted element onto an element with simple geometry in a local coordinate system of curvilinear coordinates, ξ, η.

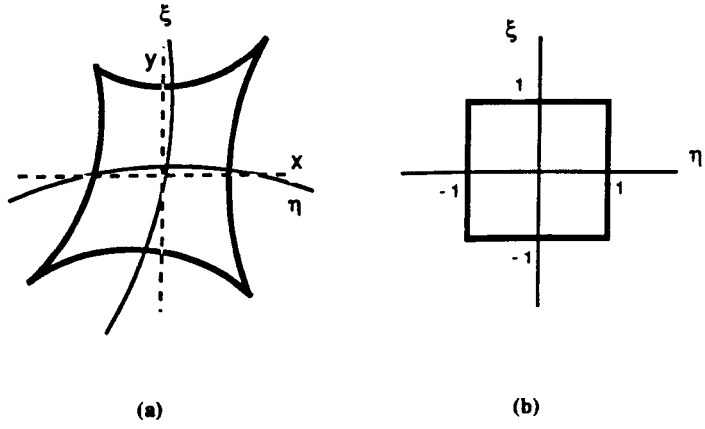

Figure A.1 - Mapping of an isoparametric element.
(a) distorted element seen in Cartesian space.
(b) element seen in ξ, η space.

It is convenient if the irregular shape shown in figure A.1 (a) becomes the square $(\pm1,\pm1)$ of figure A.1 (b). For the isoparametric elements used by PAFEC this is

achieved using the same polynomial form used to describe the displacements (c.f. equation A.1). In this case, therefore,

$$x = \beta_1 + \beta_2 \xi + \beta_3 \eta + \beta_4 \xi\eta$$

and

$$y = \beta_5 + \beta_6 \xi + \beta_7 \eta + \beta_8 \xi\eta \qquad \text{- A.16}$$

The shape matrix, [N], is obtained as before, but in terms of mapped coordinates ξ, η and a more complex integral results since the strains are not readily available in terms of ξ, η.coordinates. The integral is evaluated using the Gauss quadrature. This is described in [ZIENKIEW71].

All models presented in the thesis produce a state of stress that is truly three-dimensional. In some cases, however, the structure and loading is arranged to be symmetrical about a common axis, i.e the problem is axisymmetric. In these cases the stress and strain in one generator plane only need be considered and two-dimensional elements in such a plane may be used, greatly reducing the job size and solution time.

For axisymmetric solutions using PAFEC the axis of symmetry is arranged to be the x-axis and the y are therefore radial values. The hoop strain in these problem alters the [B] and [D] matrices which become

$$[B] = \begin{bmatrix} \frac{\partial P}{\partial x} & 0 \\ 0 & \frac{\partial P}{\partial y} \\ \frac{\partial P}{\partial y} & \frac{\partial P}{\partial x} \\ 0 & P/y \end{bmatrix}$$

and

$$[D] = \frac{E}{(1+\nu)(1-2\nu)} \begin{bmatrix} 1-\nu & \nu & 0 & \nu \\ \nu & 1-\nu & 0 & \nu \\ 0 & 0 & \frac{1}{2}-\nu & 0 \\ \nu & \nu & 0 & 1-\nu \end{bmatrix}$$

using these two definitions the solution is obtained as before.

Where 3-dimensional elements are used, the polynomial used to produce the shape functions is

$$[\, 1 \;\; x \;\; y \;\; xy \;\; x^2 \;\; y^2 \;\; x^2y \;\; y^2x \,]$$

for 8-noded brick elements and all 6 terms of the stress and strain vectors are defined within the [B] and [D] matrices.

For all models presented in the thesis, the most efficient way of gaining solutions to equation A.15, in terms of unknown displacements or nodal reactions, was to use a front solution method. This is one of a number of methods of generating the stiffness matrix in a compacted form. In essence, a 'front' of elements moves through the mesh eliminating unknowns as it progresses. A full explanation of this method appears in [IRONS80], together with a summary of the merits of this and alternative solution methods.

Having calculated the unknowns, the accuracy of the approximation must be considered. It is desirable to have convergence of the solution to the exact answer as the mesh of elements is refined. The conditions for this convergence are set out in [ZIENKIEW71]. In general terms, they state that the shape functions chosen must, in the limit as element size tends to zero, be able to represent the deformation of a continuum.

Appendix B

Mesh design for flat-tipped indenter models.

This appendix presents the procedure used to develop a mesh for the flat-tipped indenter models which are presented in Chapter 3.

The trial meshes for the flat indenter model with d/h equal to 2.0 are shown in figure B.1.

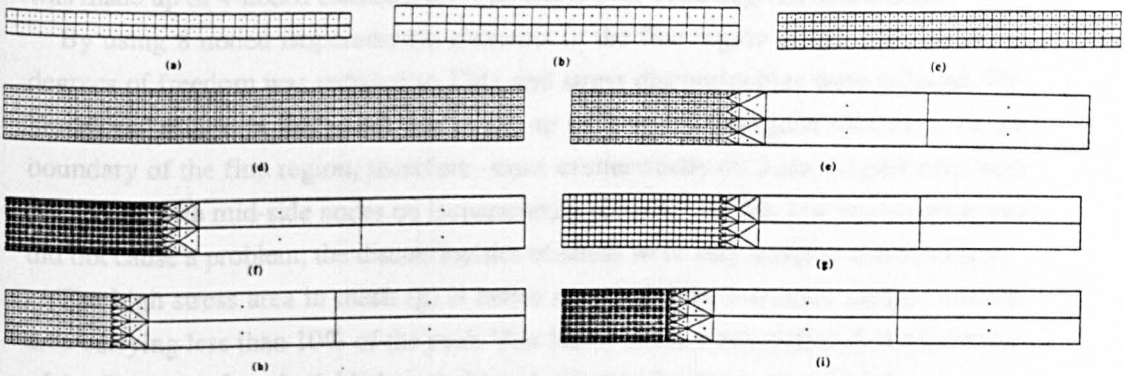

Figure B.1 Trial meshes for flat indenter model with d/h=2.0.

As discussed in section 3.2, judgement of the quality of each trial mesh was based upon the differences encountered between stress across element boundaries. For the flat tipped indenters, stresses were checked on the line of nodes below the sharp edge.

The diameter of the elastic layer was 30 mm initially in mesh (a) and this was reduced to 20 mm in (b) by removing elements which boar less than 1% of the peak Von Mises stress in the structure. Analysis of (b) showed no significant changes to the calculated stress pattern nor to the predicted structural stiffness. The apparent redundancy of the material lying outside a diameter of 20 mm in (a) may indicate that, under the circumstances, a continuous elastic layer is fairly well represented by mesh (b). The same criterion to detect redundant elements was used to fix the size of the elastic layer in models with other aspect ratios and indenter shape.

Progressive refinement ((c) and (d)) produced meshes with a roughly fourfold increase in degrees of freedom and reduced stress discontinuities and the predicted stiffness at each stage.

In order to keep the problem size to a manageable level, the mesh (e) included a coarse region where the Von Mises stress had been found to be less than 10% of the peak value in the structure. A band of 'transition' elements was used to maintain a continuous mesh between the coarse and fine regions. Results from the analysis of (d) and (e) were very similar. In the other indenter models, coarse areas of elements were located by the same criterion.

Mesh (e) became (f) by doubling the density of elements in the fine region. Mesh (f) was made up of 4-noded elements and contained over 1600 degrees of freedom.

By using 8 noded isoparametric elements in the fine region of (g), the number of degrees of freedom was reduced to 1241 and stress discontinuities were reduced. The 'transition' region in this mesh was made up of 3-noded triangular elements. At the boundary of the fine region, therefore, some corner nodes on 3-noded elements were coincident with mid-side nodes on isoparametric elements. In this low stress region this did not cause a problem; the discontinuities of stress were very small at this boundary.

The high stress area in mesh (g) is better resolved than in coarser meshes and the area carrying less than 10% of the peak Von Mises stress was smaller. A readjustment of the fine area of mesh yielded mesh (h) and a final refinement gave mesh (i).

In all of the trial meshes shown, elements beneath the indenter have an aspect ratio of 1.0. A rough test, in which the aspect ratio of the elements was changed while the degrees of freedom modelled was held roughly constant, showed predicted stiffnesses to be insensitive to element aspect ratios between 0.2 and 5.0.

For the trial meshes, maximum differences in the stresses calculated at nodes were expressed as a percentage of the peak vertical stress found. This was used as a measure of the continuity of stress within the mesh.

Below the edge of the modelled indenter in mesh (c), at the node one quarter of the way down through the elastic layer, a maximum difference of 55% of the peak stress was found. In meshes (h) and (i) these differences were 4% and 1% respectively and solutions due to these were considered to be converging. The stiffnesses predicted by these meshes differed by only 1.5% and the more time-consuming iterative runs, therefore, mesh (h) was used.

A similar mesh design process defined the meshes used to model aspect ratios of 1.0 and 4.0 and these are shown in figure B.2.

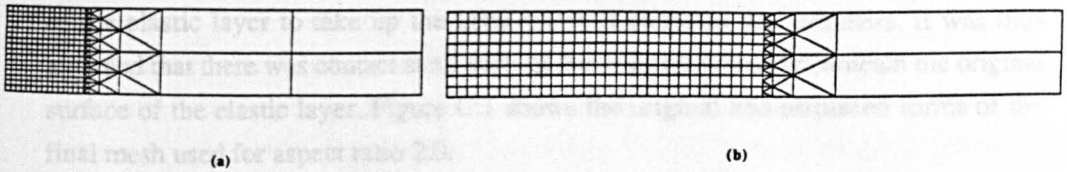

Figure B.2 - Meshes for flat-tipped indenters.

(a) d/h=1.0.

(b) d/h=4.0.

Appendix C

Mesh design for round-tipped indenter models.

The linear models used to evaluate trial meshes for indentations by round-tipped indenters prescribed displacements vertically downwards and simply forced the surface of the elastic layer to take up the hemispherical shape of the indenters. It was thus assumed that there was contact at all parts of the indenter which lay beneath the original surface of the elastic layer. Figure C.1 shows the original and displaced forms of the final mesh used for aspect ratio 2.0.

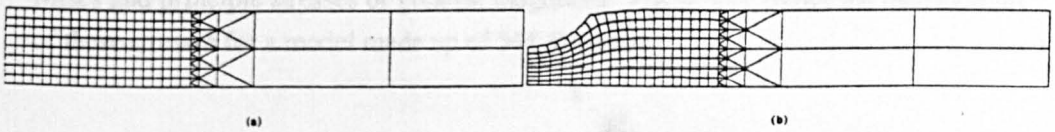

Figure C.1- Mesh for round-tipped indenter with d/h=2.0
(a) original form.
(b) displaced form

Although this was unlikely to be an accurate reflection of true indentations, it was felt to be a reasonable approximation for the sake of mesh design.

Trial meshes were checked for stress continuity and for each aspect ratio final meshes were broadly similar to those used for the flat-tipped indenters.

Appendix D

Mesh design for idealised limb models

This appendix describes the development of meshes which were used in the idealised limb models presented in Chapter 6.

For model 'A', a coarse mesh of 34 eight-noded isoparametric elements initially was used with a linear analysis in which 1 mm of bone displacement was applied. The simple axisymmetric mesh was refined using PAFEC's mesh generation module PAFBLOCKS by doubling the number of elements both along and across the elastic layer and this refinement process was repeated to create 4 meshes in all.

Using the PIGS graphical facility, areas were identified which contained the Von Mises and principle stresses of greatest magnitude. Figure D.1 shows the distributions of these stresses for a model made up of 544 elements.

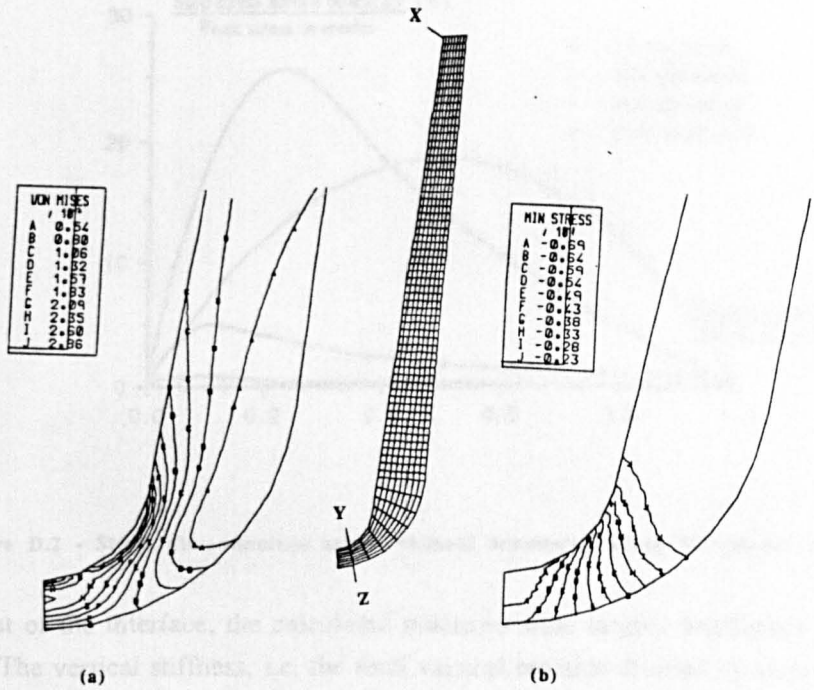

Figure D.1 - Stress distributions in model 'A' ; with end-bearing and a 'totally rough' interface.

(a) Von Mises.

(b) Minimum principle stress.

The largest stresses were, in fact, calculated at the node marked 'X'. This stress concentration was, however, highly localised and its effect on other parts of the mesh was considered to be insignificant since the applied load at node 'X' was a very small proportion of the total applied load. Improvements in the model due to mesh refinement were monitored by observing both the continuity of stresses within each trial mesh and the reactions calculated at the interface.

The continuity of stresses was checked by determining at a node the maximum difference between stresses calculated for each adjacent element. Large differences were found at nodes on the axis of symmetry and along the line YZ shown in figure D.1. Differences were calculated between minimum principle stresses at each node along the axis of symmetry and these differences were normalised by the minimum principle compressive stress found at the distal end. Figure D.2 presents plots of these normalised differences. Data are shown for each trial mesh; the solution due to the 2176 element mesh was assumed to be converging.

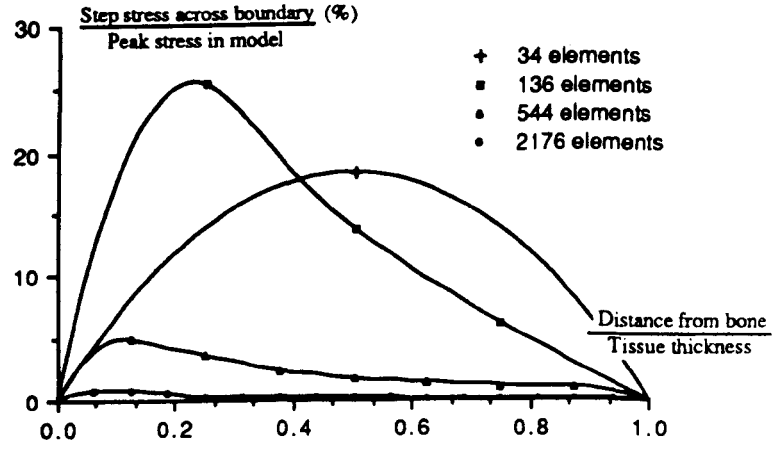

Figure D.2 - Stress discontinuities across element boundaries along YZ (model 'A').

Over most of the interface, the calculated reactions were largely unaffected by refinement. The vertical stiffness, i.e. the total vertical reaction divided by vertical displacement of the bone, of the 2176 element mesh was within 0.5% of that with 136 elements. The distribution of interface loads, however, *was* influenced by mesh refinement, mainly at the highly loaded distal end. At the node 'Z' of figure D.1, the calculated normal reaction per unit area was approximately 5% greater than at the corresponding node of the 136 element mesh. The value from the 2176 element mesh

was, however, within 1% of that with 544 elements. It was therefore presumed that further refinement of the FE mesh would be unlikely to produce significantly different interface reactions and that either of the 2 finest meshes would produce acceptable results for the purposes of the current study.

For model 'B', jobs were run using the 544 and 2176 element meshes. Stress discontinuities were small and negligibly different in the two models and differences in calculated reactions were also small. Convergence was again assumed.

The distributions of stress for model 'B' are shown in figure D.3. In the runs which created these, the total vertical reaction from the socket was the same as that which produced the figure D.1. Under the 'frictionless' conditions a larger bone displacement was required to produce this load.

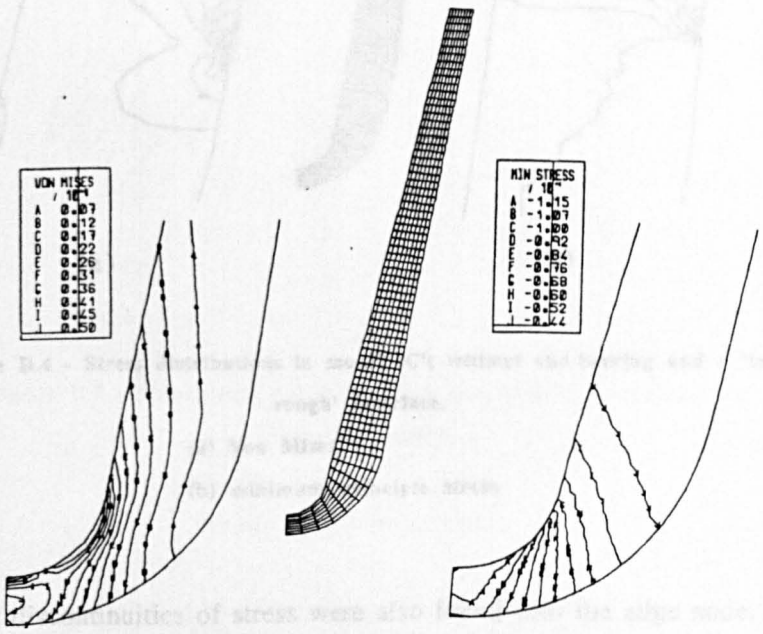

Figure D.3 - Stresses distributions in model 'B'; with end-bearing and a 'frictionless' interface.

(a) Von Mises

(b) Minimum principle stress.

For model 'C', the 544 element mesh used for the end bearing models was assessed and a sharp stress concentration was identified at the point where the modelled socket and limb surfaces part, i.e. at the most distal of the restraining nodes which modelled

the socket wall. Figure D.4 shows the distribution of the Von Mises and minimum principle stresses in this area.

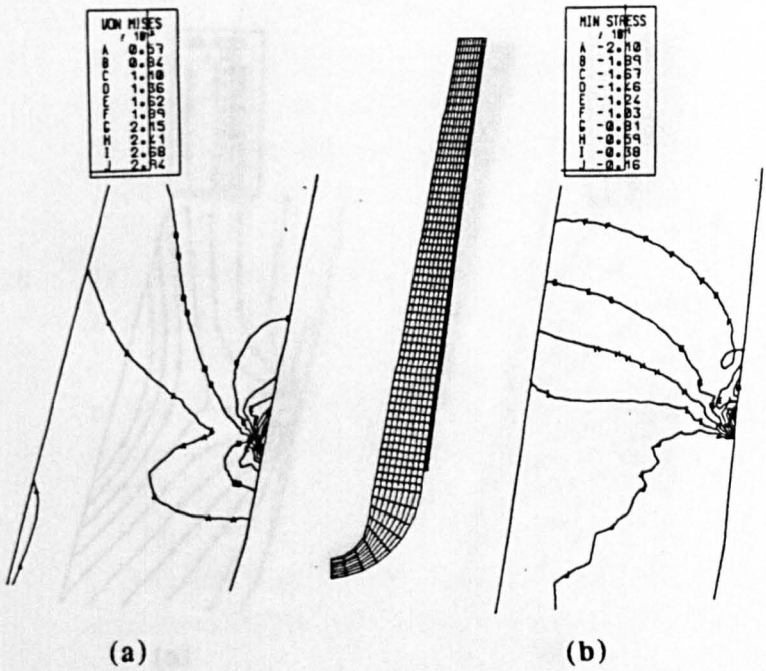

Figure D.4 - Stress distributions in model 'C'; without end-bearing and a 'totally rough' interface.

(a) Von Mises

(b) minimum principle stress.

The greatest discontinuities of stress were also found near the edge node. The differences between calculated stresses, however, were shown to be very localised when plotted for elements around this node and were thought unlikely to have wide reaching effects upon the calculated reactions; with this mesh the vertical component of the reaction at the edge was only 1% of the total load supported.

Refinement using the 2176 element mesh changed the calculated reactions per unit area for the node at the edge; however, other reactions were affected negligibly. The normal reaction per unit area at the edge with this mesh was 12.8% greater than the value calculated using the 544 element mesh. Five millimetres above the edge, however, values from the two meshes differed by only 0.8%.

For model 'D', the contribution of the edge node to the vertical reaction was smaller and the 544 element mesh was also considered acceptable. The more uniform distributions of Von Mises and minimum principle stresses are shown in figure D.5.

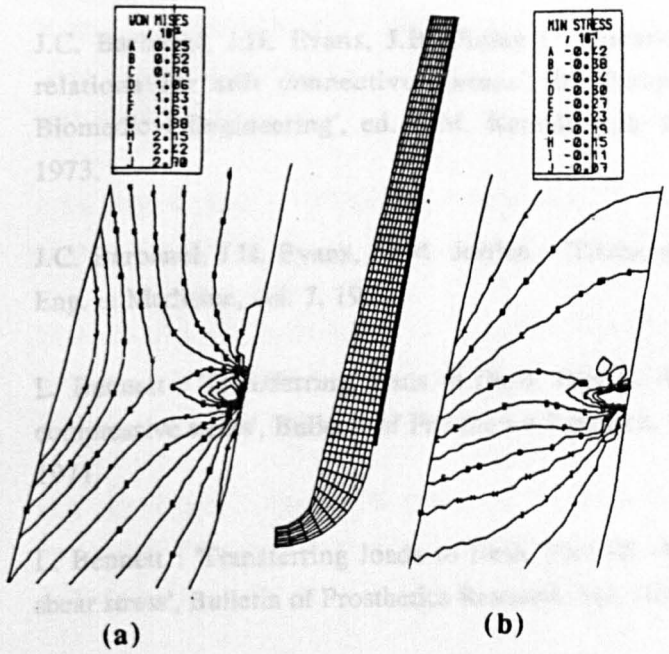

Figure D.5 - Stress distributions in model 'D'; without end-bearing and a 'frictionless' interface.

(a) Von Mises

(b) minimum principle stress.

List of references

BARBENEL73 J.C. Barbenel, J.H. Evans, J.B. Finlay : ' Stress-strain-time relations for soft connective tissues', In 'Perspectives in Biomedical Engineering', ed. R.M. Kenedi, pub. Macmillan, 1973.

BARBENEL78 J.C. Barbenel, J.H. Evans, M.M. Jordan : 'Tissue mechanics', Eng. in Medicine, vol. 7, 1978.

BENNETT71 L. Bennett : 'Transferring loads to flesh. Part II. Analysis of compressive stress', Bulletin of Prosthetics Research, vol. 10-16, 1971.

BENNETT72 L. Bennett : 'Transferring loads to flesh. Part III. Analysis of shear stress', Bulletin of Prosthetics Research, vol. 10-17, 1972.

BENNETT73 L. Bennett : 'Transferring loads to flesh. Part V Experimental work', Bulletin of Prosthetics Research, vol. 10-21, 1973.

BENNETT79 L. Bennett, D. Kavner, B.K. Lee F.A. Trainor : 'Shear vs. pressure as causative factors in skin blood flow occlusion', Arch. Phys. Med. & Rehabilitation, vol. 60, 1979.

BRAND75 P. Brand : 'Biomechanical concepts', In 'Bedsore Biomechanics', ed. R.M. Kenedi, J.M. Cowden, J.T. Scales, Baltimore University Park Press, 1976

BRUNSKI80 J.B. Brunski, V. Roth, N. Reddy, G.van B. Cochran : 'Finite element stress analysis of a contact problem pertaining to formation of pressure sores', In Advances in Bioengineering, American Society of Mechanical Engineers, 1980.

CHILDRESS87 D.S. Childress, J.W. Steege : ' Computer-aided analysis of below-knee socket pressure', J. Rehabilitation R. & D., vol. 24, 1987

CHOW78 W.W. Chow, E.I. Odell : ' Deformations and stresses in soft body tissues of a sitting person', J. Biomechanical Eng., vol. 100, 1978.

CLEGG66 E.J Clegg, C. Kent : ' Skinfold compressibility in young adults', Human Biology, 1967.

COOPER86 D.G. Cooper, J.B. Morrison, C.G. Saunders : ' Determination of in vivo bones shapes for CAD of below knee sockets', Proc. ISPO V World Congress, Copenhagen, 1986.

CRAWFORD85 H.V. Crawford, P. Gellett, S. Cousins : ' A low cost computer controlled carving machine', Bioengineering Centre Annual Report, 1985.

CRAWFORD86 H.V. Crawford, P. Gellett : ' A low cost computer controlled carving machine', Bioengineering Centre Annual Report, 1986.

DALY66 C.H. Daly : ' The biomechanical characteristics of human skin', Ph. D. Thesis, University of Strathclyde, 1966.

DAVIES85 R.M. Davies, R.B. Lawrence, P.E. Routledge, W. Knox : 'The Rapidform process for automated thermoplastic socket production', Prosthetics & Orthotics International, vol. 9,1985.

DECRAEMER80a W.F. Decraemer, M.A. Maes, V.J. Vanhuyse : 'An elastic stress-strain relation for soft biological tissues based on a structural model', J. Biomechanics, vol. 13, 1980.

DECRAEMER80b W.F. Decraemer, M.A. Maes, V.J. Vanhuyse, P. Vanpeperstraete : 'A non-linear viscoelastic constitutive equation for soft biological tissues based upon a structural model', J. Biomechanics, vol. 13, 1980.

DEMIRAY72 H. Demiray : ' A note on the elasticity of soft biological tissues', J. Biomechanics, vol. 5, 1972.

DEWAR85 M.D. Dewar, P. Jarman, D. Reynolds, H. Crawford, J. MacCoughlan, J. Wilkinson, A. Crew : ' Computer aided socket design (CASD) : UCL system based on full shape sensing', Bioengineering Centre Annual Report, 1985.

DEWAR86a M.D. Dewar, D. Reynolds : ' Development of the UCL computer aided socket design system', Bioengineering Centre Annual Report, 1986.

DEWAR86b M.D. Dewar, A. Crew, H. Crawford, P. Jarman : ' Direct carving of sockets', Bioengineering Centre Annual Report, 1986.

DEWAR86c M.D. Dewar, A. Crew, H. Crawford, P. Jarman : ' Clinical trials with the CASD system', Bioengineering Centre Annual Report, 1986.

DHSS86a Department of Health and Social Security : 'On the state of the public health', pub. HMSO, 1986.

DHSS86b Department of Health and Social Security : 'Review of artificial limb and appliance centre services', 1986.

EVANS73 F.G. Evans : 'Mechanical properties of bones', pub. C.C. Thomas, Springfield, Illinois, 1973.

FERGUSON80 M. W. Ferguson-Pell : ' Design criteria for the measurement of pressure at body/support interfaces', Eng. in Medicine, vol. 9, 1980.

FERNIE85 G.R. Fernie, G. Griggs, S. Bartlett, K. Lunau : ' Shape sensing for computer aided below-knee prosthetic socket design', Prosthetics & Orthotics, vol. 9, 1985.

FINLAY69 J.B. Finlay : ' Scanning electron microscopy of the dermis under uniaxial strain', Biomedical Eng., vol. 4, 1969.

FISHMAN87 S. Fishman, N. Berger, D.E. Krebs : ' Development of the ISNY belwo-knee flexible socket system', J. Rehabilitation R. & D., vol. 24, 1987.

FOORT63 J. Foort ' Adjustable brim fitting of total contact above-knee socket', Biomechanics Laboratory, University of California, Berkeley, 1963.

FUNG67 Y.C.B. Fung : 'Elasticity of soft tissues in simple elongation', Am. J. of Physiology, vol. 213, 1967.

FUNG72 Y.C.B. Fung : ' Stress-strain-history relations of soft tissues in simple elongation', In 'Biomechanics - Its foundations and objectives', pub. Prentice-Hall, 1972.

GOU70 P.F. Gou : ' Strain energy function for biological tissues', J. Biomechanics, vol. 3, 1970

GREEN57 A.E. Green, R.S. Rivlin : 'The mechanics of non-linear materials with memory', Arch. Rat. Mech. Analysis, vol. 1, 1957.

GREEN60 A.E. Green, J.E. Adkins : 'Large elastic deformations', pub. Clarendon Press, 1960.

GUYTON71 A.C. Guyton : 'Textbook of medical physiology', pub. W.B. Saunders, Philadelphia, 1971.

HANNAH84 R.E. Hannah, J.B. Morrison, A.E. Chapman : ' Prosthesis alignment : effect on gait of persons with below-knee amputation', Arch. Phys. Med. & Rehabilitation, vol. 65, 1984.

HAUT72 R.C. Haut, R. W. Little : ' A constitutive equation for collagen fibers', J. Biomechanics, vol. 5, 1972.

HAYES72 W.C Hayes, L.M. Keer, G. Herrmann, L.F. Mockros : 'A mathematical analysis for indentation test of articular cartilage', J. Biomechanics, vol. 5, 1972.

HICKMAN66 K.E. Hickman, O. Lindan, J.B. Reswick, R.H. Scanlan : 'Deformation and flow in compressed skin tissues', Biomedical Fluid Mechnics Symposium, ASME, 1966.

HUISKES83 Huiskes, E.Y.S Chao : ' A survey of finite element analysis in orthopaedics biomechanics : the first decade', J. Biomechanics, vol. 16, 1983.

HUSAIN53 T. Husain : ' An experimental study of some pressure effects on tissue with reference to the bed-sore problem', J. Path. & Bact, vol. 66, 1953.

IRONS80 B. Irons, S. Ahmad : 'Techniques of finite elements', pub. Ellis Horwood, 1980.

ISHERWOOD78 A. Isherwood : 'Simultaneous PTB pressures and force plate values', Bioengineering Centre Annual Report, 1978.

JARMAN85 P. Jarman, M.D. Dewar : ' Carving blanks for CASD project', Bioengineering Centre Annual Report, 1985.

JARMAN86a P. Jarman, M.D. Dewar : ' Carving blanks for the computer aided socket design project', Bioengineering Centre Annual Report, 1986.

JARMAN86b P. Jarman, M. Dewar, A. Crew, K. Jones : ' Static alignment in CASD sockets', Bioengineering Centre Annual Report, 1986.

JENKINS74 R.B. Jenkins, R.W. Little : ' A constitutive equation for parallel-fibered elastic tissue', J. Biomechanics, vol. 7. 1974.

KAY75 H.W. Kay, J.D. Newman : 'Relative incidences of new amputations', Orthopaedic Prosthetics, vol. 29, 1975.

KENEDI64 R.M. KENEDI, T. Gibson, C.H. Daly, ' Bioengineering studies of the human skin - I', NATO advanced study course on connective tissue, St. Andrews, pub. Butterworths, 1964.

KENEDI65 R.M. Kenedi, T. Gibson, C.H. Daly : ' Bioengineering studies of the human skin II', In ' Biomechanics and related Bioengineering topics', pub. Pergamon Press, 1964.

KIRK49 E. Kirk, S.A. Kvorning : 'Quantitative measurements of the elastic properties of skin and subcutaneous tissue in young and old individuals', J. Gerontology, vol. 4, 1949.

KOSIAK58 M. Kosiak, W.G. Kubicek, M. Olson, J.N. Danz, F.J. Kottke : 'Evaluation of pressure as factor in production of ishial ulcers', Arch. Phys. Med & Rehabilitation, vol. 39, 1958.

KROUSKOP87a T.A. Krouskop, A.L. Muilenberg, D.R. Doughtery, D.J. Winningham : ' Computer-aided design of a prosthetic socket for an above-knee amputee', J. Rehabilitation R. & D., vol. 24, 1987

KROUSKOP87a T.A. Krouskop, D.R. Doughtery, F.S. Vinson : ' A pulsed Doppler ultrasonic system for making noninvasive measurements of the mechanical properties of soft tissue', J. Rehabilitation R. & D., vol. 24, 1987

LANIR88 ' Structural modeling of soft tissue mechanics', Proc. World Congress Med. Phys. & Biomed. Eng., San Antonio, USA, 1988.

LARRABEE86 W.F. Larrabee, D. Sutton : 'A finite element model of skin deformations II. The finite element model', Laryngoscope, vol. 96, 1986.

LAWRENCE85 R.B. Lawrence, W. Knox, H.V. Crawford : ' Prosthetic replication using a computer controlled carving technique', Prosthetics & Orthotics International, vol. 9, 1985.

LOCKETT72 F.J. Lockett : ' Nonlinear viscoelastic solids', pub. Academic Press, 1972.

MANSCHOTT86 J.F.M. Manschott, A.J.M. Brakkee : 'The measurement and modelling of the mechanical properties of human skin in vivo - II. The modelling' J. Biomechanics, vol. 19, 1986.

MEIER73 R.H. Meier, E.D.Meeks, R.M. Herman : ' Stump-socket fit of below-knee prostheses: comparison of three methods of measurement', Arch. Phys. Med & Rehabilitation, vol. 54, 1973.

MILLER80 G.J. Miller, W.W. Purkey jr. : ' The geometric properties of paired human tibia', J. Biomechanics, vol. 13, 1980.

NAKAJIMA82 H. Nakajima, M. Suzuki, Y. Inatomi : ' Application of CAD/CAM technology for socket design of artificial legs', Proc. of Conference on CAD/CAM technology in Mechanical Engineering, MIT, 1982.

NAKAMURA81 S. NAKAMURA, R.D. CROWNINSHIELD, R.R. COOPER : 'An analysis of soft tissue loading in the foot - A preliminary report' Bulletin of Prosthetics Research, vol. 18, 1981.

OOMENS87 C.W.J. Oomens, D.H. van Campen, H.J Grootenboer : ' A mixture approach to the mechanics of the skin', J. Biomechanics, vol. 9, 1987.

PAFEC84 PAFEC limited : 'PAFEC theory', PAFEC, Strelley Hall, Nottingham,1984.

PEARSON73 J.R. Pearson, G. Holmgren, L. March, K. Oberg : ' Pressures in the critical regions of the below-knee patellar -tendon-bearing prosthesis', Bulletin of Prosthetics Research, vol. 10-19, 1973.

RADCLIFFE61 C.W. Radcliffe, J. Foort : 'The patellar-tendon-bearing below-knee prosthesis', Biomechanics Laboratory, University of California, Berkeley, 1961.

RIDGE64 M.D. Ridge, V. Wright : 'A rheological study of skin', In 'Biomechanics and related Bioengineering topics', pub. Pergamon Press, 1964.

ROAF76 R. Roaf : ' Causation and prevention of bed sores', In ' Bedsore Biomechanics', ed. R.M. Kenedi, J.M. Cowden, J.T. Scales, Baltimore University Park Press, 1976

SAUNDERS64 D.W. Saunders : 'Large deformations in amorphous polymers', In 'Biomechanics and related Bioengineering topics', pub. Pergamon Press, 1964.

SAUNDERS85 C.G. Saunders, J. Foort, M. Bannon, D. Lean, L. Panych : 'Computer aided design of prosthetic sockets for below-knee amputees', Prosthetics & Orthotics International, vol. 9, 1985.

SAUNDERS88 C. Saunders : ' Latest developments in computer aided socket design based on the results of clinical trials', Orthopædie & Rehatechnik 1988 International Congress, 1988.

SCHADE12 H. Schade : 'Untersuchegen zur Organfunction des Bindegewebes. 1. Die Elasticitatsfunction des Bindegewebes und die initiale Messung ihrer Storungen.' Zeitschrift fur exp. Path. und Therapie, 11. 1912.

SCHOCK81 R.B. Schock : ' A problem related to the biomechanics of pressure sores : stress and strain analysis of soft tissue indentations', Ph. D. dissertation, Rensselaer Polytechnic Institute, Troy, NY, 1981.

SCHUCK86 C.M. Schuck, A.B. Wilson : ' The use of surlyn and polypropylene in flexible brim socket desings for below-knee prostheses', Clinical Prosthetics & Orthotics, vol. 10, 1986.

SHARMA76 M.G. Sharma, T.M. Hollis : 'Rheological properties of arteries under normal and experimental hypertension conditions', J. Biomechanics, vol. 9, 1976.

SLOCUM49 D.B. Slocum : ' An atlas of amputations', pub. Kimpton, London, 1949.

SMITH85 D.M. Smith, M. Lord : ' A tool for standing load line assessment', In 'Biomechanical measurement in orthopaedic practice', ed. Whittle & Harris, pub. Clarendon Press.

SMITH86 D.M. Smith, A. Crew, A. Hankin : ' Silhouette shape sensor', Bioengineering Centre Annual Report, 1986.

SNYDER72 R.W. Snyder : ' Large deformations of isotropic biological tissue', J. Biomechanics, vol. 5, 1972.

SONCK70 W.A. Sonck, J.L. Cockrell, G.H. Koepke : 'Effect of liner materials on interface pressures in below-knee sockets', Arch. Phy. Med & Rehabilitation, vol. 51, 1970.

STARK71 H. L. Stark : ' The surgical limits of extension and compression of human skin', Ph. D. Thesis, University of Strathclyde, 1971.

TIMOSHENK34 S. Timoshenko : ' Theory of elasticity', McGraw-Hill, New York, 1934.

TONG76 P. Tong, Y.C.B. Fung : 'The stress-strain relationship for the skin', J. Biomechanics, vol. 9, 1976.

VANDERLIN86 J. Vanderlinden : 'Introducing new possibilities of data collection and processing in computer-aided socket design', Proc. ISPO V World Congress, Copenhagen, 1986.

VERONDA70 D.R. Veronda, R.A. Westmann : 'Mechanical characterization of skin - finite deformations', J. Biomechanics, vol. 3, 1970.

WASHIZU75 K. Washizu : 'Variational methods in elasticity and plasticity', pub. Pergamon, 1975.

WILSON79 A.B. Wilson Jr., C. Pritham, T. Cook : ' A force line visualization system', Prosthetics & Orthotics International, vol. 3, 1979.

WINTER76 In ' Bedsore Biomechanics', ed. R.M. Kenedi, J.M. Cowden, J.T. Scales, Baltimore University Park Press, 1976

YAMADA70 H. Yamada : 'Strength of biological materials', pub. Williams & Wilkins, Baltimore, 1970.

ZAHEDI86 M.S. Zahedi, W.D. Spence, S.E. Solomonidis, J.P.Paul : 'Alignment of lower-limb prostheses', J. of Rehabilitation R & D., vol. 23, 1986.

ZIEGERT78 J.C. Ziegert, J.L. Lewis : ' In vivo mechanical properties of soft tissue covering bony prominences', vol. 100, 1978.

ZIENKIEW71 O.C. Zienkiewicz : ' The finite element method in engineering science', pub. McGraw-Hill, 1971.